Model predictive control of Type 4 wind turbines

Master thesis

Rasmus Løvschall Kristiansen

Aalborg University
Electronics and IT

AALBORG UNIVERSITY
STUDENT REPORT

Electronics and IT
Aalborg University
http://www.aau.dk

Title:
Model predictive control of Type 4 wind turbines

Theme:
Control and Automation master thesis

Project Period:
Spring Semester 2023

Project Group:
1038

Participant(s):
Rasmus Løvschall Kristiansen

Supervisor(s):
Jan Dimon Bendtsen (AAU)
Lars Meyer (Vestas Wind Systems A/S)

Copies: 1

Page Numbers: 125

Date of Completion:
June 1, 2023

Abstract:

This thesis investigates the viability of MPC as a converter control strategy for Type 4 wind turbines. The thesis demonstrates the proposed controllers ability to handle grid fault events and robustness to grid strength variations. The thesis proposes a useful prediction model for the MPC controller, which contains the relevant dynamics of the controlled system. The proposed MPC controller is formulated as a quadratic optimization problem with linear constraints. The constraints limit the ranges of the controlled outputs and the control signals. The thesis also demonstrates how the developed model predictive controller can be implemented in c code, which is a necessity for future implementations on an embedded hardware platform. Tests have been conducted in a high fidelity simulation environment. The results indicate that MPC is indeed a viable control strategy, as it provides stable and accurate control, reliable fault handling capabilities and impressive robustness.

Elektronik og IT
Aalborg Universitet
http://www.aau.dk

AALBORG UNIVERSITET
STUDENTERRAPPORT

Titel:
Model predictive control af Type 4 vindmøller

Tema:
Control and Automations speciale

Projektperiode:
Forårssemestret 2023

Projektgruppe:
1038

Deltager(e):
Rasmus Løvschall Kristiansen

Vejleder(e):
Jan Dimon Bendtsen (AAU)
Lars Meyer (Vestas Wind Systems A/S)

Oplagstal: 1

Sidetal: 125

Afleveringsdato:
1. juni 2023

Abstract:

Dette speciale undersøger potentialet af MPC som en converter kontrol strategi for Type 4 windmøller. Rapporten kortlægger kontrol strategiens stabilitet i forbindelse med grid-fejl og robusthed overfor variationer i grid styrke. Specialet foreslår en prædiktionsmodel til MPC controlleren, der i rette omfang beskriver den nødvendige systemdynamik. Den udviklede MPC controller er formuleret som et kvadratisk optimeringsproblem med linære begrænsninger. Begrænsninger limiterer operationsområdet af systems kontrollede outputs og kontrolsignaler. Specialet demonstrerer hvordan kontrol strategien kan implementeres i c kode, hvilket er en nødvendighed for fremtidige implementationer på en nedlejret hardware platform. Tests er blevet udført på en high fidelity simuleringsplatform. Resultaterne bekræfter at MPC er en brugbar kandidat til converter kontrol, da den viser stabil og nøjagtigt kontrol, såvel som pålidelig håndtering af netfejl og god robusthed.

Contents

Preface

This report was written by Rasmus Løvschall Kristiansen, as a Master thesis during the 4th semester of the Control and Automation Master programme at Aalborg university. The project has been supervised by Jan Dimon Bendtsen from Aalborg university and Lars Meyer from Vestas Wind Systems A/S. The project has been developed at Vestas main office in Aarhus. Vestas has provided the student with assistance and tools during the development of the project.

This project is an extension of the work presented in [6], which was produced by the student as a 3rd semester project in collaboration with Vestas Wind Systems. The case study of this master thesis is focused on the development of a model predictive control strategy for control of a Type 4 wind turbine.

Readers Guide

It is a prerequisite for understanding the case study of the report that the readers has a basic understanding of electrical circuits, state space modelling and optimal control theory. The report provides references to material from various sources. These references are listed in a bibliography 6.1, and are presented using the IEEE standard. All figures and and graphs are listed with respect to the chapter in which they are presented. As an example the second figure in chapter 3 is referenced to as figure 3.2. All figures and graphs used in the report are either created by the student, or have references to their source appended to their label.

Aalborg University, June 1, 2023

Rasmus Kristiansen

Rasmus Løvschall Kristiansen
rkrist21@student.aau.dk

Nomenclature

Abbreviation	Meaning
MPC	Model predictive control
LQR	Linear quadratic regulator
LMI	Linear matrix inequality
SCR	Short circuit ratio
FRT	Fault ride through
HiFi	High fidelity
pu	Per unit

Chapter 1

Introduction

This chapter will discuss the motivation for the project, along with a high-level description of the system considered in the case study. Furthermore, the previous work[6] by the author will be discussed, as it is relevant for the thesis. The specific project description and hypotheses will be presented, followed by an extended summary of the thesis, which prepares the reader for the rest of the thesis.

1.1 Motivation

Energy is one of the fundamental demands of modern society. From the private household to the largest industries, a reliable and affordable source of energy is an absolute necessity. Furthermore, public services such as healthcare, sanitation, communication and security are integral to our society and are extremely dependent on a reliable energy supply.

With the global unrest brought on by the 2022 Russian invasion of Ukraine, energy prices have reached an all time high[13]. This puts a strain on all parts of society: The private consumer has to pay more for both electricity and common goods. Entire industries are struggling to overcome the increasing costs, such as energy heavy steel industry[11]. Furthermore, the war has increased the global interest in reliable energy sources other than natural gas, so as to be more energy-independent of Russia.

One way to combat the rising energy prices is to increase the global energy supply, which by supply and demand will reduce the prices. This can be aligned well with another global interest, which is to increase the market share of green energy. The European Commission has set a target for 2030, that 32% of the EU's power consumption must be supplied by renewable energy sources[10]. As of 2021 22% of EU's power comes from renewables sources. The wind industry is a growing source of energy, of which Vestas Wind Systems A/S is a pioneer. The danish company has since it founded in 1945 been a driving force towards a sustainable future, and in 2022 alone, Vestas shipped more than 3000 wind turbines with a total capacity of over 13 gigawatts of power[14].

As a consequence of the growing market penetration of renewables, the power grid is shifting towards a larger share of converter based power supplies, such as wind turbines. This implies that a lower percentage of power is supplied by traditional power plants, such as coal and gas, which utilize large synchronous generators connected to the grid[3]. These generators contain a massive inertia, which helps stabilize the grid, as the frequency of the grid is tied to the rotational speed of the generators. As the relative amount of generator based power plants gradually decreases, the power grid gets weaker. Therefore, it is an increasing priority that wind turbines must be robustly stable to the strength of the power grid.

Another important factor for modern control of wind turbines, is that they should be able to support the power grid during faults. One such fault could be a low voltage drop. One way to support the grid during a low voltage fault is to lower the active power production while injecting reactive power into the grid, which will help raise the voltage.

To ensure that the wind turbines can support the power grid during faults and operate robustly on weaker grids, this master thesis proposes and investigates the use of an optimal control strategy for power converters. The specific control strategy, which will be tested, is the model predictive controller. It is a control strategy which uses a model to predict the future behavior of the plant, and calculates the optimal control signals based on those predictions. As such, it takes the system dynamics into account, on a level not seen in classical cascaded control. Another benefit of optimal control strategies is the intuitive tuning procedures, which potentially can reduce the complexities of working with converter control applications.

1.2 Type 4 wind turbines

IEC defines 4 types of wind turbines[4], with the most discernible differences being their generator type and their converter strategy or lack thereof. Both Type 1 and Type 2 wind turbines uses asynchronous generators directly connected to the grid. The difference between them is primarily that Type 2 has a variable rotor resistance. Type 3 uses a double fed asynchronous generator. The Type 4 wind turbine is the focus of this case study, as a growing amount of new wind turbines shipped use this technology. It utilizes a full scale power converter: A back-to-back AC/DC/AC converter with a DC link connecting the rectifier and inverter.

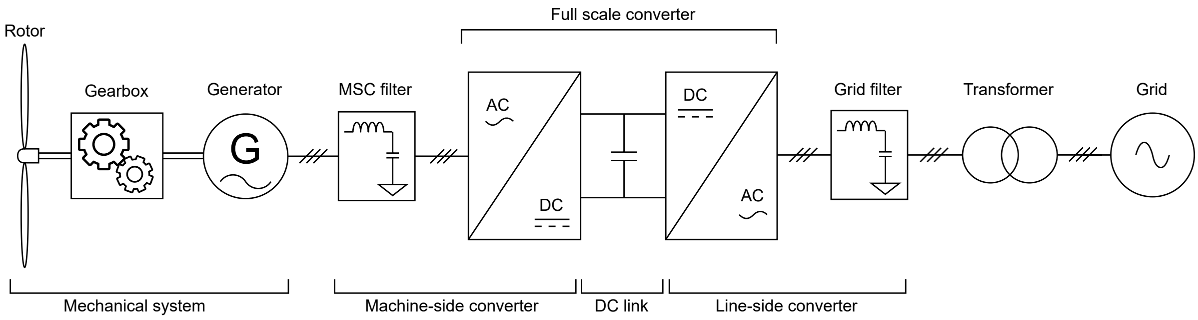

Figure 1.1: Block diagram of the power route of a Type 4 wind turbine. Double-lined connections represent mechanical connections. Connections marked with three lines represent 3 phased electrical signals. Single line connections with no indicators represent DC signals.

The block diagram of a Type 4 wind turbine is seen if figure 1.1. Going left to right the turbine contains:

The mechanical system
The mechanical system is comprised of three elements: The rotor, the gearbox, and the generator. The rotor is an aeromechanical unit, with 3 blades which capture the energy of the wind. It is connected by a shaft to a gearbox, that converts the slow rotational speed of the rotor to a speed which fits the generator. The outgoing shaft of the gearbox connects to the generator, which converts mechanical power to three phased electrical power.

The machine-side converter
The machine-side converter is comprised of a lowpass filter and an AC-DC rectifier. The lowpass filter acts as a $\frac{dv}{dt}$ filter, which limits the rate of change of voltage, smoothing the slopes of the PWM signals. The machine side converter operates as an active rectifier, converts the AC power to DC power which is fed to the DC link.

The DC link
The DC link transfers the power from the machine-side to the line-side. It contains a large capacitor, which removes ripples from the voltage, mitigating DC link voltage spikes. The capacitor helps decouple the mechanical and electrical systems, as it effectively filters out everything besides the active power being transferred. The capacitor is designed to handle the switching average power, but is not capable of mitigating major power imbalances between the MSC and LSC.

For that, the DC link also contains a chopper. The chopper is connected in parallel with the capacitor and consists of a series resistor and gate. During grid events where active power cannot be delivered to the grid, the switch is opened so the chopper resistor can dissipate the excess power from the machine side. Thus, an increase in DC link voltage can be avoided. This is preferred over the alternative solution, which is to lower the MSC power, resulting in damaging torque spikes.

The line-side converter
The line-side converter consists of the DC-AC inverter, and the grid filter. The inverter converts the power from the DC link to 3 phased AC power. The power is passed through the grid filter, which attenuates switching harmonics of the signal delivered to the grid.

Transformer and grid
The filtered power is delivered to the grid through the transformer. This greatly increases the voltage of the power, while lowering the current, which minimizes power loss when transferring power.

There are several benefits inherent to the Type 4 wind turbine structure. A prime benefit is the decoupling between the mechanical system and the electrical system. The use of a full scale converter ensures that variations of the voltage and frequency on the grid will not impact the mechanics. Similarly, the exact manner of power generation (the specific frequency, voltage etc.) on the machine-side will not be visible on the line-side.

The decoupling is attributed to the DC link, seperating the two converters. If the DC link voltage is well regulated, all that is seen is a DC link current, corresponding to the active power received from the machine-side. Similarly, the line-side simply consumes a given amount of active power from the DC link.

A final benefit of the Type 4 wind turbine is the increased control capability on the line-side. Since the line-side converter is isolated from the slow mechanical dynamics, the active and reactive powers can be rapidly changed. Quickly being able to reduce the active power is beneficial during low grid voltage events, as it allows the line side converter to avoid overcurrent operation. Further, increasing the reactive power during low voltage faults, helps stabilize the grid by raising the voltage.

1.2.1 Classical control of full scale converters

The control strategy for full scale converters is normally comprised of cascaded PI controllers. Separate control units regulate the MSC and LSC independently. Furthermore, these units typically consist of several cascaded PI controllers, such that the complete control strategy for a full scale converter can consist of more than 10 independent PI controllers. This poses a challenge in and of itself: The task of locally tuning a single PI controller is made difficult by the complex couplings to and from the other parts of the control. What is more, tuning the entire control system such that it is robust to parameter and grid variations becomes a difficult task, requiring extensive testing.

1.3 Previous work by the author

This report will as act as a natural extension of previous work by the author[6]. The author has previously written a report on the subject of full scale converters as part of their 3rd semester project in collaboration with Vestas. The case study of the report was an investigation of how model-based control could be used for full scale converters.

The project was focused mainly on the development of a linear state space model of a full scale converter. Referring to figure 1.1, the model included the DC link, line-side converter, transformer and grid. The machine-side was also simplified as a controllable current source. The system dynamics were inherently nonlinear, so linearization methods were used to obtain a LTI model. The methodology and know-how refined during the development of the model will be reused for this project, since modifications to the model will be made. This will be described in chapter 2.

Previous work also includes the development and testing of an LQI controller for the full scale converter. The controller used reference tracking to successfully control the DC link voltage as well as the active and reactive power delivered to the grid. The system tests indicated that while stability in the full range of operation was obtainable, the system proved challenging to control when operating far from the operating point. A gain scheduling strategy was implemented to further stabilize the system in the full range of operation. The proposed control strategy constituted a proof of concept that model was sufficiently accurate and that model based control is a viable strategy for wind turbine power converter.

Throughout the thesis there will be references to the previous work by the author. The associated report is however confidential and can thus not be accessed on the Aalborg University student project library. When referencing topics, findings or methods from the previous work, the author will therefore describe the subject in greater detail than is common. The description will either be written directly in this report or in an appendix, depending on the volume and subject.

1.4 Project description

1.4.1 Problem definition and hypotheses

To ensure that wind turbines also in the future can support the power grid during faults and operate robustly on weaker grids it is foreseen that more advanced control strategies must be considered. Thereby the following thesis statement has been formulated:

> How can a model predictive controller be implemented and used as a viable control strategy for a wind turbine full scale converter?

To evaluate the theses statement the following hypotheses had been deduced:

Hypothesis 1.
Model predictive control can be used to stably control a wind turbine full scale converter. The controller maintains system stability during slow changes in active and reactive power references, and it can regulate the active and reactive power to meet those references with zero steady state error.

Hypothesis 2.
Model predictive control can be used to stabilize a full scale power converter during a symmetric low voltage grid fault, while maintaining production of active current and reactive power.

Hypothesis 3.
Model predictive control for full scale power converter is a robust control strategy with respect to grid strength. The controller maintains stability at low short circuit ratios.

1.4.2 Project scope and limitations

The case study of this thesis is the development, implementation and test of a model predictive control strategy for a Type 4 wind turbine. A state space model of the system dynamics will be created, based on findings from previous work. The model is required, as the MPC controller uses a prediction model for its operation.

The proposed control strategy must adhere to the system limitations, such as hard constraints on the actuator ranges and relevant signal ranges. It must provide control signals which satisfy these constraints, while keeping the system stable. It must also be able to quickly control specific outputs to reference points with zero steady state error. Furthermore, the controller must be implemented in C code, so it can be tested on a high fidelity simulation platform.

On this simulation platform several applications will be tested. Firstly, normal operation must be verified. That is, the controller can stabilize the system and bring the outputs to their references.

Secondly, a symmetric grid fault will be applied to the system. The controller must be able to stabilize the system during the fault: an event known as a Fault Ride-Through (FRT). The fault in this thesis will be a rapid drop in grid voltage, during which the wind turbine will not be able to deliver nominal active power to the grid. During the fault, the controller must deliver a certain amount of active and reactive power, specified later in the thesis. The fault ends by restoring the grid voltage to its nominal value, at which point the controller must continue normal operation and deliver nominal power.

Lastly, the controllers robustness will be tested by varying the short circuit ratio (SCR) by adjusting the grid impedance. The controller is expected to perform well when the grid is strong - that is, a high SCR. The thesis will in simulation investigate the MPC controllers performance towards lower short circuit ratios.

To balance the scope of the thesis, the following boundaries has been set. The mechanical system will not be considered, as the primary focus is the control of the line side converter and DC link. No considerations has been done with respect to the pitch and yaw control, nor to speed control, or to control the machine side converter. The machine side converter is conceptually included in the thesis, but it is simplified as an ideal controllable current source.

The thesis considers only a single turbine connected to an infinite bus power grid. Thus the potential interaction between multiple converter has not been considered.

The thesis does not benchmark the achieved results versus the performance of the existing control. The thesis is intended to investigate the viability of using MPC for wind turbine converters, which requires a thorough analysis, that must naturally precede any bench marking. Optimizing and tuning MPC to compete directly with the existing control will be left as a project for future work.

1.5 Extended summary

This section summarizes the the key points of the entire thesis.

Chapter 2 discusses how the Type 4 wind turbine is modelled. A accurate model is critical to the MPC algorithm, as it is used to predict future system behavior. The chapter shows how a LTI state-space model has been derived using first principles modelling and how the non-linear power relations have been linearized. While the foundation of the model was made in previous work[6], revisions have been made to the model during this thesis. The model includes the dymanics of the system seen in figure 1.2. The model interfaces are described in the table below.

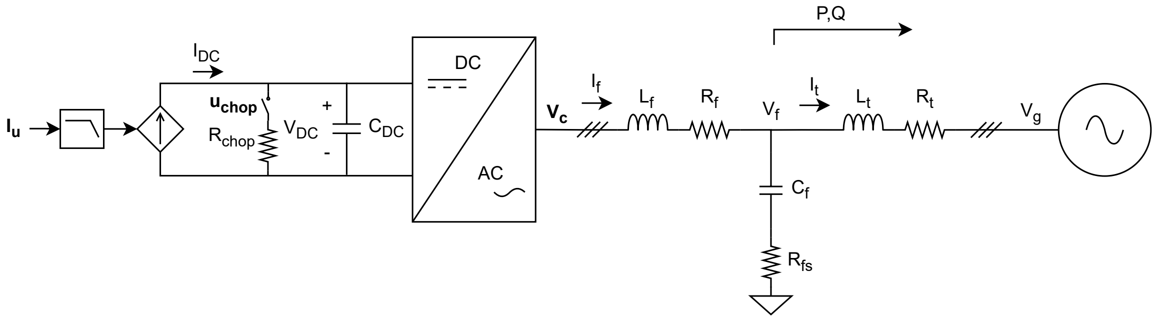

Figure 1.2: Block diagram of the Type 4 wind turbine model considered in this thesis

The model interfaces are:

Measured outputs:	Controlled outputs:	Controlled inputs (actuators):
I_t	I_t	V_c
V_{DC}	V_{DC}	I_u*
V_f		U_{chop}*
I_{DC}		

*Note, that during normal operation the chopper not used; the signal I_u is used to control the DC link voltage. During a grid fault, I_u is held constant at its nominal value, and the chopper is used to control the DC link voltage.

A list of the main features and limitations of the derived model:

- The system is modelled as a LTI discrete-time state space model in the rotating dq frame
- The model is both controllable and observable, and the matrices are decently conditioned
- The model is open-loop unstable due to the DC link dynamics
- The model includes the synchronizing effect of the PLL, however does not include the PLL dynamics - that is, the PLL is assumed to be ideal and infinitely fast

- The grid voltage is expressed in the dq frame of the model, although it operates in its own independent dq frame.

Chapter 3 discusses the implemented control strategy for the system. A MPC algorithm has been developed based on the method proposed by Maciejowski. This MPC method seeks to minimize the cost function

$$\mathcal{J}(k) = \sum_{i=0}^{H_p} ||\hat{y}(k+i) - r(k+i)||_Q + \sum_{i=0}^{H_u} ||\Delta\hat{u}(k+i)||_R \tag{1.1}$$

where

$\|\|x\|\|_P = x^T P x$	Convenient notation
$Q, R \geq 0$	Positive semi-definite weight matrices
$H_p \geq 1$	Prediction horizon
$H_u \leq H_p$	Control horizon

The control objective is to minimize the error between the controlled outputs and their respective references, while minimizing the changes in control signals. It is important to note that the absolute values of the control signals are not directly penalized, only their movement.

The practical system limitations rae specified as linear constraints. These can be constraints on input ranges, inputs slew-rates and output ranges:

$$\begin{aligned} u_{Low} &\leq u \leq u_{Low} \\ \Delta u_{Low} &\leq \Delta u \leq \Delta u_{Low} \\ y_{Low} &\leq y \leq y_{Low} \end{aligned} \tag{1.2}$$

By performing techniques known as augmenting and lifting, the MPC problem can be reformulated as a quadratic optimization problem with linear constraints. This is a equivalent to the cost function of equation 1.1 and the constraints of equation 1.2:

$$\min_{\Delta\mathcal{U}(k)} \mathcal{J}(k) = \Delta\mathcal{U}(k)^T \mathcal{H} \Delta\mathcal{U}(k) - \Delta\mathcal{U}(k)^T \mathcal{G} \tag{1.3}$$

subject to

$$\begin{bmatrix} \mathbf{F} \\ \Gamma\Theta \\ W \end{bmatrix} \Delta\mathcal{U}(k) \leq \begin{bmatrix} -\mathbf{F_1} u(k-1) - f \\ -\Gamma\psi\hat{x}(k) - g \\ w \end{bmatrix} \tag{1.4}$$

where

$$\Delta\mathcal{U}(k) = \begin{bmatrix} \Delta\hat{u}(k) \\ \vdots \\ \Delta\hat{u}(k+H_u-1) \end{bmatrix} \tag{1.5}$$

Solving this optimization problem yields the optimal input sequence $\Delta\mathcal{U}(k)$. This is a sequence of input signal over the next H_u samples. Only the first signal of the sequence is applied:

$$\hat{u}_{opt}(k) = \begin{bmatrix} I & 0 & \dots & 0 \end{bmatrix} \Delta\mathcal{U}_{opt}(k) + u(k-1) \tag{1.6}$$

Chapter 4 discusses the practical implementation of the controller. The controller was initially implemented in Simulink. The purpose of this was to verify the MPC functionality in a controlled and well-known environment. The implementation uses the solver OSQP[12] through the software tool CasADI[2]. Essentially, CasADI can act as a translator between a high level syntax in MATLAB to the low level syntax of OSQP. As such it smooths the learning curve of how to implement solver based controllers. The Simulink implementation was stable and served as a proof of concept that the MPC controller could be implemented using OSQP.

The next phase of the project was to write the MPC optimization in C code. The objective of the C implementation was to test the controller in a high fidelity wind turbine simulation built in Plecs. The controller was implemented in C code using OSQP libraries. The implementation was verified by comparing the results of an optimization in Plecs (C code) and Simulink.

The C code implementation actually realizes two optimization problems. The two problems both solve the MPC problem, however the difference is in the control signals they have available. The first problem can control the converter voltage and the MSC current, and the second problem can control converter voltage and the chopper resistor. The first problem is solved during normal operation, where the chopper should not be used. The second problem is solved during FRT events, where the MSC current should not be changed.

Chapter 5 demonstrates the three categories of tests has been conducted in Plecs:

Normal operation
A simple test case where references to the active and reactive power are varied over time. The references are passed through a math function which converts them to the d and q references of the output current. These references are passed to the MPC algorithm which controls the system. It was observed that there was no steady state error, and the system remained stable during transients. During normal operation the MPC controller must not and does not use the chopper resistor. This a hard coded behaviour, so as to avoid wasting power and in a real life application damaging the chopper resistor.

Fault ride through
This test sees the grid voltage being rapidly lowered 1 pu to 0.5 pu. The voltage remains low for 0.5 seconds and then rapidly returns to 1 pu. During the fault the converter is unable to deliver nominal power, as that would require too much active current. As such the active current is kept at its nominal value, resulting in a lower active power output. The fast decrease in line side power must be handled at the DC link, as to avoid a sudden rise in DC link voltage. The proposed solution

is to not change the DC link current during a FRT event, but rather let the chopper resistor absorb the excess power.

It was observed that the controller could stabilize the system during a FRT event, without excessive spikes in current and voltage. The controller would rapidly increase the chopper resistors gates duty cycle, matching the lowered active power consumption of the grid.

Grid SCR robustness

Lastly it was investigated how the short circuit ratio of the grid impacted the performance of the controller. By varying the from a strong grid with a SCR of 20 to a very weak grid of SCR 2, the following tendencies was observed. It should be noted that the X/R ratio was constant for the different SCR tests. The controller was robustly stable down to a SCR of 3 without chaning the tuning. At a SCR of 2, the system became marginally stable, as the DC link voltage and reactive current began oscillating.

As an extension, combining the FRT test with the robustness test, it was observed that a FRT could be handled with a SCR as low as 3. Lastly the predicted trajectories of the MPC controller were investigated, which revealed some unintended (but not critical) behavior that should be mitigated in future MPC implementations.

Chapter 2

Modelling

2.1 Chapter objective

The objective of the modelling chapter is to document the development of a state space model of the relevant elements of a type 4 wind turbine. The relevant elements include the DC link, line side filter, and grid impedance. The purpose of the model is to act as a prediction model for the model predictive controller. As such it should be accurate enough to predict the relevant dynamics, but simple enough as to not make the MPC predictions excessively time consuming.

The Type 4 wind turbine has been modelled in previous work[6]. The model will be reused in this thesis, albeit with modifications. This chapter will first present the methodology used to derive the model in previous work, and then present the modifications applied to make the model suitable for this thesis. The outline below provides an overview of the various sections and their content.

2.1.1 Outline of the modelling chapter

Section 2.2 - Model from previous work: This section recaps the model that was developed in previous work. It covers the following subjects:

- **2.2.1:** The electrical three-phased circuitry in the stationary abc frame
- **2.2.2:** The dq transformation of the AC system
- **2.2.3:** Linearizing the non-linear DC link voltage dymanics
- **2.2.4:** Linearizing the non-linear power outputs
- **2.2.5:** Finding a relevant operating point for linearization
- **2.2.6:** Discretization of the model

Section 2.3 - Model modifications: This section discusses the various changes made to the model for this thesis. Many changes were made based on findings from previous work. The section convers the following subjects:

- **2.3.1:** Simplifications made to the grid model
- **2.3.2:** The synchronizing effect of the PLL and its relation to the dq signals
- **2.3.3:** A model of the chopper, which is a new component in this thesis
- **2.3.4:** A transformation of the grid voltage from its own dq frame, to the dq frame defined by the PLL
- **2.3.5:** Changing the controlled outputs from powers to currents

2.2 Model from previous work

The system that was modelled in previous work is seen in figure 2.1. The mechanical system and machine side is modelled as a controllable bandwidth-limited current source I_{DC}. The DC link is modelled as a capacitor C_{DC} with voltage V_{DC}. The grid side filter is modelled as a LC lowpass filter, with impedances L_f and C_f. Each have a series resistance, with value R_f and R_{fs} respectively. The transformer impedance is represented by L_t and R_t. The remaining passive components represent the grid impedance.

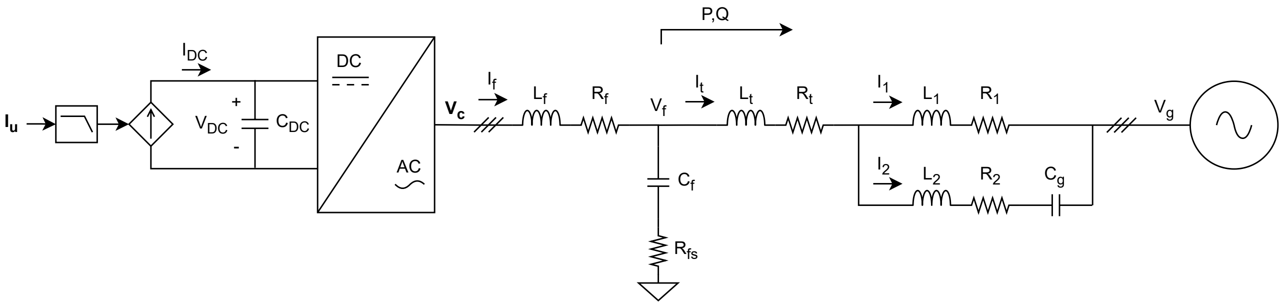

Figure 2.1: Block diagram of the Type 4 wind turbine model from previous work

The model interfaces are:

Measured outputs:	Controlled outputs:	Controlled inputs (actuators):
V_{DC}	V_{DC}	V_c
I_{DC}	P	I_u
V_f	Q	
I_t		
P		
Q		

The system states are the energy storing elements of the circuit. That is, the voltage across the capacitors and the current through the inductors. The grid voltage V_g is an unmeasured disturbance.

The system can be described by the linear discrete time state space model

$$\Delta x(k+1) = A\Delta x(k) + B\Delta u(k) + E\Delta d(k) \tag{2.1}$$

$$\Delta y(k) = C\Delta x(k) \tag{2.2}$$

where

$$x = \begin{bmatrix} I_{f_d} \\ I_{f_q} \\ I_{t_d} \\ I_{t_q} \\ I_{2_d} \\ I_{2_q} \\ V_{C_{f_d}} \\ V_{C_{f_q}} \\ V_{C_{g_d}} \\ V_{C_{g_q}} \\ V_{DC} \\ I_{DC} \end{bmatrix}, \quad u = \begin{bmatrix} V_{c_d} \\ V_{c_q} \\ I_u \end{bmatrix}, \quad d = \begin{bmatrix} V_{g_d} \\ V_{g_q} \end{bmatrix}, \quad y = \begin{bmatrix} I_{t_d} \\ I_{t_q} \\ V_{f_d} \\ V_{f_q} \\ V_{DC} \\ I_{DC} \\ P \\ Q \end{bmatrix}, \tag{2.3}$$

and

$$\Delta x(k) = x(k) - x' \tag{2.4}$$

The model is a linear approximation of the nonlinear dynamics, hence the Δ notation. Furthermore, the system is described in the rotating dq frame. The d and q subscripts denote the d and q components of the relevant three phased signal. The dq frame in previous work, was synchronized to the grid voltage. This is an erroneous simplification in previous work, as the PLL that provides the angle for the dq transformations is synchronized to the filtered converter voltage V_f.

The following subsections will briefly describe how the different elements of the model was derived.

2.2.1 AC system model

Consider first the AC subsystem, depicted in figure 2.2

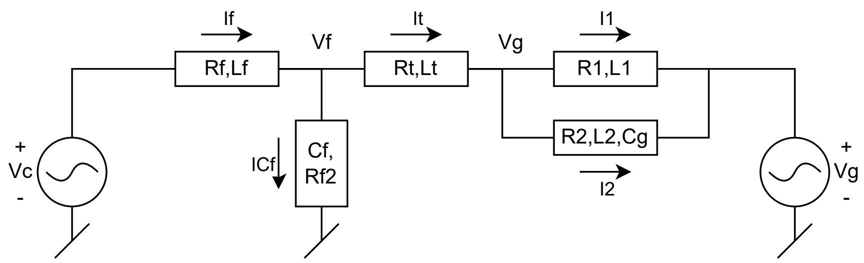

Figure 2.2: Single phase AC system. Blocks represent a series connection of the listed components

The dynamical behaviour of a single phase of the AC system can be described with a linear state space model. The state vector of the single-phase AC subsystem is

$$x = \begin{bmatrix} I_f \\ I_t \\ I_1 \\ I_2 \\ V_{C_f} \\ V_{C_g} \end{bmatrix} \tag{2.5}$$

The inputs to the subsystem is the converter voltage V_c and the grid voltage V_g. The converter voltage is a controllable input, while the grid voltage will act as a disturbance:

$$u = \begin{bmatrix} V_c \end{bmatrix}, \quad d = \begin{bmatrix} V_g \end{bmatrix} \tag{2.6}$$

The outputs of the AC subsystem are the measured values. That is the voltage V_f and the current I_t. Thus the output vector is defined as

$$y = \begin{bmatrix} V_f \\ I_t \end{bmatrix} \tag{2.7}$$

Using standard electrical relations such as Ohm's law, Kirchhoffs mesh and node laws and superposition, one can derive the differential equations describing the dynamics of the state vector. It can be expressed as a linear combination of the states and inputs in the state space format. Furthermore, the outputs can be expressed as a linear combination of the states. The model of the system in figure 2.1 becomes

$$\dot{x} = Ax + Bu + Ed \tag{2.8}$$

$$y = Cx \tag{2.9}$$

The system matrices A, B and C can be found in Appendix A.

The model can be expanded to contain two independent phases. The third phase need not be modelled, as the system is symmetric and with no neutral wire. Therefore, $I_a + I_b + I_c = 0$, which implies that the third phase always can be reconstructed from the two. Kirchhoffs current law is also used as an argument to exclude the state I_1 from the model, as $I_1 + I_2 - I_t = 0$.

The dynamics of the phase b are identical to that of phase a. The state, input and output vectors are thus expanded as such:

$$x_{ab} = \begin{bmatrix} I_{f_a} \\ I_{f_b} \\ I_{ta} \\ I_{tb} \\ I_{1a} \\ I_{1b} \\ I_{2a} \\ I_{2b} \\ V_{C_{f_a}} \\ V_{C_{f_b}} \\ V_{C_{g_a}} \\ V_{C_{g_b}} \end{bmatrix}, \quad u_{ab} = \begin{bmatrix} V_{ca} \\ V_{cb} \end{bmatrix}, \quad d_{ab} = \begin{bmatrix} V_{g_a} \\ V_{g_b} \end{bmatrix}, \quad y_{ab} = \begin{bmatrix} V_{f_a} \\ V_{f_b} \\ I_{ta} \\ I_{tb} \end{bmatrix} \tag{2.10}$$

The extended system matrices A_{ab}, B_{ab}, E_{ab} and C_{ab} are constructed from the original matrices A, B, E and C. Every element in A, B, E and C is replaced with a 2x2 diagonal matrix as such:

$$A_{1,1} \to \begin{bmatrix} A_{1,1} & 0 \\ 0 & A_{1,1} \end{bmatrix} \tag{2.11}$$

2.2.2 Transformation to rotating reference frame

The AC system can be described in the rotating dq frame, rather than the stationary abc frame. The dq frame rotates with the same frequency as the system (50 Hz) such that the three phases are stationary when observed in the frame. This allows the three phase system to be described by two DC values: their Direct "d" and Quadrature "q" components. There is commonly a third component "0", which is only non-zero when the system is unbalanced. The 0 component is omitted in this application, as the system is symmetrical and without a neutral wire.

When the system is balanced and linear time invariant, the dq transformation is simple to implement. The only difference in the state space models in the two frames, is a change to the A matrix. That is, to convert the system from the stationary frame

$$\dot{x}_{ab} = A_{ab}x_{ab} + B_{ab}u_{ab} + E_{ab}d_{ab} \tag{2.12}$$
$$y_{ab} = C_{ab}x_{ab} \tag{2.13}$$

to the rotating frame

$$\dot{x}_{dq} = A_{dq}x_{dq} + B_{dq}u_{dq} + E_{dq} \tag{2.14}$$
$$y_{dq} = C_{dq}x_{dq} \tag{2.15}$$

Previous work by the author[6] and other literature [7] has derived the transformation between the two frames. Both conclude that only the the state transition matrix A changes during the transformation:

$$A_{dq} = (A_{ab} + W_c) \tag{2.16}$$

where

$$W_c = \begin{bmatrix} W & & 0 \\ & \ddots & \\ 0 & & W \end{bmatrix}, \quad W = \begin{bmatrix} 0 & 2\pi\omega_s \\ -2\pi\omega_s & 0 \end{bmatrix} \tag{2.17}$$

Conveniently the ab→ dq transformation does not change the B, E and C matrices

$$B_{dq} = B_{ab}, \qquad E_{dq} = E_{ab}, \qquad C_{dq} = C_{ab}$$

2.2.3 DC link capacitor model

The dynamics of the DC link capacitor voltage V_{DC} are described by

$$\dot{V}_{DC} = \frac{I_{Cap}}{C_{DC}} \tag{2.18}$$

The capacitor current I_{Cap} can be extracted by using the power relationship of the circuit, shown in figure 2.3.

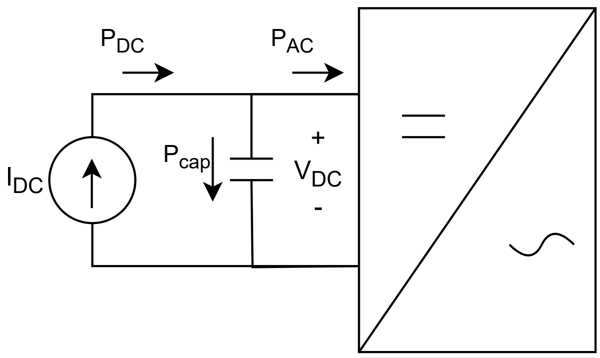

Figure 2.3: Power flow of the DC link.

The power balance can be defined as

$$P_{Cap} = P_{DC} - P_{AC} \tag{2.19}$$

By expressing the powers as functions of voltage and current the power relationship can be expressed as

$$V_{DC} I_{Cap} = V_{DC} I_{DC} - \frac{3}{2} \left(V_{c_d} I_{f_d} + V_{c_q} I_{f_q} \right) \tag{2.20}$$

The capacitor current I_{Cap} can be isolated and substituted into equation 2.18 to express the nonlinear dynamics of the DC link voltage

$$\dot{V}_{DC} = \frac{I_{DC} - \frac{3}{2} \left(\frac{V_{c_d} I_{f_d} + V_{c_q} I_{f_q}}{V_{DC}} \right)}{C_{DC}} \tag{2.21}$$

By applying a first-order Taylor approximation to equation 2.21 it can be linearized around a operating point given by x' and u', which yields the linear model

$$\begin{aligned} \Delta \dot{V}_{DC} \approx & \left[\frac{-\frac{3}{2} V_{c_d}{}'}{C_{DC} V_{DC}{}'} \right] \Delta I_{f_d} + \left[\frac{-\frac{3}{2} V_{c_q}{}'}{C_{DC} V_{DC}{}'} \right] \Delta I_{f_q} + \left[\frac{\frac{3}{2} \left(I_{f_d}{}' V_{c_d}{}' + I_{f_q}{}' V_{c_q}{}' \right)}{C_{DC} V_{DC}{}' V_{DC}{}'} \right] \Delta V_{DC} \\ & + \left[\frac{-\frac{3}{2} I_{f_d}{}'}{C_{DC} V_{DC}{}'} \right] \Delta V_{c_d} + \left[\frac{-\frac{3}{2} I_{f_q}{}'}{C_{DC} V_{DC}{}'} \right] \Delta V_{c_q} + \left[\frac{1}{C_{DC}} \right] \Delta I_{DC} \end{aligned} \tag{2.22}$$

where the variables are expressed as deviations from the operating point:

$$\Delta x = x - x' \tag{2.23}$$

Equation 2.22 is included in the state space model. As the dynamics of the existing states are linear, one can freely use Δ variables for those, without changing the system matrices. Going forward, states, inputs and outputs will be modelled in terms of Δ values.

As one control objectives is to regulate the DC link voltage, ΔV_{DC} is also included as a output of the model.

2.2.4 Active and reactive power outputs

Two additional measured outputs of the system is the active power P and reactive power Q delivered to the grid. In the dq frame these can be expressed as

$$P = \frac{3}{2} \left(V_{C_{f_d}} I_{td} + V_{C_{f_q}} I_{tq} \right) \tag{2.24}$$

$$Q = \frac{3}{2} \left(V_{C_{f_q}} I_{td} - V_{C_{f_d}} I_{tq} \right) \tag{2.25}$$

These nonlinear equations can be linearized with a Taylor approximation, which yields

$$\Delta P = \frac{3}{2}V_{C_{f\,d}}{}'\Delta I_{td} + \frac{3}{2}I_{td}{}'\Delta V_{C_{f\,d}} + \frac{3}{2}V_{C_{f\,q}}{}'\Delta I_{tq} + \frac{3}{2}I_{tq}{}'\Delta V_{C_{f\,q}} \tag{2.26}$$

$$\Delta Q = \frac{3}{2}V_{C_{f\,q}}{}'\Delta I_{td} + \frac{3}{2}I_{td}{}'\Delta V_{C_{f\,q}} - \frac{3}{2}V_{C_{f\,d}}{}'\Delta I_{tq} - \frac{3}{2}I_{tq}{}'\Delta V_{C_{f\,d}} \tag{2.27}$$

These equations are included in the state space model as outputs.

2.2.5 Operating point

A operating point for the system is found numerically using MATLAB®. The nonlinear model $\dot{x} = f(x, u)$ is solved as follows

$$f(x, u) = 0 \tag{2.28}$$

subject to

$$V_{DC} = V_{DC}{}' \tag{2.29}$$
$$V_{f\,dq} = V_{f\,dq}{}' \tag{2.30}$$
$$P = P' \tag{2.31}$$
$$Q = Q' \tag{2.32}$$

The values $V_{DC}{}'$, $V_{f\,dq}{}'$, P' and Q' are chosen by the designer as criteria for the operating point. MATLAB® then calculates the remaining state and input values that satisfy the equation. Solving $f(x, u) = 0$ ensures that the operating point is an equilibrium. That is, the system is at rest at the point x', u'.

2.2.6 Discretization

The model is discretized using the zero-order hold method. The sampling frequency is 8kHz. The discrete system matrices are given by

$$\begin{aligned} A_d &= e^{AT_s} \\ B_d &= A^{-1}(A_d - I)B \\ E_d &= A^{-1}(A_d - I)E \\ C_d &= C \end{aligned} \tag{2.33}$$

where A_d, B_d, E_d and C_d are the discrete system matrices, A, B, E and C are the continuous system matrices, and T_s is the sample time.

2.3 Model modifications

The following will discuss the modifications made to the model, to make it suitable for this thesis.

2.3.1 Grid model simplification

The grid model used in previous work consist of two parallel impedances, seen in figure 2.4. The

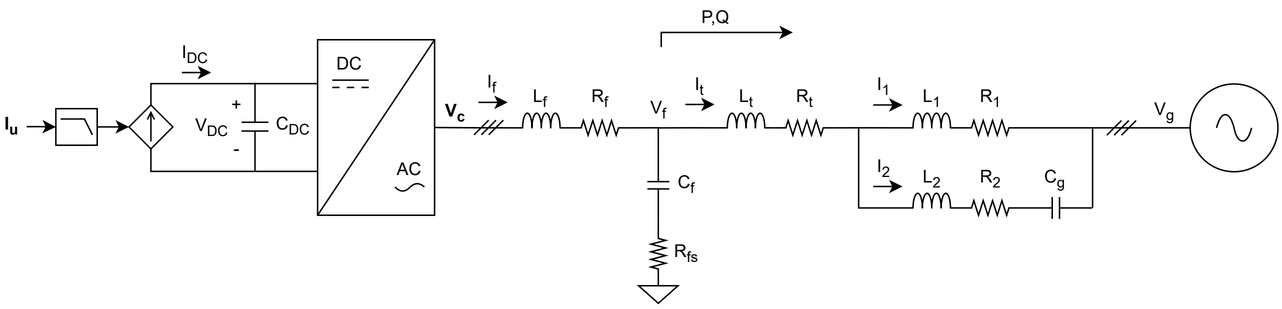

Figure 2.4: Block diagram of the Type 4 wind turbine model from previous work

specific grid model was chosen, as the original goal of the previous work was a case study in sub synchronous resonance (SSR). The grid model seen in figure 2.4 is the standard configuration used for SSR tests. However, since the focus of this thesis is on non-SSR specific control, the grid model can be simplified, which greatly reduces system complexity. The grid impedance is replaced with an RL series connection, which is added to the transformer impedance R_t and L_t. The resulting system is depicted in figure 2.5.

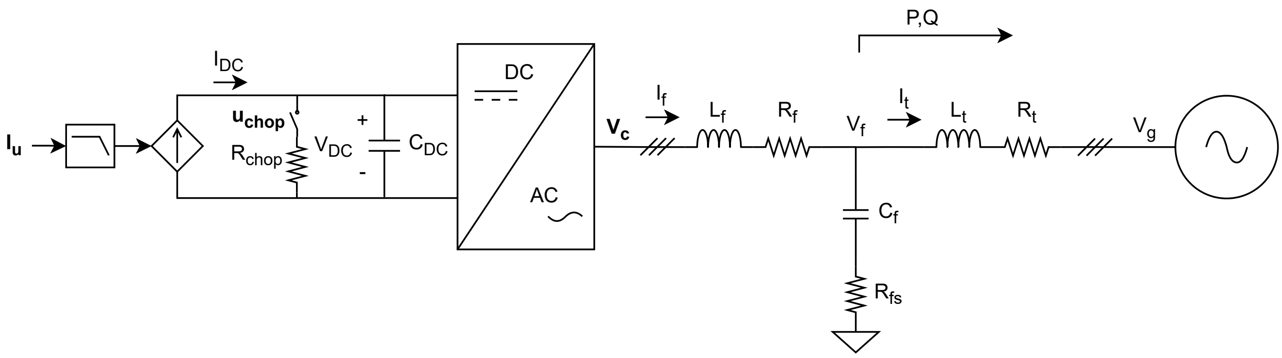

Figure 2.5: Block diagram of the Type 4 wind turbine model considered in this thesis

Where R_t and L_t represent the combined impedance of the grid and transformer. The simplification effectively eliminates 6 states from the AC subsystem. The single-phase AC subsystem of the reduced model can be described by the following state space model.

$$
\begin{bmatrix} \dot{I_f} \\ I_t \\ V_{C_f} \end{bmatrix} = \underbrace{\begin{bmatrix} \frac{-R_f - R_{fs}}{L_f} & \frac{R_{fs}}{L_f} & \frac{-1}{L_f} \\ \frac{R_{fs}}{L_t} & \frac{-R_t - R_{fs}}{L_t} & \frac{1}{L_t} \\ \frac{1}{C_f} & \frac{-1}{C_f} & 0 \end{bmatrix}}_{A} \begin{bmatrix} I_f \\ I_t \\ V_{C_f} \end{bmatrix} + \underbrace{\begin{bmatrix} \frac{1}{L_f} \\ 0 \\ 0 \end{bmatrix}}_{B} \begin{bmatrix} V_c \end{bmatrix} + \underbrace{\begin{bmatrix} 0 \\ \frac{-1}{L_t} \\ 0 \end{bmatrix}}_{E} \begin{bmatrix} V_g \end{bmatrix} \tag{2.34}
$$

$$
\begin{bmatrix} I_t \\ V_f \end{bmatrix} = \underbrace{\begin{bmatrix} 0 & 1 & 0 \\ R_{fs} & -R_{fs} & 1 \end{bmatrix}}_{C} \begin{bmatrix} I_f \\ I_t \\ V_{C_f} \end{bmatrix} \tag{2.35}
$$

The differential equations, which constitute the model, have been derived in Appendix B. The model must, like in previous work, by expanded to two phases and transformed to the rotating dq frame.

$$
\begin{bmatrix} \dot{I_{f_{dq}}} \\ I_{tdq} \\ V_{C_{f_{dq}}} \end{bmatrix} = \begin{bmatrix} \mathbf{I}_2 A_{11} + W & \mathbf{I}_2 A_{12} & \mathbf{I}_2 A_{13} \\ \mathbf{I}_2 A_{21} & \mathbf{I}_2 A_{22} + W & \mathbf{I}_2 A_{23} \\ \mathbf{I}_2 A_{31} & \mathbf{I}_2 A_{32} & \mathbf{I}_2 A_{33} + W \end{bmatrix} \begin{bmatrix} I_{f_{dq}} \\ I_{tdq} \\ V_{C_{f_{dq}}} \end{bmatrix} + \begin{bmatrix} \mathbf{I}_2 B_{11} \\ \mathbf{I}_2 B_{21} \\ \mathbf{I}_2 B_{31} \end{bmatrix} \begin{bmatrix} V_{cdq} \end{bmatrix} + \begin{bmatrix} \mathbf{I}_2 E_{11} \\ \mathbf{I}_2 E_{21} \\ \mathbf{I}_2 E_{31} \end{bmatrix} \begin{bmatrix} V_{g_{dq}} \end{bmatrix} \tag{2.36}
$$

$$
\begin{bmatrix} I_{tdq} \\ V_{f_{dq}} \end{bmatrix} = \begin{bmatrix} \mathbf{I}_2 C_{11} & \mathbf{I}_2 C_{12} & \mathbf{I}_2 C_{13} \\ \mathbf{I}_2 C_{21} & \mathbf{I}_2 C_{22} & \mathbf{I}_2 C_{23} \end{bmatrix} \begin{bmatrix} I_{f_{dq}} \\ I_{tdq} \\ V_{C_{f_{dq}}} \end{bmatrix} \tag{2.37}
$$

where $\mathbf{I}_2$ is a 2x2 identity matrix and the subscript $_{ab}$ indicates a 2x1 vector as such:

$$
I_{f_{ab}} = \begin{bmatrix} I_{f_a} \\ I_{f_b} \end{bmatrix}
$$

and

$$
W = \begin{bmatrix} 0 & 2\pi\omega_s \\ -2\pi\omega_s & 0 \end{bmatrix} \tag{2.38}
$$

The linearized model of the DC link voltage dynamics are unchanged by the AC subsystem simplification.

2.3.2 The consequences of the PLL

In previous work, the angle signal θ used for the dq transformation was not considered properly. That is, the model assumed that an external clock was generating the signal:

$$
\theta(t) = \omega_s t
$$

In practice θ is generated by a phase locked loop. The PLL synchronizes to the frequency of the measured voltage V_f and aligns θ with phase a of V_f. This effectively drives the q component of V_f to 0 in steady state.

There are several implications of this implementation. Firstly, from the perspective of the dq frame, the phase of V_f never changes. Rather other signals change their phase relative to V_f. As an example, the grid voltage V_g has a constant phase, frequency and amplitude in the time domain. But from the perspective of the dq frame, which is synchronized to V_f, the d and q components of V_g can vary.

Secondly, recall that the PLL will always aim to drive the q component of V_f to 0. One can then make the assumption that $V_{f_q}(t) = 0$ for all t. This introduces an error, since it implies the PLL is infinitely fast, which is naturally wrong. However, this assumption allows the model to ignore the PLL dynamics, and the state V_{f_q} can be removed from the model, which is utilized in this case study.

Removing the state V_{f_q} also simplifies the calculations of the outputs ΔP and ΔQ. Recall from earlier that

$$\Delta P = \frac{3}{2} V_{C_{f_d}}{}' \Delta I_{td} + \frac{3}{2} I_{td}{}' \Delta V_{C_{f_d}} + \frac{3}{2} V_{C_{f_q}}{}' \Delta I_{tq} + \frac{3}{2} I_{tq}{}' \Delta V_{C_{f_q}} \tag{2.39}$$

$$\Delta Q = \frac{3}{2} V_{C_{f_q}}{}' \Delta I_{td} + \frac{3}{2} I_{td}{}' \Delta V_{C_{f_q}} - \frac{3}{2} V_{C_{f_d}}{}' \Delta I_{tq} - \frac{3}{2} I_{tq}{}' \Delta V_{C_{f_d}} \tag{2.40}$$

As $V_{f_q} = 0$ it follows that

$$\Delta P = \frac{3}{2} V_{C_{f_d}}{}' \Delta I_{td} + \frac{3}{2} I_{td}{}' \Delta V_{C_{f_d}} \tag{2.41}$$

$$\Delta Q = -\frac{3}{2} V_{C_{f_d}}{}' \Delta I_{tq} - \frac{3}{2} I_{tq}{}' \Delta V_{C_{f_d}} \tag{2.42}$$

2.3.3 Chopper model

The chopper is a passive component mounted in parallel to the DC link capacitor as seen in figure 2.6. It has a series gate, which can be opened with a PWM signal. The purpose of chopper resistor is to dissipate excess power from the machine side, when a fault occurs on the grid. During a grid voltage drop, the active power delivered to the grid is suddenly lowered. This has potential to cause a rise in DC link voltage, as the machine side power cannot be lowered quickly enough to balance the power flow. The strategy is thus to open the chopper gate, letting the resistor dissipate the power.

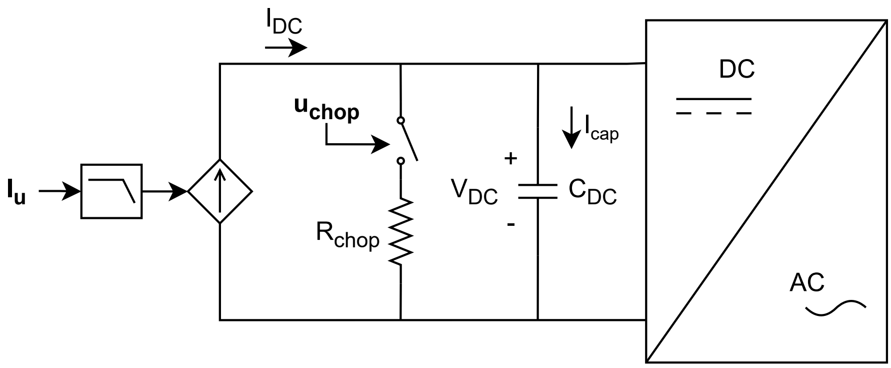

Figure 2.6: DC link block diagram. The chopper is a combination of a series resistor R_{chop} and a gate, here depicted as a switch controlled by the signal u_{chop}.

The power flows of the circuit are defined in figure 2.7.

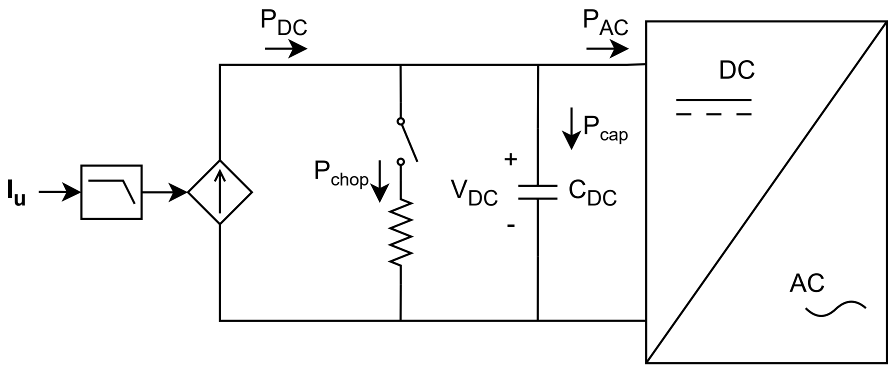

Figure 2.7: DC link power flows.

The chopper resistor affects the DC link voltage dynamics:

$$\dot{V}_{DC} = \frac{I_{Cap}}{C_{DC}} \tag{2.43}$$

The capacitor current I_{Cap} can be extracted by using the power relationship of the circuit, as depicted in figure 2.7:

$$P_{Cap} = P_{DC} - P_{AC} - P_{chop} \tag{2.44}$$

The powers are defined as

$$V_{DC} I_{cap} = V_{DC} I_{DC} - \frac{3}{2}\left(V_{c_d} I_{f\,d} + V_{c_q} I_{f\,q}\right) - V_{DC} I_{chop} u_{chop} \tag{2.45}$$

I_{chop} can be substituted using Ohm's law

$$V_{DC} I_{cap} = V_{DC} I_{DC} - \frac{3}{2}\left(V_{c_d} I_{f\,d} + V_{c_q} I_{f\,q}\right) - \frac{V_{DC}^2}{R_{chop}} u_{chop} \tag{2.46}$$

Isolating I_{cap}

$$I_{cap} = I_{DC} - \frac{3}{2}\left(\frac{V_{c_d} I_{f\,d} + V_{c_q} I_{f\,q}}{V_{DC}}\right) - \frac{V_{DC}}{R_{chop}} u_{chop} \tag{2.47}$$

Dividing I_{cap} by C_{DC} yields the DC link voltage dynamics

$$\dot{V}_{DC} = \frac{I_{DC} - \frac{3}{2}\left(\frac{V_{c_d} I_{f\,d} + V_{c_q} I_{f\,q}}{V_{DC}}\right) - \frac{V_{DC}}{R_{chop}} u_{chop}}{C_{DC}} \tag{2.48}$$

where $0 \leq u_{chop} \leq 1$ is the duty cycle of an ideal switch in series with the chopper resistor. That is, when $u_{chop} = 0$ no current can flow in the chopper resistor, thus it does not affect the DC link voltage dynamics. When $u_{chop} > 0$ power is being dissipated in the resistor.

2.3.4 Grid voltage in dq frame

The grid is modelled as infinite bus, with fixed frequency, phase and voltage. Let a rotating reference frame be synchronized to the grid voltage. In this supposed frame, the grid voltage will be described by

$$V_{g_{dq}} = \begin{bmatrix} |V_g| \\ 0 \end{bmatrix} \tag{2.49}$$

where $|V_g|$ is the amplitude of the voltage signal in the time domain. However, in the reference frame synchronized to V_f, $V_{g_{dq}}$ will vary. This issue can be approached from a steady state perspective.

If the voltage V_f is known, and the voltage drop $I_t Z_t$ is known, the residual voltage V_g can be calculated as

$$V_{g_{dq}} = V_{f_{dq}} - I_{t_{dq}} Z_t \tag{2.50}$$

This is an accurate calculation of $V_{g_{dq}}$ but is it not sufficient from a modelling perspective. That is because it defines $V_{g_{dq}}$ as a function of converter circuitry, without considering the actual grid source. This is understood by letting $V_{f_{dq}}$ and $I_{t_{dq}}$ be 0 in equation 2.50. As a result, $V_{g_{dq}}$ would then be 0 as well, which is nonsensical.

One method to resolve this issue is to express only one of the dq components using 2.50. The other can then be solved using the trigonometric relation in the dq frame:

$$|V_g|^2 = V_{g_d}^2 + V_{g_q}^2 \tag{2.51}$$

The q component will be expressed as a function of the converter circuitry. Firstly, appendix B derives the differential equation describing the current I_t in the abc domain:

$$\dot{I}_t = V_{C_f} \frac{1}{L_t} + I_f \frac{R_{fs}}{L_t} + I_t \frac{-R_t - R_{fs}}{L_t} - V_g \frac{1}{L_t} \tag{2.52}$$

In the dq frame, the q component is affected by the d component as described in equation 2.17

$$\dot{I}_{t_q} = V_{C_{f_q}} \frac{1}{L_t} + I_{f_q} \frac{R_{fs}}{L_t} + I_{t_q} \frac{-R_t - R_{fs}}{L_t} - V_{g_q} \frac{1}{L_t} - 2\pi\omega_s I_{t_d} \tag{2.53}$$

In steady state, $\dot{I}_{t_q} = 0$ and $I_{t_q} = I_{f_q}$. Futhermore, the PLL drives $V_{C_{f_q}}$ to 0:

$$0 = 0\frac{1}{L_t} + I_{t_q} \frac{R_{fs}}{L_t} + I_{t_q} \frac{-R_t - R_{fs}}{L_t} - V_{g_q} \frac{1}{L_t} - 2\pi\omega_s I_{t_d} \tag{2.54}$$

Rearrange to isolate V_{g_q}

$$V_{g_q} \frac{1}{L_t} = I_{t_q} \frac{R_{fs}}{L_t} + I_{t_q} \frac{-R_t - R_{fs}}{L_t} - 2\pi\omega_s I_{t_d} \tag{2.55}$$

Multiply both sides by L_t

$$V_{g_q} = I_{t_q} R_{fs} + I_{t_q}(-R_t - R_{fs}) - 2\pi\omega_s L_t I_{t_d} \tag{2.56}$$

Remove parentheses

$$V_{g_q} = I_{t_q} R_{fs} \text{ - } I_{t_q} R_t \text{ - } I_{t_q} R_{fs} \text{ - } 2\pi\omega_s L_t I_{t_d} \tag{2.57}$$

Remove cancelling terms

$$V_{g_q} = \text{-} I_{t_q} R_t \text{ - } 2\pi\omega_s L_t I_{t_d} \tag{2.58}$$

The q component of V_g is now expressed as a function of the converter circuitry. Furthermore, V_{g_d} can be expressed using Pythagoras theorem:

$$|V_g|^2 = V_{g_d}^2 + V_{g_q}^2 \tag{2.59}$$

where $|V_g|$ is the amplitude of V_g. Assuming $|V_{g_d}| \gg |V_{g_q}|$ one can approximate that

$$|V_g|^2 \approx V_{g_d}^2 \tag{2.60}$$

which is rearranged as

$$V_{g_d} \approx |V_g| \tag{2.61}$$

The validity of the assumption $|V_{g_d}| \gg |V_{g_q}|$ must be analyzed. This is done by evaluation the maximum error introduced by the assumption under different grid conditions. The simplification error can be defined as

$$e = \frac{\hat{V}_{g_d} - V_{g_d}}{V_{g_d}} \tag{2.62}$$

where

$$\hat{V}_{g_d} = |V_g| \tag{2.63}$$

$$V_{g_d} = \sqrt{|V_g|^2 - \max\left(V_{g_q}\right)^2} \tag{2.64}$$

Equation 2.58 shows that V_{g_q} is a function of the grid impedance and the currents $I_{t_{dq}}$. The error increases with $I_{t_{dq}}$, so the error is evaluated at the maximum rated current. The error also increases with the grid impedance. Figure 2.8 plots the error as a function of the grid impedance.

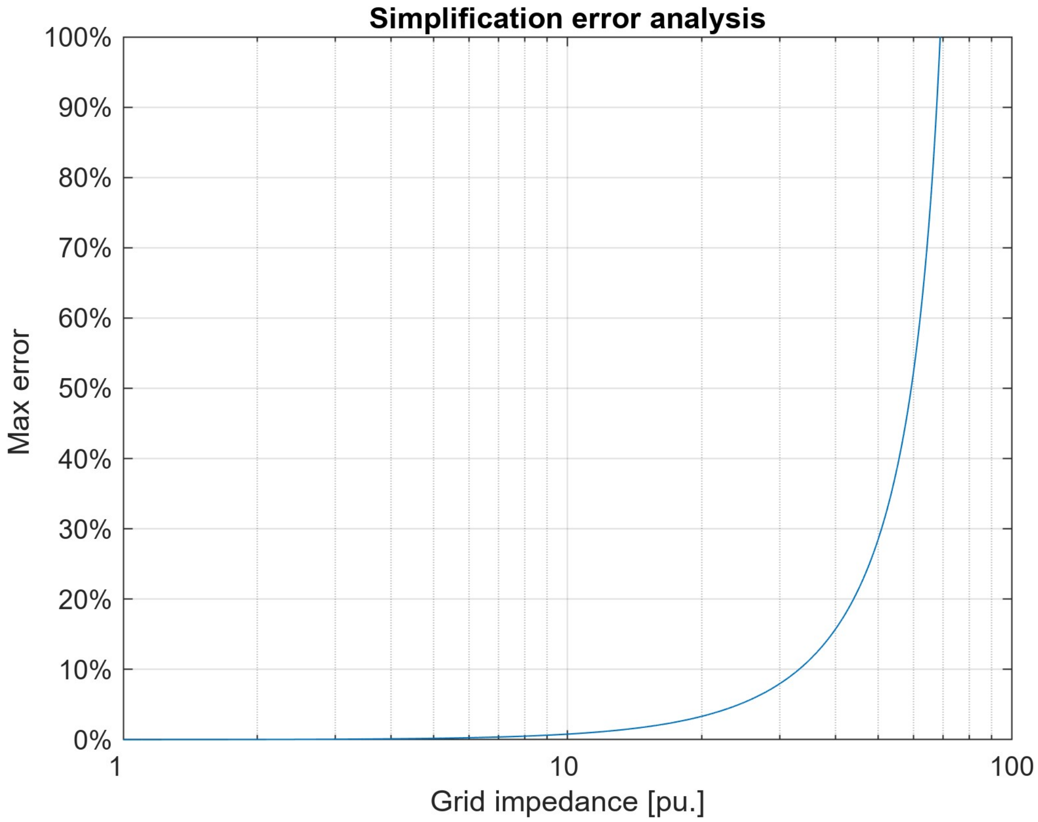

Figure 2.8: The error in V_{g_d} introduced when assuming $V_{g_d} \gg V_{g_q}$. The error is dependent on the current and the grid impedance. The current is at maximum value, and the grid impedance ($Z_g = R_t + j\omega L_t$) is swept from $Z_g = 1$pu. to $Z_g = 70$pu., where 1pu. is the nominal grid impedance. The test is conducted with the amplitude $|V_g| = 1$pu.

It is observed that at nominal grid impedance, the error is negligible at ≈0%. Even when the grid impedance is 35pu. the error is still only 10%. As such it is concluded that the simplification is valid for this case study. Going forward, the grid voltage will be defined as:

$$\begin{bmatrix} V_{g_d} \\ V_{g_q} \end{bmatrix} = \begin{bmatrix} |V_g| \\ -I_{t_q} R_t - 2\pi\omega_s L_t I_{t_d} \end{bmatrix} \tag{2.65}$$

2.3.5 Model outputs

In previous work the outputs of the model were the following measured signals:

$$y = \begin{bmatrix} I_{tdq} \\ V_{C_f dq} \\ V_{DC} \\ I_{DC} \\ P \\ Q \end{bmatrix} \tag{2.66}$$

The controlled outputs were

$$y_{con} = \begin{bmatrix} V_{DC} \\ P \\ Q \end{bmatrix} \tag{2.67}$$

The control structure in previous work used reference tracking and integral action to drive the controlled outputs to the desired values. However, in this case study the P and Q outputs will not be used. Rather, the controlled outputs will be the d and q components of the I_t current (as well the DC link voltage). These map directly into P and Q by

$$P = \frac{3}{2} V_{C_{fd}} I_{td} \tag{2.68}$$

$$Q = -\frac{3}{2} V_{C_{fd}} I_{tq} \tag{2.69}$$

$$\tag{2.70}$$

Thus the powers can still be controlled indirectly.

The motivation for controlling the currents rather than powers is twofold: Firstly, the powers are nonlinear. Thus, they must be linearized, which results in an increasing error when moving away from the operating point. This can be avoided by controlling the currents directly, since the currents dynamics are linear. Secondly, when operating during fault scenarios - such as grid voltage dips - the converter will be unable to deliver full power to the grid. Thus, it makes practical sense to control currents during faults, as the nonlinear power outputs will be far away from their linearization points during faults.

The power plant controller defines the reference signals for the converter. The reference signals are commonly a P and Q reference. These references can be translated to I_{tdq} references, by

$$I_{td} = \frac{P}{\frac{3}{2} V_{C_{fd}}} \tag{2.71}$$

$$I_{tq} = \frac{-Q}{\frac{3}{2} V_{C_{fd}}} \tag{2.72}$$

The proposed current control reference strategy is thus as follows. The system receives reference signals: expressed as P/Q power references. During **normal operation**, a math block translates these to current references, using the equations 2.71-2.72. The dq current references are passed to the controller.

During faults the external power references are ignored. The controllers fault system will generate optimal references, which depend on the type and severity of the fault. How these are generated is described later in the thesis.

2.4 Model summary

The chapter has documented the development of the desired model. The final discrete time linear state space model of this case study is given by

$$\begin{bmatrix} \Delta I_{f_d} \\ \Delta I_{f_q} \\ \Delta I_{td} \\ \Delta I_{tq} \\ \Delta V_{C_{fd}} \\ \Delta V_{DC} \\ \Delta I_{DC} \end{bmatrix}(k+1) = A_d \begin{bmatrix} \Delta I_{f_d} \\ \Delta I_{f_q} \\ \Delta I_{td} \\ \Delta I_{tq} \\ \Delta V_{C_{fd}} \\ \Delta V_{DC} \\ \Delta I_{DC} \end{bmatrix}(k) + B_d \begin{bmatrix} \Delta V_{cd} \\ \Delta V_{cq} \\ \Delta I_u \\ \Delta u_{chop} \end{bmatrix}(k) + E_d \begin{bmatrix} \Delta |V_g| \end{bmatrix}(k) \tag{2.73}$$

$$\begin{bmatrix} \Delta I_{td} \\ \Delta I_{tq} \\ \Delta V_{f_d} \\ \Delta V_{DC} \\ \Delta I_{DC} \end{bmatrix}(k) = C_d \begin{bmatrix} \Delta I_{f_d} \\ \Delta I_{f_q} \\ \Delta I_{td} \\ \Delta I_{tq} \\ \Delta V_{C_{fd}} \\ \Delta V_{DC} \\ \Delta I_{DC} \end{bmatrix}(k) \tag{2.74}$$

where

$$A_d = e^{AT_s} \tag{2.75}$$

$$B_d = A^{-1}(A_d - I)B \tag{2.76}$$

$$E_d = A^{-1}(A_d - I)E \tag{2.77}$$

$$C_d = C \tag{2.78}$$

T_s is the sample time, and the system matrices A, B, E and C are shown in equations 2.79 - 2.80.

The model is open loop unstable due to the dynamics of the DC link capacitor. This can be verified by inspection of the eigenvalues of A_d, but an intuitive explanation makes it obvious. The DC link voltage will increase if more power is supplied by the MSC than is consumed by the LSC. Otherwise, if the MSC supplies less power than the LSC consumes, the voltage will decrease. Only in the special case where the supply and consumption of active power exactly match, will the DC link voltage be constant. Achieving this singular matching point naturally requires feedback control.

It should further be noted that the inputs i_u and u_{chop} are not intended to be used at the same time. u_{chop} should be zero during normal operating. During grid low-voltage faults the i_u should remain constant, at whichever value it had before the fault occurs. Meanwhile u_{chop} should be increased so the chopper can dissipate the excess power from the machine side. This will be further discussed in the implementation and test chapters.

$$A = \begin{bmatrix} \frac{-R_f - R_{fs}}{L_f} & 2\pi\omega_s & \frac{R_{fs}}{L_f} & 0 & \frac{-1}{L_f} & 0 & 0 \\ -2\pi\omega_s & \frac{-R_f - R_{fs}}{L_f} & 0 & \frac{R_{fs}}{L_f} & 0 & 0 & 0 \\ \frac{R_{fs}}{L_t} & 0 & \frac{-R_t - R_{fs}}{L_t} & 2\pi\omega_s & \frac{1}{L_t} & 0 & 0 \\ 0 & \frac{R_{fs}}{L_t} & 0 & \frac{-R_{fs}}{L_t} & 0 & 0 & 0 \\ \frac{1}{C_f} & 0 & \frac{-1}{C_f} & 0 & 0 & 0 & 0 \\ \frac{-\frac{3}{2}V_{c_d}'}{C_{DC}V_{DC}'} & \frac{-\frac{3}{2}V_{c_q}'}{C_{DC}V_{DC}'} & 0 & 0 & 0 & \frac{\frac{3}{2}\left(I_{f_d}'V_{c_d}' + I_{f_q}'V_{c_q}'\right)}{C_{DC}V_{DC}'V_{DC}'} & \frac{1}{C_{DC}V_{DC}'} \\ 0 & 0 & 0 & 0 & 0 & 0 & -2\pi I_{DC_{bw}} \end{bmatrix} \tag{2.79}$$

$$B = \begin{bmatrix} \frac{1}{L_f} & 0 & 0 & 0 \\ 0 & \frac{1}{L_f} & 0 & 0 \\ 0 & 0 & 0 & 0 \\ 0 & 0 & 0 & 0 \\ 0 & 0 & 0 & 0 \\ \frac{-\frac{3}{2}I_{f_d}'}{C_{DC}V_{DC}'} & \frac{-\frac{3}{2}I_{f_q}'}{C_{DC}V_{DC}'} & 0 & \frac{-V_{DC}'}{R_{chop}C_{DC}} \\ 0 & 0 & 2\pi I_{DC_{bw}} & 0 \end{bmatrix} \quad E = \begin{bmatrix} 0 \\ 0 \\ \frac{-1}{L_t} \\ 0 \\ 0 \\ 0 \\ 0 \end{bmatrix} \quad C = \begin{bmatrix} 0 & 0 & 1 & 0 & 0 & 0 & 0 \\ 0 & 0 & 0 & 1 & 0 & 0 & 0 \\ R_{fs} & 0 & -R_{fs} & 0 & 1 & 0 & 0 \\ 0 & 0 & 0 & 0 & 0 & 1 & 0 \\ 0 & 0 & 0 & 0 & 0 & 0 & 1 \end{bmatrix} \tag{2.80}$$

Chapter 3

Controller design

3.1 Chapter objective

The objective of this chapter is to document the development of the model predictive control strategy for this thesis. The chapter will document how the control objective is formulated and how the problem is eventually reformulated as a quadratic constrained optimization problem. The outline below provides an overview of the various sections and their content.

3.1.1 Outline of the modelling chapter

Section 3.2 - MPC overview: This section presents the fundamental concepts of model predictive control. The cost function is presented and the concepts of horizons and tuning matrices are introduced.

Section 3.3 - Model augmentation: This section demonstrates how the state space model is augmented to include the outputs in the state vector. This facilitates zero steady state error during reference tracking.

Section 3.4 - Lifting: This section demonstrates how the augmented model is lifted. That is, expressing the trajectory of the future state vector as a function of the current state vector and a sequence of input signals.

Section 3.5 - Reformulation: This section demonstrates how the lifted cost function is reformulated in terms of a sequence of control signal changes. This results in a single quadratic minimization problem.

Section 3.6 - Constrained optimization problem: This section adds constraints to the optimization problem. It demonstrates how the constraints also can be expressed in terms of the sequence of control signal changes. This section concludes by expressing the MPC problem as a quadratic minimization problem with linear matrix inequality constraints.

Section 3.7 - MPC tuning This section present guidelines and considerations for tuning MPC control systems. It also documents the tuning in the controller of this thesis.

3.1.2 Nomenclature of control section

In the previous chapter the Δ symbol was used to show deviations from an operating point. However as all signals in the model are defined as deviations from an operating point due to the Taylor expansion, the Δ symbol is redundant and will thus be omitted. The motivation for this is, that we instead wish to use the Δ symbol to indicate changes in a signal between samples. That is:

$$\Delta x(k) = x(k) - x(k-1)$$

Furthermore, MPC uses future predictions abundantly. The standard notation of a prediction is

$$\hat{x}(k+i|k)$$

The circumflex ˆshows that the signal is a prediction, not a measurement. In this report the index "$|k$" will be omitted for the sake of clarity. It is implied that all future values are predictions made at index k.

3.2 MPC overview

Model Predictive Control is an advanced optimal control strategy. It is conceptually related to the classical LQ regulator, but it differs in some key points. While the LQ regulator seeks to minimize a cost function over an infinite horizons, the MPC controller considers two finite receding horizons. This is a major difference, as the infinite horizon of LQ regulator facilitates the calculation of a constant state feedback gain. With the receding horizons of MPC this is not possible. Instead, the MPC algorithm will predict the future outputs and optimize future control signals over two horizons.

The first horizon to discuss is the prediction horizon. This is the number of samples into the future the MPC controller predicts the behaviour of the system. A visualisation of this is provided in figure 3.1.

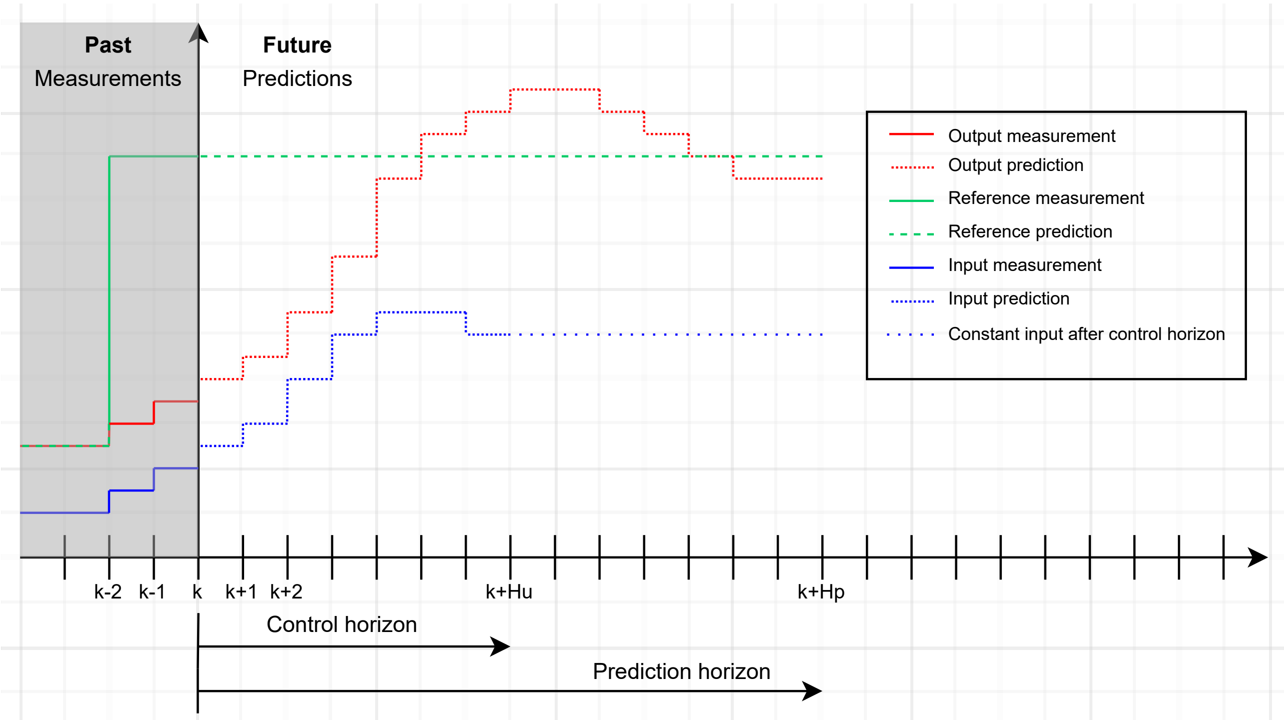

Figure 3.1: Model predictive controller prediction visualisation. At time k the controller predicts the optimal future input sequence, which will produce the optimal output trajectory. The input sequence has a length of H_u samples, while the output trajectory is H_p samples long. The controller drives the output error (output-reference) towards zero. The optimal performance is dictated by the cost function.

The future behaviour is dependent on 3 things: The current measurements of the system, the current reference signals and the future control signals. While measurements and references are inputs to the controller, the future control signals are the optimization variables of the MPC algorithm. Simply put the controller will calculate the sequence of future control signals which yields the optimal system performance.

The optimal performance is dependent on the cost function, which is being minimized. The standard MPC cost function is

$$\min_{\Delta u} \mathcal{J}(k) = \sum_{i=0}^{H_p} ||\hat{y}(k+i) - r(k+i)||_Q + \sum_{i=0}^{H_u} ||\Delta\hat{u}(k+i)||_R \tag{3.1}$$

where

$\|\|x\|\|_P = x^T P x$	Notation
$Q, R \geq 0$	Positive semi-definite weight matrices
$H_p \geq 1$	Prediction horizon
$H_u \leq H_p$	Control horizon

subject to the system dynamics given by

$$x(k+1) = Ax(k) + Bu(k) \tag{3.2}$$

$$y(k) = Cx(k) \tag{3.3}$$

This cost function penalizes the error between the output signals and the references, while minimizing the changes in control signals. The priorities between the signals are specified by the weight matrices Q and R. They are diagonal matrices, such that the designer intuitively can modify the desired closed loop response. Consider for example a system with 2 outputs, where an error in output 1 is much more critical than an error in output 2. Then the designer can specify a relatively large weight for the entry $Q_{1,1}$ and a relatively small weight for $Q_{2,2}$.

The cost function is formulated in terms of $\Delta\hat{u}(k)$ rather than absolute values of $\hat{u}(k)$. This implies that the absolute values of the control signals are irrelevant, as long as the output error is zero and the control signals are steady. It also implies that the control signal applied to the plant must be the sum of the previous signal and the newly calculated change in signal:

$$u(k) = \Delta\hat{u}(k) + u(k-1)$$

An important feature of the MPC controller is the capability of defining constraints for various signals. Specifically, the standard MPC formulation solves the optimization problem of equation 3.1 subject to the following constraints:

$$\begin{aligned} u_{Low} &\leq u \leq u_{Low} \\ \Delta u_{Low} &\leq \Delta u \leq \Delta u_{Low} \\ y_{Low} &\leq y \leq y_{Low} \end{aligned} \tag{3.4}$$

Under this formulation, one can constrain the range of both control signals and outputs, as well as the slewrate of the control signals.

Before investigating the MPC controller further, a describtion of the controller interfaces is provided below.

MPC interfaces

Figure 3.2 depicts the concepts of the internal structure of the MPC controller.

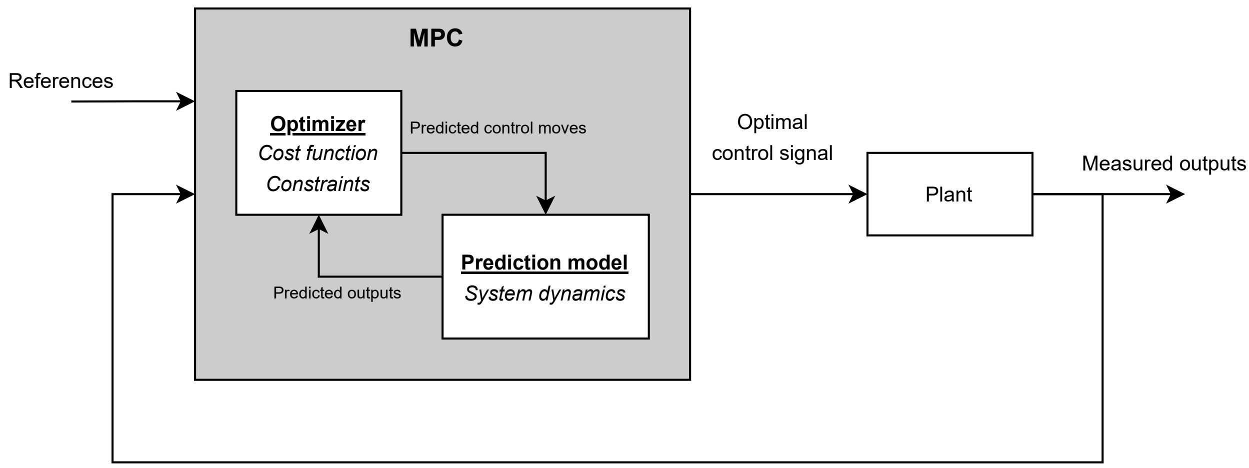

Figure 3.2: MPC internal structure concept. The figure highlights the iteratize process of optimizing control signals, then predicting the resulting system behavior. The graphics is inspired by art by Mathworks[8].

The inputs to the MPC controller are the measurements of the current plant outputs, and the reference signals. The internal model uses information about the system dynamics to predict the future output trajectory of the system.

The optimizer block predicts a sequence of control signals, which are passed to the prediction model. It then observes the resulting predicted outputs, and iterates the control sequence until a solution has been found: that is, a minimum of the cost function.

When the optimal control signal sequence has been found, the first sample of the sequence is set as the output of the MPC controller. Futhermore, since the control strategy is *incremental* (that is, it optimizes over *changes* in control signals), the control signal change must be added to the previous signal.

3.3 Model augmentation

As the MPC algorithm optimizes over the Δu sequence, it will prove beneficial to reformulate the system dynamics as a function of Δu. This can be done by first substituting the state vector for the incremental state vector as such:

$$x(k+1) = Ax(k) + Bu(k) \tag{3.5}$$
$$y(k) = Cx(k) \tag{3.6}$$

$$\Delta x(k+1) = A\Delta x(k) + B\Delta u(k) \tag{3.7}$$
$$\Delta y(k) = C\Delta x(k) \tag{3.8}$$

where $\Delta x(k+1) = x(k+1) - x(k)$. However the output should be expressed in absolute quantities rather than Δ values. One way to achieve this is by augmenting the state vector with the output vector. To do so, one must first describe the output dynamics.

$$y(k+1) = \Delta y(k+1) + y(k) \tag{3.9}$$
$$y(k+1) = C\Delta x(k+1) + y(k) \tag{3.10}$$
$$y(k+1) = C\left(A\Delta x(k) + B\Delta u(k)\right) + y(k) \tag{3.11}$$
$$y(k+1) = CA\Delta x(k) + CB\Delta u(k) + y(k) \tag{3.12}$$

The augmented system can then be constructed as such

$$\begin{bmatrix} \Delta x(k+1) \\ y(k+1) \end{bmatrix} = \begin{bmatrix} A & 0 \\ CA & I \end{bmatrix} \begin{bmatrix} \Delta x(k) \\ y(k) \end{bmatrix} + \begin{bmatrix} B \\ CB \end{bmatrix} \Delta u(k) \tag{3.13}$$
$$y(k) = \begin{bmatrix} 0 & I \end{bmatrix} \begin{bmatrix} \Delta x(k) \\ y(k) \end{bmatrix} \tag{3.14}$$

The system dynamics are now expressed as a function of control signal changes. Another feature of the augmented system is the inclusion of the output directly in the state vector. This will facilitate zero steady state error, which will be demonstrated later in the thesis.

The following sections uses the augmented state space model.

3.4 Lifting

Since the cost function in eq. 3.1 is a quadratic sum of future predictions, it is beneficial to reformulate the system dynamics to include the future behavior. This is done using a technique known as lifting. The technique involves defining the vector of future predicted states as a function of the current state vector and the sequence of input signal changes. This is written as such

$$\mathcal{X}(k) = \mathcal{A}\hat{x}(k) + \mathcal{B}\Delta\mathcal{U}(k) \tag{3.15}$$

where

$$\mathcal{X}(k) = \begin{bmatrix} \hat{x}(k+1) \\ \vdots \\ \hat{x}(k+H_p) \end{bmatrix} \tag{3.16}$$

$$\Delta\mathcal{U}(k) = \begin{bmatrix} \Delta\hat{u}(k) \\ \vdots \\ \Delta\hat{u}(k+H_u-1) \end{bmatrix} \tag{3.17}$$

Deriving the lifted state matrices $\mathcal{A}$, $\mathcal{B}_u$ and $\mathcal{B}_{\Delta u}$ is no simple process. Appendix C demonstrates how the method is applied on a small system. The matrices for the general case with arbitrary prediction- and control horizons are:

$$\mathcal{A} = \begin{bmatrix} A \\ \vdots \\ A^{H_p} \end{bmatrix} \tag{3.18}$$

$$\mathcal{B} = \begin{bmatrix} B & 0 & \dots & 0 \\ B + AB & B & \ddots & 0 \\ \vdots & \ddots & \ddots & 0 \\ \sum_{i=0}^{H_p-1} A^i B & \dots & \dots & \sum_{i=0}^{H_p-H_u} A^i B \end{bmatrix} \tag{3.19}$$

The output equation must also be lifted. Given that $\hat{y}(k) = C\hat{x}(k)$ it is inferred that

$$\begin{bmatrix} \hat{y}(k) \\ \vdots \\ \hat{y}(k+H_p) \end{bmatrix} = \begin{bmatrix} C & & 0 \\ & \ddots & \\ 0 & & C \end{bmatrix} \begin{bmatrix} \hat{x}(k) \\ \vdots \\ \hat{x}(k+H_p) \end{bmatrix} \tag{3.20}$$

which is denoted in the compact form

$$\mathcal{Y}(k) = \mathcal{C}\mathcal{X} \tag{3.21}$$

Substituting equation 3.15 into 3.21 reveals the lifted output vector.

$$\mathcal{Y}(k) = \mathcal{C}\left(\mathcal{A}\hat{x}(k) + \mathcal{B}\Delta\mathcal{U}(k)\right) \tag{3.22}$$

For convenience the following notation is adopted

$$\mathcal{Y}(k) = \psi\hat{x}(k) + \Theta\Delta\mathcal{U}(k) \tag{3.23}$$

where

$$\psi = \mathcal{C}\mathcal{A}, \qquad \Theta = \mathcal{C}\mathcal{B}_{\Delta u}$$

Furthermore, the lifted reference vector is constructed as

$$\mathcal{T}(k) = \begin{bmatrix} r(k) \\ \vdots \\ r(k+H_p) \end{bmatrix} \tag{3.24}$$

and the Q and R matrices can be lifted as

$$\mathcal{Q}(k) = \begin{bmatrix} Q(k) & & 0 \\ & \ddots & \\ 0 & & Q(k+H_p) \end{bmatrix}, \quad \mathcal{R}(k) = \begin{bmatrix} R(k) & & 0 \\ & \ddots & \\ 0 & & R(k+H_u-1) \end{bmatrix} \tag{3.25}$$

3.5 Reformulation

The cost function can now be reformulated

$$\mathcal{J}(k) = \sum_{i=1}^{H_p} ||\hat{y}(k) - r(k)||_Q + \sum_{i=1}^{H_u} ||\Delta\hat{u}(k)||_R \tag{3.26}$$

$$\mathcal{J}(k) = ||\mathcal{Y}(k) - \mathcal{T}(k)||_{\mathcal{Q}} + ||\Delta\mathcal{U}(k)||_{\mathcal{R}} \tag{3.27}$$

The cost can be written as a quadratic function in $\Delta\mathcal{U}(k)$. For convenience constant terms with respect to $\Delta\mathcal{U}(k)$ will be colored blue. First, expand the terms of the cost function.

$$\mathcal{J}(k) = \mathcal{Y}(k)^T\mathcal{Q}\mathcal{Y}(k) - \mathcal{Y}(k)^T\mathcal{Q}\mathcal{T}(k) - \mathcal{T}(k)^T\mathcal{Q}\mathcal{Y}(k) + \mathcal{T}(k)^T\mathcal{Q}\mathcal{T}(k) + \Delta\mathcal{U}(k)^T\mathcal{R}\Delta\mathcal{U}(k) \tag{3.28}$$

The second and third term can be combined. For further use, each term is labeled with a number, as such:

$$\mathcal{J}(k) = \underbrace{\mathcal{Y}(k)^T\mathcal{Q}\mathcal{Y}(k)}_{1} - \underbrace{2\mathcal{Y}(k)^T\mathcal{Q}\mathcal{T}(k)}_{2} + \underbrace{\mathcal{T}(k)^T\mathcal{Q}\mathcal{T}(k)}_{3} + \underbrace{\Delta\mathcal{U}(k)^T\mathcal{R}\Delta\mathcal{U}(k)}_{4} \tag{3.29}$$

Recall the definition of $\mathcal{Y}$, and group the constant terms as $\mathcal{K}$:

$$\begin{aligned} \mathcal{Y} &= \psi\hat{x}(k) + \Theta\Delta\mathcal{U}(k) \\ &= \mathcal{K} + \Theta\Delta\mathcal{U}(k) \end{aligned} \tag{3.30}$$

Substituting equation 3.30 into the first and second term of equation 3.29 yields:

Term 1:

$$\begin{aligned}
&\mathcal{Y}(k)^T \mathcal{Q} \mathcal{Y}(k) \\
&= (\mathcal{K} + \Theta \Delta \mathcal{U}(k))^T \mathcal{Q} (\mathcal{K} + \Theta \Delta \mathcal{U}(k)) \\
&= (\mathcal{K}^T + \Delta \mathcal{U}(k)^T \Theta^T) \mathcal{Q} (\mathcal{K} + \Theta \Delta \mathcal{U}(k)) \\
&= \mathcal{K}^T \mathcal{Q} \mathcal{K} + \Delta \mathcal{U}(k)^T \Theta^T \mathcal{Q} \Theta \Delta \mathcal{U}(k) + \Delta \mathcal{U}(k)^T 2 \Theta^T \mathcal{Q} \mathcal{K}
\end{aligned} \tag{3.31}$$

Term 2:

$$\begin{aligned}
&-2\mathcal{Y}(k)^T \mathcal{Q} \mathcal{T}(k) \\
&= -2(\mathcal{K} + \Theta \Delta \mathcal{U}(k))^T \mathcal{Q} \mathcal{T}(k) \\
&= -2(\mathcal{K}^T + \Delta \mathcal{U}(k)^T \Theta^T) \mathcal{Q} \mathcal{T}(k) \\
&= -\Delta \mathcal{U}(k)^T 2 \Theta^T \mathcal{Q} \mathcal{T} - 2\mathcal{K}^T \Theta^T \mathcal{T}
\end{aligned} \tag{3.32}$$

All constant terms are combined in const. As such, the cost can be rewritten as

$$\mathcal{J}(k) = \Delta \mathcal{U}(k)^T \left(\Theta^T \mathcal{Q} \Theta + \mathcal{R} \right) \Delta \mathcal{U}(k) + \Delta \mathcal{U}(k)^T 2 \Theta^T \mathcal{Q} (\mathcal{K} - \mathcal{T}) + \mathrm{const} \tag{3.33}$$

or compactly as

$$\mathcal{J}(k) = \Delta \mathcal{U}(k)^T \mathcal{H} \Delta \mathcal{U}(k) - \Delta \mathcal{U}(k)^T \mathcal{G} + \mathrm{const} \tag{3.34}$$

where

$$\mathcal{H} = \Theta^T \mathcal{Q} \Theta + \mathcal{R} \tag{3.35}$$

$$\mathcal{G} = -2\Theta^T \mathcal{Q} (\mathcal{K} - \mathcal{T}) \tag{3.36}$$

The cost function is now a quadratic function in $\Delta \mathcal{U}(k)$. Minimizing $\mathcal{J}(k)$ over $\Delta \mathcal{U}(k)$ is now a trivial task, as the quadratic function is convex. The minimum of $\mathcal{J}(k)$ is found by setting the gradient to 0

$$0 = \nabla_{\Delta \mathcal{U}(k)} \mathcal{J}(k) = 2\mathcal{H} \Delta \mathcal{U}(k) - \mathcal{G} \tag{3.37}$$

The optimal control action sequence $\Delta \mathcal{U}(k)_{opt}$ is thus

$$\Delta \mathcal{U}_{opt}(k) = \frac{1}{2} \mathcal{G} \mathcal{H}^{-1} \tag{3.38}$$

The optimal control action at time k is the first entry in $\Delta \mathcal{U}(k)_{opt}$:

$$\Delta \hat{u}_{opt}(k) = \begin{bmatrix} I & 0 & \dots & 0 \end{bmatrix} \Delta \mathcal{U}_{opt}(k) \tag{3.39}$$

However, the control action is incremental, so the actual signal which should be applied is

$$\hat{u}_{opt}(k) = \Delta \hat{u}_{opt}(k) + u(k-1) \tag{3.40}$$

3.6 Constrained optimization problem

In practical applications, the dynamics of the controlled system are commonly constrained. Examples of constraints are limitations on the actuator signal range, or limitations of the slew rate of the actuator signals. For instance, a duty cycle cannot exceed 100%, or the system may not respond linearly to large steps in the duty cycle. Another common constraint is the limitations of the controlled output signals.

The constraints on the system are formulated as linear matrix inequalities (LMIs). For the three types of constraints described above, let the LMIs be defined as

Actuation slew rate constraint:

$$\mathcal{E}\begin{bmatrix}\Delta\mathcal{U}(k)\\1\end{bmatrix} \leq 0, \qquad \Delta\mathcal{U}(k) = \begin{bmatrix}\Delta\hat{u}(k)\\ \vdots \\ \Delta\hat{u}(k+H_u-1)\end{bmatrix} \tag{3.41}$$

Actuation range constraint:

$$\mathcal{F}\begin{bmatrix}\mathcal{U}(k)\\1\end{bmatrix} \leq 0, \qquad \mathcal{U}(k) = \begin{bmatrix}\hat{u}(k)\\ \vdots \\ \hat{u}(k+H_u-1)\end{bmatrix} \tag{3.42}$$

Output range constraint:

$$\mathcal{G}\begin{bmatrix}\mathcal{Y}(k)\\1\end{bmatrix} \leq 0, \qquad \mathcal{Y}(k) = \begin{bmatrix}\hat{y}(k)\\ \vdots \\ \hat{y}(k+H_p)\end{bmatrix} \tag{3.43}$$

An example of how the matrices $\mathcal{E}$, $\mathcal{F}$ and $\mathcal{G}$ are constructed from the constraints, is provided in Appendix D.

As the optimization problem is concerned with minimizing the cost function over $\Delta\mathcal{U}(k)$, it is beneficial to reformulate the constraints in terms of $\Delta\mathcal{U}(k)$ as well. That is, a stacked LMI containing the three constraint types, all with respect to $\Delta\mathcal{U}(k)$:

$$\mathcal{M}\Delta\mathcal{U}(k) \leq \mathcal{N}$$

Each LMI can be rewritten in terms of $\Delta\mathcal{U}(k)$. First, the constraint of the actuator slew rate:

$$\mathcal{E}\begin{bmatrix}\Delta\mathcal{U}(k)\\1\end{bmatrix} \leq 0 \tag{3.44}$$

The constraint matrix $\mathcal{E}$ can be rewritten as

$$\mathcal{E} = \begin{bmatrix} W & \text{-}w \end{bmatrix} \tag{3.45}$$

which is used to reformulate the LMI as

$$\boxed{W\Delta\mathcal{U}(k) \leq w} \tag{3.46}$$

The input range constraint can be reformulated as well:

$$\mathcal{F}\begin{bmatrix} \mathcal{U}(k) \\ 1 \end{bmatrix} \leq 0 \tag{3.47}$$

The constraint matrix $\mathcal{F}$ can be rewritten as

$$\mathcal{F} = \begin{bmatrix} F_1 & F_2 & \cdots & F_{H_u} & f \end{bmatrix} \tag{3.48}$$

Which leads to the interpretation that

$$\begin{bmatrix} F_1 & F_2 & \cdots & F_{H_u} & f \end{bmatrix}\begin{bmatrix} \mathcal{U}(k) \\ 1 \end{bmatrix} = \sum_{i=1}^{H_u} F_i\hat{u}(k+i-1) + f \leq 0 \tag{3.49}$$

which can be expressed in terms of $\Delta\hat{u}(k)$ as

$$\sum_{j=1}^{H_u}\sum_{i=1}^{H_u} F_i\Delta\hat{u}(k+j-1) + \sum_{j=1}^{H_u} F_j u(k-1) + f \leq 0 \tag{3.50}$$

This can be written compactly as

$$\boxed{\mathbf{F}\Delta\mathcal{U}(k) \leq -\mathbf{F_1}u(k-1) - f} \tag{3.51}$$

where

$$\mathbf{F} = \begin{bmatrix} \mathbf{F_1} & \mathbf{F_2} & \cdots & \mathbf{F_{H_u}} \end{bmatrix} \tag{3.52}$$

and

$$\mathbf{F_j} = \sum_{i=j}^{H_u} F_i \tag{3.53}$$

The output range constraint can be reformulated as well:

$$\mathcal{G}\begin{bmatrix} \mathcal{Y}(k) \\ 1 \end{bmatrix} \leq 0 \tag{3.54}$$

$\mathcal{Y}$ can be substituted by equation 3.23 to show

$$\mathcal{G}\begin{bmatrix} \psi\hat{x}(k) + \Theta\Delta\mathcal{U}(k) \\ 1 \end{bmatrix} \leq 0 \tag{3.55}$$

$\mathcal{G}$ can be rewritten as $\begin{bmatrix}\Gamma & g\end{bmatrix}$:

$$\begin{bmatrix}\Gamma & g\end{bmatrix}\begin{bmatrix}\psi\hat{x}(k)+\Theta\Delta\mathcal{U}(k)\\ 1\end{bmatrix}\leq 0 \tag{3.56}$$

The matrices are multiplied to yield

$$\Gamma\left(\psi\hat{x}(k)+\Theta\Delta\mathcal{U}(k)\right)+g\leq 0 \tag{3.57}$$

which can be rearranged as an LMI in $\Delta\mathcal{U}(k)$:

$$\boxed{\Gamma\Theta\Delta\mathcal{U}(k)\leq -\Gamma\psi\hat{x}(k)-g} \tag{3.58}$$

Combining the three constraints yields the final stacked LMI:

$$\begin{bmatrix}\mathbf{F}\\ \Gamma\Theta\\ W\end{bmatrix}\Delta\mathcal{U}(k)\leq\begin{bmatrix}-\mathbf{F_1}u(k-1)-f\\ -\Gamma\psi\hat{x}(k)-g\\ w\end{bmatrix} \tag{3.59}$$

The constrained MPC problem is thus a quadratic minimization problem with LMI constraints:

$$\min_{\Delta\mathcal{U}(k)}\mathcal{J}(k)=\Delta\mathcal{U}(k)^T\mathcal{H}\Delta\mathcal{U}(k)-\Delta\mathcal{U}(k)^T\mathcal{G} \tag{3.60}$$

subject to

$$\begin{bmatrix}\mathbf{F}\\ \Gamma\Theta\\ W\end{bmatrix}\Delta\mathcal{U}(k)\leq\begin{bmatrix}-\mathbf{F_1}u(k-1)-f\\ -\Gamma\psi\hat{x}(k)-g\\ w\end{bmatrix} \tag{3.61}$$

The optimal control signal which should be applied at time k is

$$\hat{u}_{opt}(k)=\begin{bmatrix}I & 0 & \dots & 0\end{bmatrix}\Delta\mathcal{U}_{opt}(k)+u(k-1) \tag{3.62}$$

3.7 MPC tuning

Tuning MPC is an iterative process, like all other control strategies. However, some guidelines exist that can provide reasonable starting points[1]. This section presents some of these guidelines, and presents the final tuning parameters used for the MPC algorithm in this thesis. Tuning the MPC controller can be divided into three sections: The horizons, the cost function weights and the constraints.

MPC horizons

The prediction and control horizons are commonly chosen first and are changed the least during the tuning process. The following considerations should be made when choosing the prediction horizon:

- The horizon should be long enough as to cover the majority of the desired closed loop dynamics. If the desired settling time of the system is 10ms, the horizon should not be significantly less than 10ms. Increasing the horizon beyond this points yields little improvent to performance.
- If the sample time is low, caution should be taken. Predicting many samples ("many" depends on the application) into future, becomes extremely computationally difficult, even for simple prediction models.
- If the open loop dynamics are unstable, the prediction horizon should not be too long. Predictions well into the future will be inaccurate due to the ill conditioned nature of open loop instability.
- In general, increasing the prediction horizon yields more stable controllers, at the cost of computational effort and potentially inaccurate predictions.

The following considerations should be made when choosing the control horizon:

- Increasing the control horizon increases the aggresiveness of the controller, and increases the controllers ability to stabilize unstable plants[1].
- Decreasing the control horizon increases the controller robustness.
- The control horizon is strongly coupled to the computational cost of the algorithm, as H_u dictates the amount of variables the algorithm must optimize over.

The following horizons are used in this thesis. The prediction horizon is shorter than the expected system dynamics, due to the low sample rate and unstable model.

Horizon	Length [samples]	Length [Time]
H_p - Prediction	50	6.25ms
H_u - Control	30	3.75ms

Cost function weights

An optimal starting point for the in- and output weights is Bryson's rule[5]. The rule states that a weight for a given variable should be chosen inversely proportional to the maximum acceptable value of the variable. Consider an arbitrary state x_1, with the maximum acceptable value of $\max(x_1)$. Then associated weight should then be

$$Q_{1,1} = \frac{1}{\max(x_1)^2}$$

Using this method effectively scales the cost function. Recalling that the cost function is quadratic sum of the states and weights, the contribution from x_1 will be

$$x_1 \left(Q_{1,1}\right) x_1 = x_1^2 Q_{1,1} = \frac{x_1^2}{\max(x_1)^2}$$

If this method is used on all states and inputs, the maximum contribution from any variable to the total cost will be 1. This is beneficial for variables with different units, that result in numerical values very different from each other.

Bryson's rule has been used as a starting point for tuning, but the final weights are a result of a trial-and-error process.

Signal	Function	Matrix entry	Weight
V_{DC}	Output	$Q_{1,1}$	40
I_{f_d}	Output	$Q_{2,2}$	100
I_{f_q}	Output	$Q_{3,3}$	2
V_{c_d}	Input	$R_{1,1}$	40000
V_{c_q}	Input	$R_{2,2}$	40000
I_u	Input	$R_{3,3}$	100
u_{chop}	Input	$R_{4,4}$	100

Constraints

The choice of constraints is more tied to the physical system than the other parameters. The constraints on the output signals are derived from the limits of the physical components. Most electrical components have specified operating regions in which they operate optimally and degrade the least.

Constraints on the input ranges are a result of the physical capabilities of the actuators. A prime example is the chopper, which is driven by a PWM signal, which can natually only have a dutycyle between 0% and 100%.

Signal	**Function**	**Lower limit**	**Upper limit**
V_{DC}	Output	0.95 pu	1.05 pu
I_{f_d}	Output	-0.15 pu	1.25 pu
I_{f_q}	Output	-0.15 pu	1.25 pu
V_{c_d}	Input	-0.1 pu	1.10 pu
V_{c_q}	Input	-0.1 pu	1.10 pu
I_u	Input	-0.15 pu	1.15 pu
u_{chop}	Input	0 pu	1 pu

3.8 MPC summary

The chapter has documented how the rather complex MPC formulation can be reduced to a common quadratic optimization problem with LMI constraints. The optimization problem is constructed from the prediction model, the horizons, the cost function weights and the constraints. Solving the MPC problem is equivalent to solving the following optimization problem:

$$\min_{\Delta\mathcal{U}(k)} \mathcal{J}(k) = \Delta\mathcal{U}(k)^T \mathcal{H} \Delta\mathcal{U}(k) - \Delta\mathcal{U}(k)^T \mathcal{G} \tag{3.63}$$

subject to

$$\begin{bmatrix} \mathbf{F} \\ \Gamma\Theta \\ W \end{bmatrix} \Delta\mathcal{U}(k) \leq \begin{bmatrix} -\mathbf{F_1} u(k-1) - f \\ -\Gamma\psi\hat{x}(k) - g \\ w \end{bmatrix} \tag{3.64}$$

The optimal control signal which should be applied at time k is

$$\hat{u}_{opt}(k) = \begin{bmatrix} I & 0 & \dots & 0 \end{bmatrix} \Delta\mathcal{U}_{opt}(k) + u(k-1) \tag{3.65}$$

Chapter 4

Implementation

4.1 Implementation of MPC

The optimization problem must be solved at each sample time. This a is computationally demanding task, as the matrices in the problem formulation can be very large, depending on the horizons chosen. Due to computational complexity, the solving algorithm should be chosen to suit the problem type: that is, a solver that has been developed specifically for the quadratic convex optimization problem with LMI constraints.

4.1.1 OSQP

One such solver is OSQP[12], which is being used in this thesis. The algorithm is developed to solve problems on the form

$$\begin{aligned} \min_{x} \quad & \frac{1}{2} x^T H x + g^T x \\ \text{subject to} \quad & l \leq Ax \leq u \end{aligned}$$

where H must be a positive semidefinite matrix - that is, the problem must be convex. This is the structure of the MPC optimization problem. Some of the features of OSQP are listed below.

Efficiency:

OSQP uses a method of optimization called ADMM[1], which requires only one matrix factorization to setup the problem. This is beneficial as factorization, especially on large matrices, is a very demanding task. OSQP also utilizes the sparsity patterns of the matrices, to reduce the amount of calculations requires at each sample. Essentially the matrices are only initilized once, and the numerical values are updates as needed at each sample.

[1] Alternating Direction Method of Multipliers

Reliability:

OSQP detects if the problem is infeasible online and raises a flag. Thus no erroneous control signal is used, as a result of an undetected infeasibility issue. Furthermore, the solver can use a warm-start procedure, which makes the optimization fast and robust during transients, and significantly fast during steady state.

Interfacing:

OSQP features relatively easy interfacing to MATLAB, as well as programming languages such as Python, Julia and C. OSQP can also be made to interface with Simulink, albeit not as easily as the other. In this thesis MPC will be tested on a high fidelity simulation of a wind turbine. This requires the algorithm to be implemented as C code. The actual implementation will be shown shortly.

4.1.2 Implementation in Simulink

OSQP can be used directly in Matlab without auxilary software. However, it can be a tedious process to simultaneously learn the OSQP syntax and verify the MPC functionality. Because of this, for the Simulink implementation an auxilary software, CasADI, was used. CasADi[2] is a software framework, which can be used to define and solve nonlinear optimization problems using a high level syntax. It also features easy integration with external solving algorithms, such as OSQP.

CasADI works as a intuitive bridge when going from the the high level notation of optimization problems and Matlab to the low level syntax of the solver OSQP. It features a Matlab class of helper functions called Opti, which makes defining the optimization problem very simple.

```
% Initialize workspace
opti    = casadi.Opti();             % Initialize Opti object

u       = opti.variable(3*Hu,1);     % Optimization variable
x       = opti.parameter(7,1);       % State vector
ref     = opti.parameter(3,1);       % Reference vector
y       = opti.parameter(3,1);       % Output vector
u_prev  = opti.parameter(3,1);       % Previous input vector

% Calculate linear cost
T       = repmat(ref,Hp,1);          % Repeat reference over Hp
E       = T - Psi * [x ; y];         % Calculate "Free response" E
G       = 2 * Theta' * Q_mpc * E;    % Calculate linear cost G

% Setup optimization objective
opti.minimize( -u'*G + u'*H*u )      % Define objective function

```

```
% Setup constraints
opti.subject_to( gamma*Theta*u <= -gamma*(Psi*[x;y]) - g );
opti.subject_to(            F*u <= -F1*u_prev - f );

% Setup solver
opts = struct;                           % Options struct
opts.qpsol = 'osqp';                     % Solver method is OSQP
opti.solver('sqpmethod',opts);           % Solver wrapper is sqpmethod

% Setup mapping function
f = opti.to_function('f',{x y ref u_prev},{u(1:3)});
```

At this point, the object 'opti' contains the optimization problem and solver specifications. It is defined symbolically, as the parameters are used to define the linear cost and the constraints.

The function 'f' is a CasADI function built from 'opti'. It takes as inputs the values of the parameters x, y, ref and u_{prev} and returns the optimal solution u. Notice that only the first 3 elements of u are returned. The function 'f' can be called directly in Matlab to solve the optimization problem. However, to execute it in Simulink a mex file must be constructed. A mex file is a compiled Matlab function, which is called like a C or C++ routine. It can be constructed with the following script, which is written by CasADI.

```
file_name = 'f.casadi';
f.save(file_name);

lib_path = GlobalOptions.getCasadiPath();
inc_path = GlobalOptions.getCasadiIncludePath();
mex('-v',['-I' inc_path],['-L' lib_path],'-lcasadi', 'casadi_fun.c')
```

The generated mex file can be executed in an S-Function in Simulink.

4.1.3 Implementation as C code

The MPC algorithm must now be written in C code, to be excuted on the Plecs simulation model. Plecs has a C-script block, which executes c code during runtime. The C-script block uses predefined function calls in which the user must write their code. A flowchart of these function calls is depicted in figure 4.1.

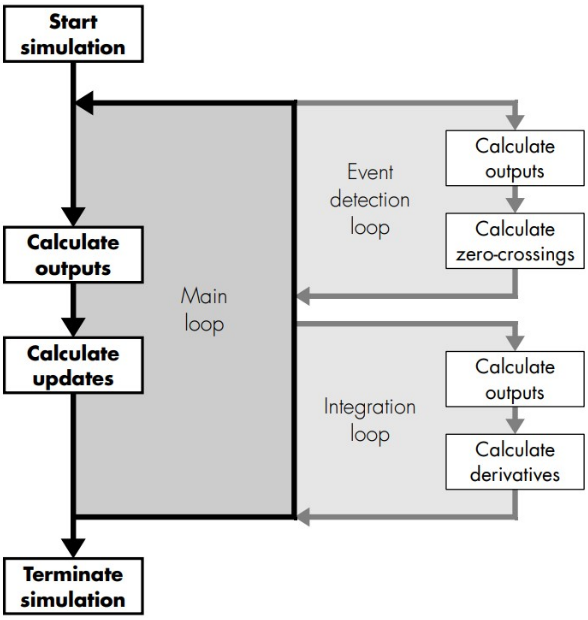

Figure 4.1: Plecs C-script block flowchart. The graphic is made by Plexim, for their Plecs C-Scipt tutorial.[9]

Not all functions need to be used. The following functions are used for the MPC algorithm:

Code declarations. Although not depicted in the diagram, this section can be used to declare global variables and functions. Global variables include constant matrices of the MPC problem, such as the quadratic cost H.

Start simulation is called only once during initialization of simulation. This function is used to initialize variables.

Calculate outputs is called repeatedly with a fixed sample time during simulation. The rate is defined by the user. This function should contain the implementation of the MPC controller. During each call to the function the system outputs and references are measured, and the optimal control signal is calculated. The control signal is passed as an output of the C-script block.

Terminate simulation is called at the end of simulation. A clean-up routine should be written in this function.

Besides these function structures, the C-script block also features macro function used to read inputs and parameters, and to set outputs.

Start simulation

```
// Exitflag
c_int exitflag = 0;

// Workspace structures
OSQPWorkspace *work;
OSQPSettings  *settings = (OSQPSettings *)c_malloc(sizeof(OSQPSettings));
OSQPData      *data     = (OSQPData *)c_malloc(sizeof(OSQPData));

// Initialize problem data
if (data) {
    data->n = n;
    data->m = m;
    data->P = csc_matrix(data->n, data->n, P_nnz, P_x, P_i, P_p);
    data->q = q;
    data->A = csc_matrix(data->m, data->n, A_nnz, A_x, A_i, A_p);
    data->l = l;
    data->u = u;
}

// Define solver settings as default
if (settings) {
    osqp_set_default_settings(settings);
    settings->alpha = 1.0; // Change alpha parameter to 1
}

// Setup workspace
exitflag = osqp_setup(&work, data, settings);
```

Update outputs

```
// -------------- Load measurements ----------------------------------------------
// Load previous input vector
for (int i = 0; i < len_u ; i++){
 uprev[i] = InputSignal(2,i);
}

// Load augmented state vector
for (int i = 0; i < len_xAug ; i++){
 x_aug[i] = InputSignal(1,i);
}

// Load reference vector
for (int i = 0; i < Hp ; i++){
 ref[3*i]   = InputSignal(0,0);
 ref[3*i+1] = InputSignal(0,1);
 ref[3*i+2] = InputSignal(0,2);
}

// -------------- Setup and solve MPC problem ------------------------------------
// Calculate new MPC matrices
MPC_calc(q_new, l_new, u_new, uprev, x_aug, ref);

// Update problem vectors
osqp_update_lin_cost(work, q_new);
osqp_update_bounds(work, l_new, u_new);

// Update problem matrices
osqp_update_P(work, P_x_new, OSQP_NULL, 3);
osqp_update_A(work, A_x_new, OSQP_NULL, 4);

// Solve Problem
osqp_solve(work);

// -------------- Output problem solution ----------------------------------------
for (int i = 0; i < len_u ; i++){
 OutputSignal(0,i) = work -> solution -> x[i];
}
```

Terminate simulation

```
    osqp_cleanup(work);
    if (data) {
        if (data->A) c_free(data->A);
        if (data->P) c_free(data->P);
        c_free(data);
    }
    if (settings) c_free(settings);

    return exitflag;
```

4.1.4 Code run-time

Solving control oriented optimization problems can be computationally heavy especially during dynamic events. The thesis has not considered to computational limitations of a practical implementations. The c code will be executed in a simulation, which has no limit on the per-sample run time of the code.

If the code was to be executed on a real-time platfrom, it should be ensured that the code is executed faster than the sample time, so a new control signal is already. Furthermore, backup strategies should be implemented to handle situations where the time limit is not met.

4.1.5 Implementation of FRT capability

As briefly mentioned in section 2.3.3, the chopper resistor should only be used during faults. Furthermore, during faults the DC link current should not be changed. This leads to the following control scheme:

During normal operation:	**During grid fault:**
I_u =variable	I_u =const.
$u_{chop} = 0$	u_{chop} =variable

The constant value of I_u during faults is whatever value it had before the fault began.

This dual structure has been made by setting up to optimization problems in the C code. For clarity only one is seen in the above code examples. The first optimization problem is used during normal operation. The matrices constituting this problem have been built from a modified version of the system matrices, where the u_{chop} input in the B matrix has been manually set to 0. This ensures that the controller will not change u_{chop} as it "does not know" that u_{chop} can alter the system.

The second optimization problem is made using the concept and is intended for use during faults. In it, the I_u input set to 0. As such it will use the chopper resistor and leave I_u unaltered.

It should be noted that in theory this could be implemented using constraints. However in practice it was discovered that this caused steady state errors and very long computation times. It was deemed much more efficient and accurate to (simply put) not the controller know that the other input existed.

During real life operation it is impossible to know when a grid fault occurs. A detection algorithm must discover the fault and pass that information to the controller. However for the scope of this thesis, it was decided to let the controller know as soon as the fault occurred. Therefore, in the majority of the upcoming tests, there is no delay between the fault happening and the controller switching strategy. If nothing else is written, there no delay. It should however be noted that tests showed that the controller was able to stabilise the system despite a delay in the switch between normal and FRT-oriented control.

4.2 Implementation summary

The chapter has documented the code implementation of the MPC controller. The controller is implemented in Simulink as a mex function, and in C code. Both implementations use the solver OSQP, which is well suited for quadratic optimization problems. OSQP has a C library which was used for the C code implementation. In Simulink, the software package CasADI was used to inferface to OSQP.

The C code implementation features two control models: one which can use the MSC current input, and another which can use the chopper. The first model will being used for normal operation, the other for fault ride through events.

Chapter 5

Test

5.1 Chapter objective

The primary objective the testing phase is to verify the hypotheses of the thesis:

Hypothesis 1.
Model predictive control can be used to stably control a wind turbine full scale converter. The controller maintains system stability during slow changes in active and reactive power references, and it can regulate the active and reactive power to meet those references with zero steady state error.

Hypothesis 2.
Model predictive control can be used to stabilize a full scale power converter during a symmetric low voltage grid fault, while maintaining production of active current and reactive power.

Hypothesis 3.
Model predictive control for full scale power converter is a robust control strategy with respect to grid strength. The controller maintains stability at low short circuit ratios.

Testing the hypthoses will demonstrate and verify the performance of the developed MPC controller. The overall goal of this thesis is to demonstrate the potential of transitioning from classical converter control to a model based optimal control strategy. This is done specifically by evaluating:

- Steady state and slow dynamics through simple reference tracking in nominal operation. This includes reference changes i.e. active and reactive power reference ramps.
- Fast dynamics through a grid event, where the grid voltage rapidly changes.
- Robust stability to variations of grid strength.

5.1.1 Structure

The chapter is divided into two primary sections. The first contains tests from Simulink, and the other contains tests from Plecs. The reason is that the following development strategy has been applied:

First develop and implement the MPC controller in a known environment (Simulink) to practically reduce the amount of debugging needed through the development stage.

Secondly implement the controller into the Vestas high fidelity model in Plecs to evaluate the performance.

All test will be documented with three primary plots:

- The active and reactive powers and currents - measured and references
- The DC link voltage - measured and reference
- The control signals produced by the MPC controller

Additional plots are provided when relevant. Signal constraints are noted in the captions of each plot.

5.1.2 Outline of the test chapter

Section 5.2 - Test in Simulink: This section documents the first test of the MPC controller. It is conducted in a reliable Simulink environment used in previous work. This ensures that the only test subject is the MPC controller. The controller was shown to be stable.

Section 5.3 - Test in Plecs: This section documents the tests performed on the high fidelity Plecs simulation model.

Subsection 5.3.1 - Baseline functionality test: This test documents the baseline MPC stability, and verifies that the control can regulate the active and reactive powers.

Subsection 5.3.2 - Fault ride through: This test documents that the MPC controller can stabilize the system when a low voltage grid fault occurs. The test also demonstrates how the FRT-oriented control is activated, which changes the control objective from power-regulation to current regulation. It is demonstrated that the chopper is used to dissipate excess power during FRT.

Subsection 5.3.3 - FRT with Q production: This test documents that the MPC controller can stabilize the system when a low voltage grid fault occurs. This test produces half of the nominal active current during the fault, and half of nominal reactive current. This is in contrast with the previous test which produced full active current and no reactive current. This reactive power injection increases the grid voltage, which helps stabilize the grid.

Subsection 5.3.4 - Low SCR test: This test documents that the MPC controller can stabilize the system, when the grid SCR is 20, 10, 5 or 3. It also demonstrates that at SCR=2, the system starts oscillating.

Subsection 5.3.5 - Low SCR FRT test: This test documents that the MPC controller can stabilize the system during FRT events, when the grid SCR is 20, 10, 5 or 3. It again demonstrates that at SCR=2, the system starts oscillating.

Subsection 5.3.6 - FRT with detection delay test: This test documents that the MPC controller can stabilize the system during a FRT event, in the presence of a detection delay from when the fault occurs to the controller switches to FRT-oriented control.

Subsection 5.4 - MPC predictions investigation: This test documents an investigation of the MPC controllers prediction behavior. It will be shown that control features such as terminal contraints and equal horizons could be useful in future control revisions.

5.1.3 Test applications

The upcoming tests will be concerned with three primary applications. These are introduced here.

Baseline functionality.
The purpose of the baseline functionality tests is to verify nominal stability of the controller. The tests will use slow reference signal changes, which will reveal if the controller is stable in steady state applications. The test features a nominal grid strength of SCR=20 (SCR will explained shortly).

Fault ride through
Fault ride through (or FRT) is an application in which the controllers disturbance rejection is tested. The tests will see a sudden symmetric decrease in grid voltage from 1pu to 0.5pu. When this happens the controller will switch from normal to FRT-oriented control. The grid voltage will remain low for a set duration, then rapidly return to its normal value. The grid voltage fault is seen in figure 5.1.

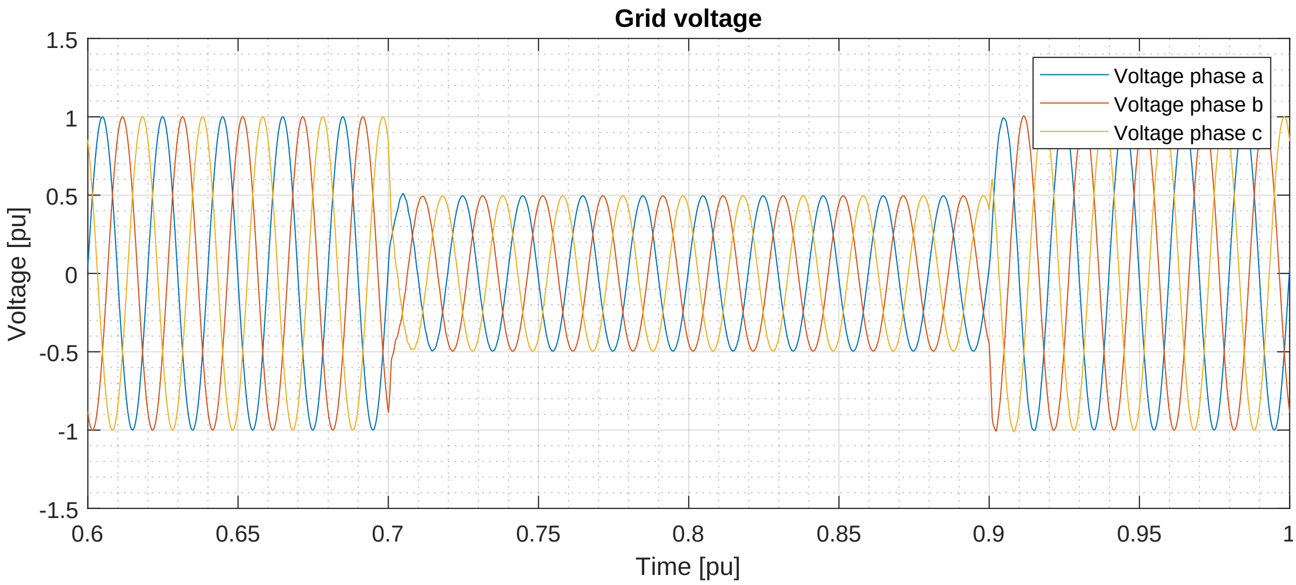

Figure 5.1: Low voltage grid fault

Low SCR tests

Short circuit ratio is used to describe the strength of the grid. An intuitive understanding of the metric is, that the a higher SCR implies a stronger grid, that is a lower grid impedance. A strong grid leads to a more stable converter control, since the local voltages of the converter are strongly coupled to the stable voltage of the grid. If the grid is weak (low SCR), the coupling between the stable grid voltage and the local converter voltage is weaker. This makes the local voltage more volatile, which makes instability a more likely risk.

The low SCR tests comprise of several executions of the same test sequences, each with a different SCR. The SCR values used range from 20 (nominal strong grid) to 2 (very weak grid).

It should be noted, that lower SCR values are often accompanied by lower X/R values. X/R is a metric that simply defines the ratio between imaginary and real impedance of the grid. However, the tests in thesis applies the same X/R values for all SCR test cases.

5.2 Test in Simulink

The initial tests of MPC were performed in Simulink. In previous work[6], Simulink had been the platform for all tests, so it was natural to use the experience in that environment to test the proposed MPC controller. The Simulink tests were performed before the FRT-oriented control strategy was proposed, and do therefore neither test the chopper functionality nor FRT capability.

The Simulink test setup consists of the following

- A mathematical model of the nonlinear system dynamics derived in chapter 2.
- A kalman filter which estimates the system states.
- A reference generator block which translates some predefined power references to current references based on the measurements.
- The MPC controller which generates the control signals for the mathematical model.

The structure and I/O relations of the simulation is seen in figure 5.2.

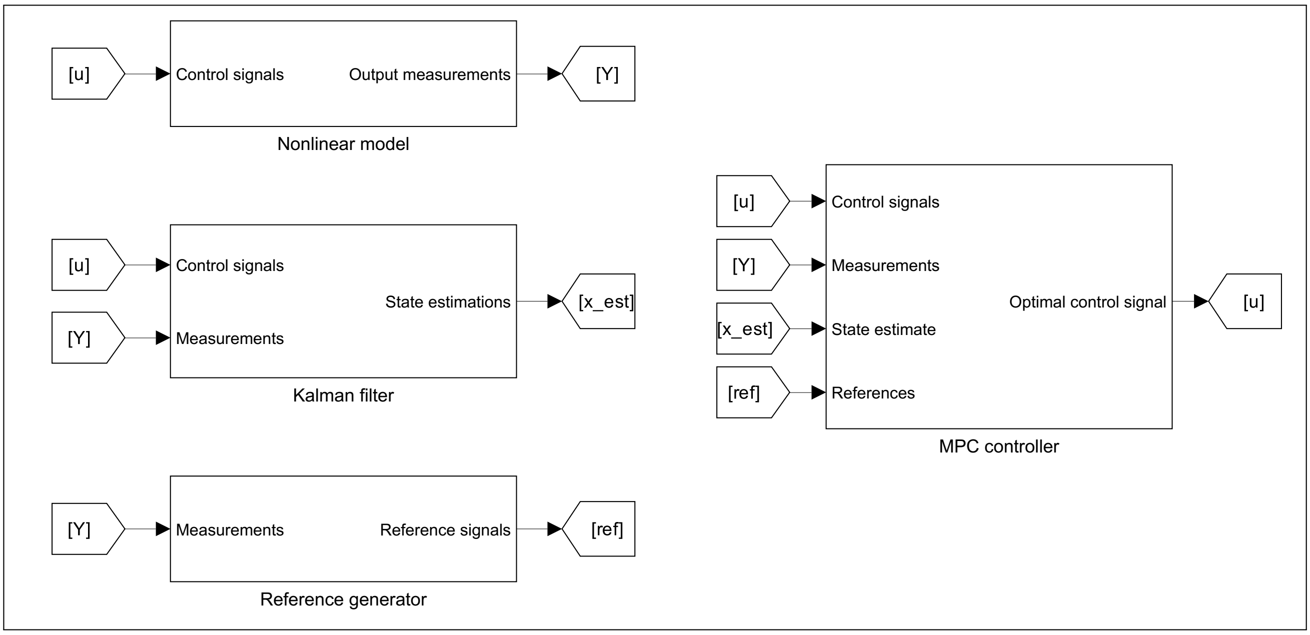

Figure 5.2: Block diagram depicting the functional blocks and I/O relationsships of the Simulink test framework

5.2.1 Baseline functionality test

This test seeks to verify the MPC stability by applying a variety of active and reactive power references. During the test the reference for the DC link voltage is constant, and the grid voltage is constant.

The success-criteria are:

- The system must be stable.
- There must be zero steady state error in P, Q, V_{DC} and the output currents.
- There should be minimal coupling from P and Q changes to V_{DC}.

Power outputs and references

The test sequence for the generic Simulink test is seen in figure 5.3. The active power ramps from 0.5pu to 1pu, followed by a reactive power ramp from 0pu to 0.16pu. Lastly, the active power ramps down from 1pu to 0.5pu.

The power references are being met, with zero steady state error. The active and reactive power appear to couple slightly to each other, as they spike slighty when the other ramps. The reactive power oscillates more than the active power. This is a result of the tuning: The cost weight for the active current is 100, whereas the reactive current is 2.

The powers are only controlled indirectly, as the power references are being translated to current references. These are shown in the figure as well. They appear identical to the power signals, except the sign of the reactive current is inverted, as expected.

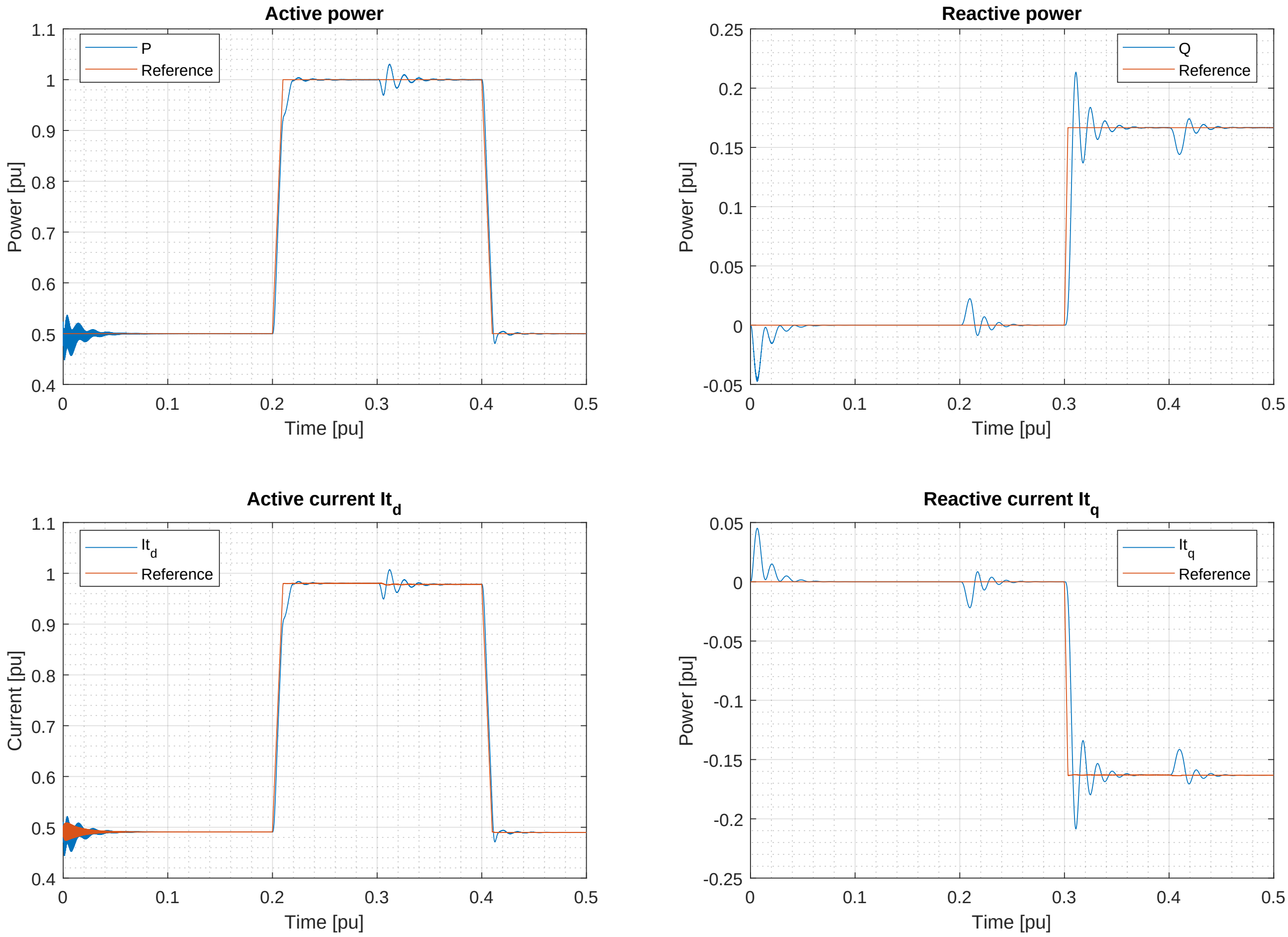

Figure 5.3:
Top left: P not directly constrained
Bottom left: I_d constraint = [-0.15pu to 1.25pu]
Top right: Q not directly constrained
Bottom right: I_q constraint = [-0.15pu to 1.25pu]

DC link voltage

During the test, the DC link voltage reference is constant at 1pu. This is seen in figure 5.4. It can be observed that the DC link voltage converges to 1pu with zero steady state error.

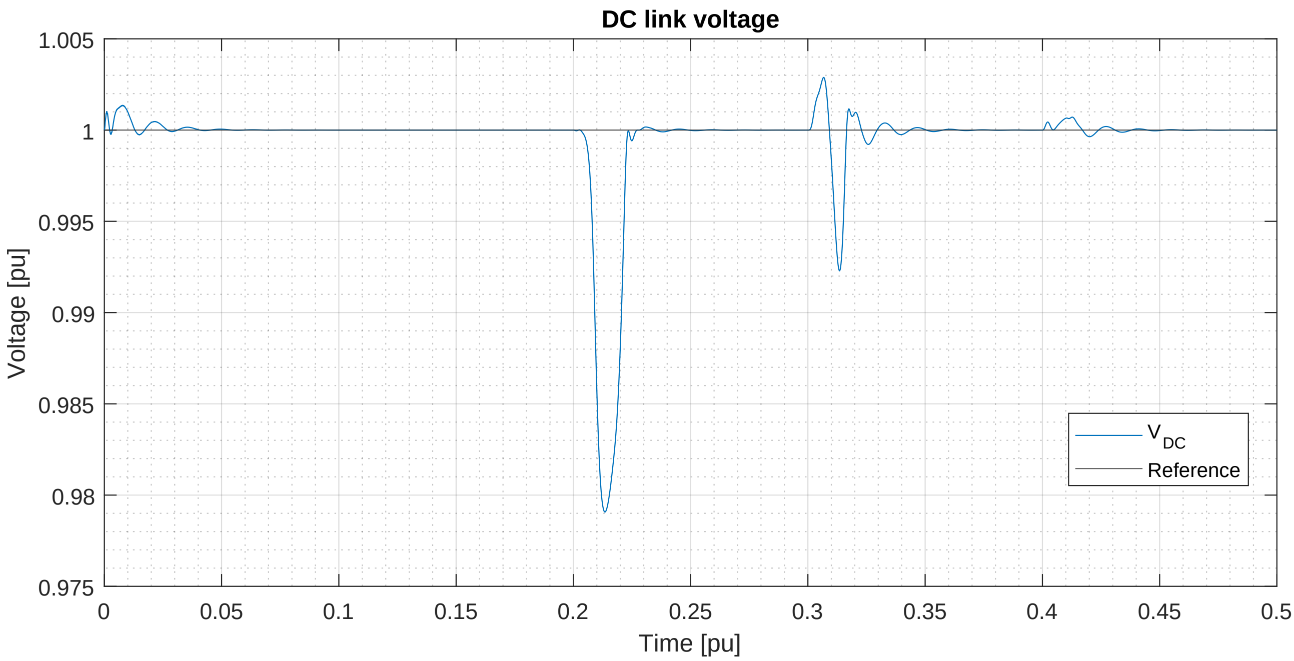

Figure 5.4: V_{DC} constraint = [0.95pu to 1.05pu]

When the active power ramps up, there is a decrease in DC link voltage. This is expected, as the sudden increase in LSC power consumpted, is not instantly matched by an increase in MSC power production. The energy difference is drawn from the DC link capacitor. The voltage is regulated back to 1pu once the ramp is over. Similar deviations appear as well, when the reactive power is changed and (less noticably), when the active power ramps down.

It is somewhat unexpected that the DC link reacts to the change in reactive power, as the DC link dynamics are tied to the active power flows. But by inspection of the power figures, it is clear that the active powers do change during a Q ramp. Thus the DC link voltage change is a secondhand result of the the Q to P coupling:

$$Q \text{ ramps up} \rightarrow P \text{ reacts} \rightarrow V_{DC} \text{ reacts}$$

It was expected that the down ramp of active power, would cause an large increase in DC link voltage - using the inverse argument of how the up ramp cause a decrease in voltage. This does not happen. The reason may be the simplified nature of the mathematical model, since later simulations in Plecs reveal that the DC link voltage *does* increase when the active power decreases.

Control signals

Figure 5.5 depicts the control signals during the simulation. The tendencies in control behavior that can be deducted from these plots repeats themselves in many of the future tests as well - they are common tendencies for converter control. Therefore, they will be described in detail here:

- Vc_d will match the movement of the reactive power. This is because Q is directly linked to the amplitude of the voltage, which is described by the voltage d component.
- Vc_q controls the LSC active power. The q component of the voltage relates (nonlinearly) to the phase of the voltage, and the phase of the voltage is directly couple to the amount of active power delivered to the grid. Therefore Vc_q will have similar behavior as the active power reference.
- I_u controls the active power delivered by the MSC. This is clear as the DC power is simply $P = V_{DC}I_{DC}$, and the DC link voltage is being held constant. I_u therefore also follows the LSC active power reference, so as to maintain the power balance at the DC link.

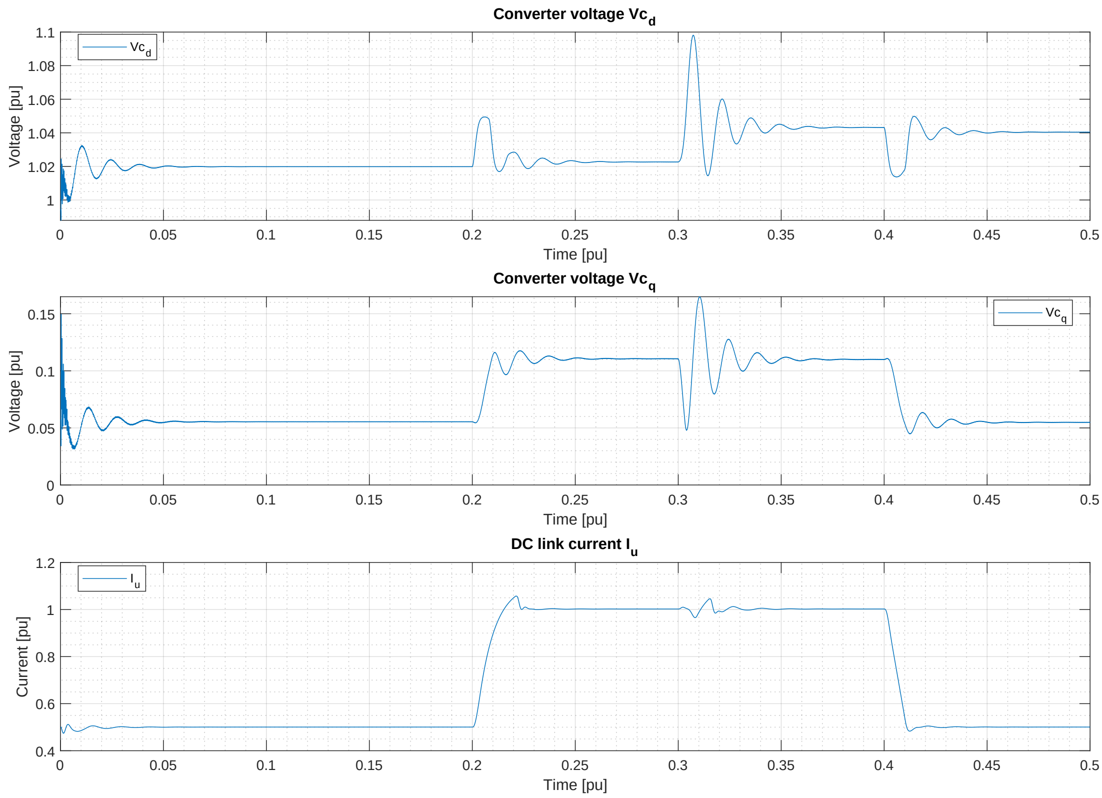

Figure 5.5:
Top: V_{c_d} constraint = [-0.1pu to 1.1pu]
Middle: V_{c_q} constraint = [-0.1pu to 1.1pu]
Bottom: I_u constraint = [-0.15pu to 1.15pu]

Simulink test summary

The Simulink test has verified the basic MPC functionality. It has been demonstrateted that the MPC controller is stable in a range of P and Q values. The translation from P/Q to Id/Iq references produce stable internal reference signals. The DC link voltage is well regulated during ramps. The general relation between the inputs and outputs are as expected.

The success-criteria were met:

- ✓ The system must be stable.
- ✓ There must be zero steady state error in P, Q, V_{DC} and the output currents.
- ✓ There should be minimal coupling from P and Q changes to V_{DC}.

5.3 Test in Plecs

The objective of the tests in Plecs is to evalutate the MPC performance on the high fidelity converter simulation. The previously discussed applications (baseline, FRT and SCR) will be tested.

Common test conditions

All tests in Plecs are initialized in the following way: While the simulation time is less than 0.4pu, the MPC controller is **inactive**. During this time frame the system is controlled using the following procedure:

- The converter voltage $V_{c_{dq}}$ is kept fixed, at values corresponding to P=0.5pu and Q=0pu.
- The DC link current is controlled by a PI controller, which regulates the DC link voltage to 1pu.

The LSC converter is implemented as average model, which does not use PWM signals. The chopper uses PWM signals.

Kalman filter and state measurements

A kalman filter was developed during this thesis, with the intent to be used for state estimation. It is however not being used for the Plecs tests. During the initial integration tests in Plecs, the observer acted unexpectedly and did not estimate the states accurately. When using the kalman filter in combination with the MPC controller, the system became unstable, likely due to estimation errors.

Fortunately, the kalman filter is not strictly necessary for state estimation in this thesis. This is because the physical (and simulation) platform has sensors for all the states of model. Therefore, it is possible to simply use full state measurements for the controller, thus bypassing the kalman filter entirely. The downside to this strategy, is that the noise filtering properties of the kalman filter are lost.

It is hypothesised that the estimation errors during integration were caused by the LSC converter model; during integration the converter used PWM signals, rather than the average-model used for the final tests. These PWM signals may cause the instability seen in the kalman filter. Due to time constraints no further investigation has been put towards this issue. The following test section uses full state measurements.

5.3.1 Baseline functionality test

This test seeks to verify the MPC stability by applying a variety of active and reactive power references. During the test the reference for the DC link voltage is constant, and the grid voltage is constant. The test is conduction with nominal grid: SCR = 20.

The success-criteria are:

- The system must be stable.
- There must be zero steady state error in P, Q, V_{DC} and the output currents.
- There should be minimal coupling from P and Q changes to V_{DC}.
- The controller should not use the chopper, as no fault is applied to system.

Power outputs and references

The primary reference signals for the simulation is the active and reactive power references, as seen in the upper plots of figure 5.6. The figure show that the MPC controller can control the active and reactive powers with zero steady state error. The reactive power has a small error during ramps. It is hypothesised that the ramp error is caused by the lower cost weight associated with the reactive current.

The reactive power has a positive error when the active power in ramping up, and a negative error when the active power is ramping down. This is two likely causes for this behavior:

- Firstly, one might suggest that the controller should be able to increase P in a way that makes no change in Q. But then recall that the controller is only *optimal* with respect to the defined cost function. And the cost function penalizes P must more than Q. As such the optimal performance might be to let Q increase slightly when ramping P up.
- Another cause for the behaviour may lie in the reference signals the controller uses. At time k, the controller measures the references and assumes they will be constant over the next H_p samples. But in practice the references increase with every sample.

The lower plots show the corresponding I_d and I_q references. The current references are calculated based on the P and Q references, and the measured converter voltage V_f.

The d component of the current follows the movement of the active power, seen on the previous figure. However, when the reactive power increases the current reference decreases. This is because an increase in reactive power causes a rise of voltage, which lowers the current need to produce the same amount of power.

The q component of the current follows the movement of the reactive power, with a change of sign.

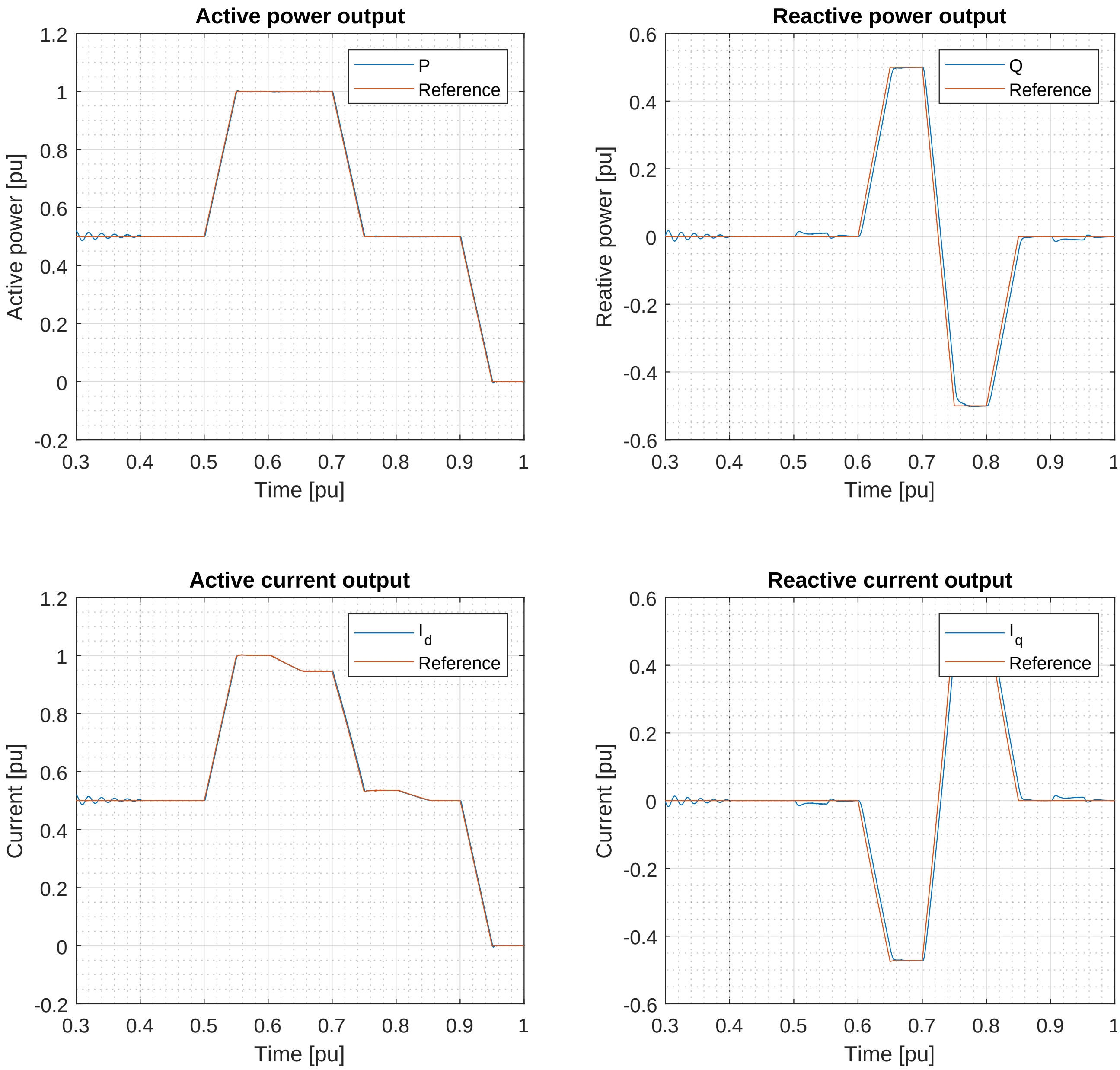

Figure 5.6:
Top left: P not directly constrained
Top right: Q not directly constrained
Bottom left: I_d constraint = [-0.15pu to 1.25pu]
Bottom right: I_q constraint = [-0.15pu to 1.25pu]

DC Link voltage

The reference for the DC link voltage is constant at 1 pu. Figure 5.7 shows the behaviour of the DC voltage during the test. Notably the DC link voltage is lowered when the active power is ramping up, and increased when the active power is ramping down.

This happens because a increase in power on the line side requires an equal increase in power from the machine side. The machine side power is not increased instantly, so there is a drop in DC link voltage, as the line side extracts energy from the capacitor. When the power balance is restored the DC link voltage settles, but not on its reference value. This is because there is no additional integration to remove errors during ramps. In classical control theory, this is known as a type 1 system, which has zero error to step signals, but a constant error to ramp signals.

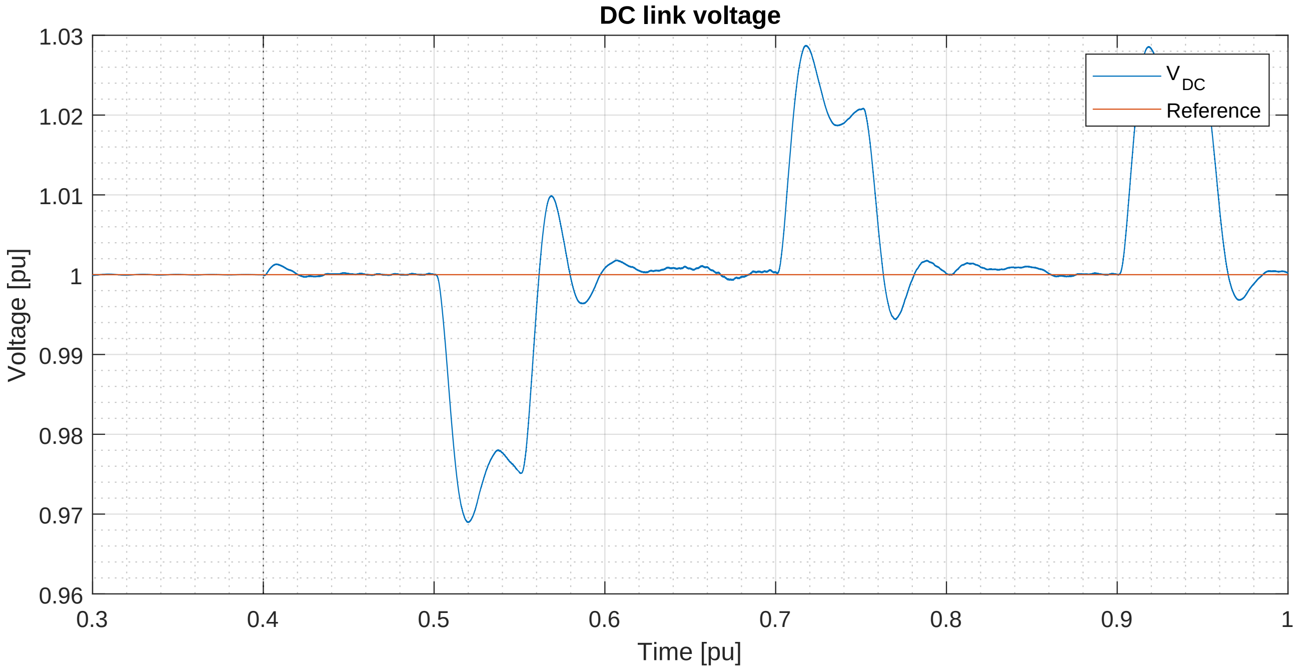

Figure 5.7: V_{DC} constraint = [0.95pu to 1.05pu]

Control signals

Figure 5.8 depicts the control signals of the test. The tendencies observed in the figure will be seen in many of the

- The d component of the converter voltage V_{c_d} controls the reactive power (and vicariously the reactive current). It follows the Q reference.
- The q component of the converter voltage V_{c_q} and the MSC current I_u both follow the active power P. This is because V_{c_q} controls the LSC power and I_u controls the MSC power.
- The chopper control signal is zero, when no grid fault is happening

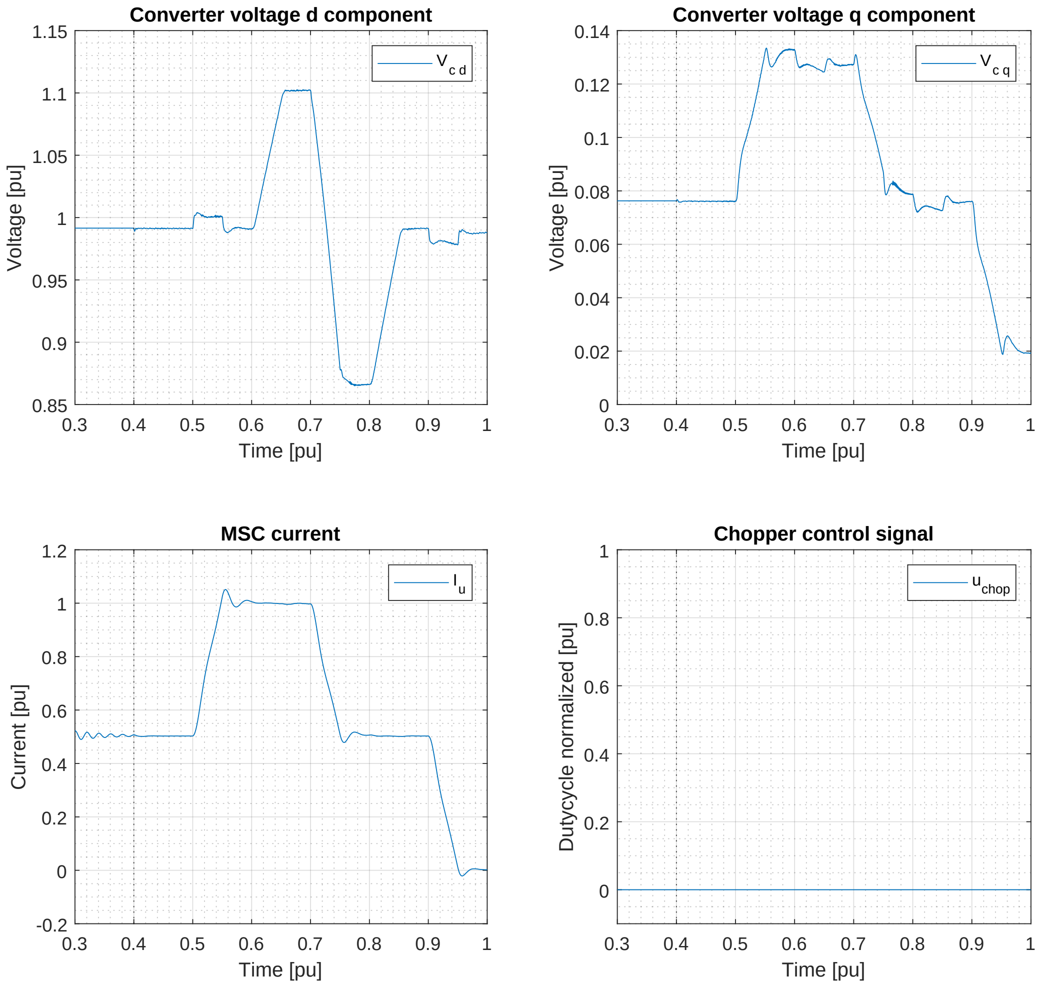

Figure 5.8:
Top left: V_{c_d} constraint = [-0.1pu to 1.1pu]
Top right: V_{c_q} constraint = [-0.1pu to 1.1pu]
Bottom left: I_u constraint = [-0.15pu to 1.25pu]
Bottom right: u_{chop} constraint = [0pu to 1pu]

Baseline functionality test summary

The test has demonstrated that the MPC controller is stable during normal operation. The controller is capable of controlling the active and reactive powers independently, while maintaining a constant DC link voltage. Furthermore it is demonstrated that the controller does not use the chopper during normal operation. The general trends of the control have been observed, such as the various inputs relation the the outputs.

The success-criteria were met:

- ✓ The system must be stable.
- ✓ There must be zero steady state error in P, Q, V_{DC} and the output currents.
- ✓ There should be minimal coupling from P and Q changes to V_{DC}.
- ✓ The controller should not use the chopper, as no fault is applied to system.

5.3.2 Fault ride through

This test investigates the controllers stability to external disturbances. The primary disturbance will be a rapid decrease in grid voltage, from 1pu to 0.5pu. After a short period the grid voltage will return to 1pu.

During the fault the controller switches from normal operation to FRT-oriented control. This includes severel things:

- As described in section 4, the controller will not change the MSC current during a FRT event. It will instead use the chopper to balance the power.
- During FRT events, the primary P and Q references are **not** used. This is because it is infeasible to deliver nominal power to a low voltage grid, without exceeding the current limitations.
- During FRT events, the controller uses predefined I_{dq} references. These are planned before simulation, and are thus **not** calculated online, as a function of the specific grid fault.
- The controller switches to FRT-oriented control instantly when the fault occurs; There is no detection delay in this test.
- The controller leaves FRT-oriented control when the chopper control signal has returned to zero. This ensures that the controller does not resume normal performance while the chopper is not completely close, as the normal control cant change the chopper signal.

During FRT-oriented control in this test the I_{dq} references are:

$$I_{d_{ref}} = 1\text{pu}$$
$$I_{q_{ref}} = 0\text{pu}$$

The fault begins at time = 0.7pu and ends at time = 0.9pu. The test is conduction with nominal grid: SCR = 20.

The success-criteria are:

- The system must be stable during and after the fault.
- There must be zero steady state error in P and Q before and after the fault.
- There must be zero steady state error in the active and reactive currents during the fault.
- The currents must not exceed their constraints
- The controller must use the chopper to control the DC link voltage during the fault, and return the chopper signal to zero after the fault.
- The controller must not change the DC link current during the fault.

Grid voltage

The upper plot of figure 5.9 depicts the grid voltage, which is lowered to 0.5pu when the fault occurs.

The lower plot depicts the resulting decrease of the converter output voltage V_f. Both signals converge to 0.5pu. This is because no reactive power is being delivered, which would raise the voltage.

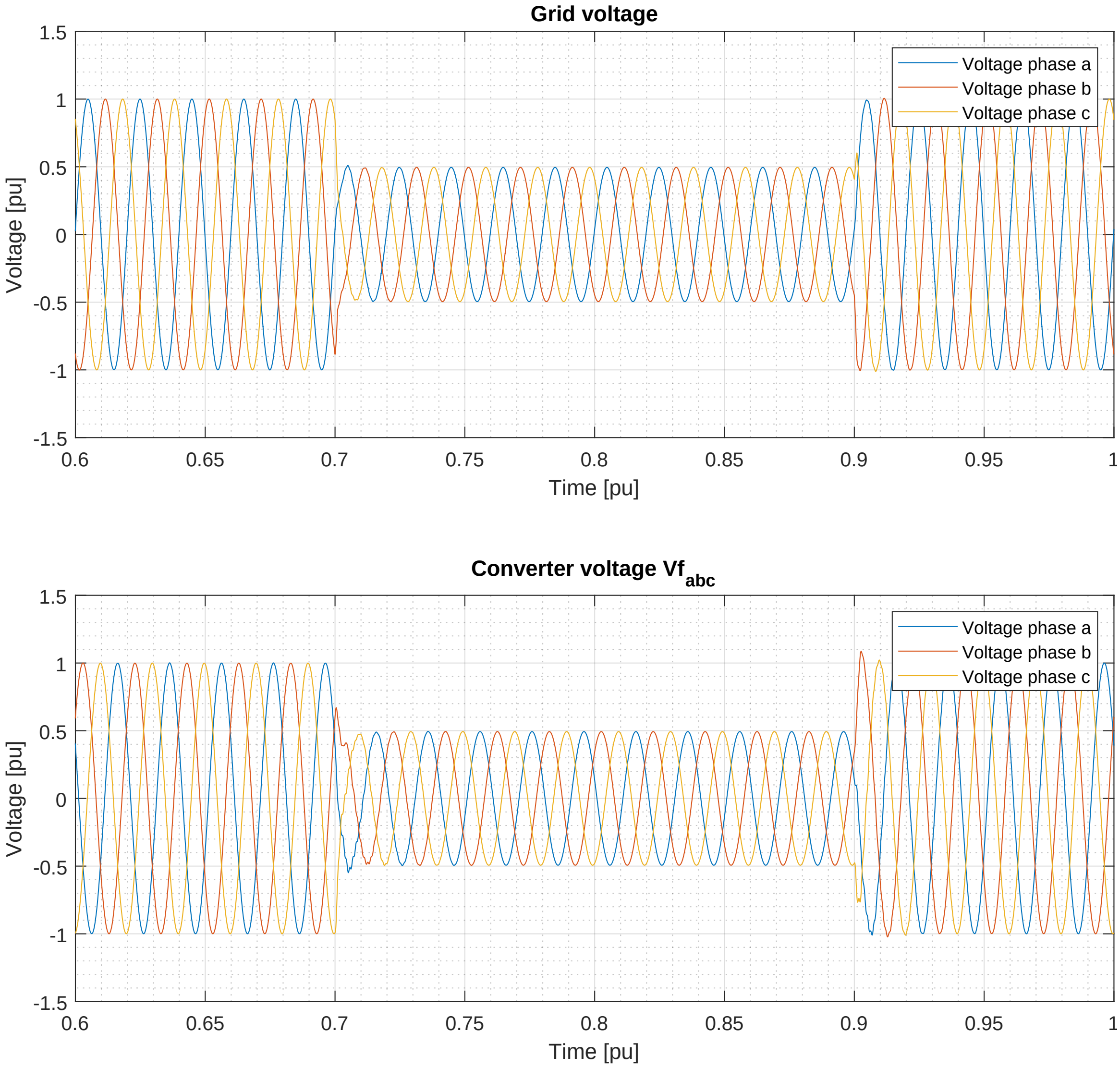

Figure 5.9:
Top: Grid voltage V_g **Bottom left:** Converter voltage V_f

Power outputs and references

Figure 5.10 shows the active and reactive powers being delivered to the grid (upper plots). It is clear that during the fault, the active power reference is not being used. During the beginning and end of the fault there are noticeable spikes in the active and reactive powers. The active current in particular exceeds the controller constraint of 1.25pu. Future test demonstrate how these spikes can be reduced by instantly reducing the current references.

During the fault the current references are being followed with zero steady state error.

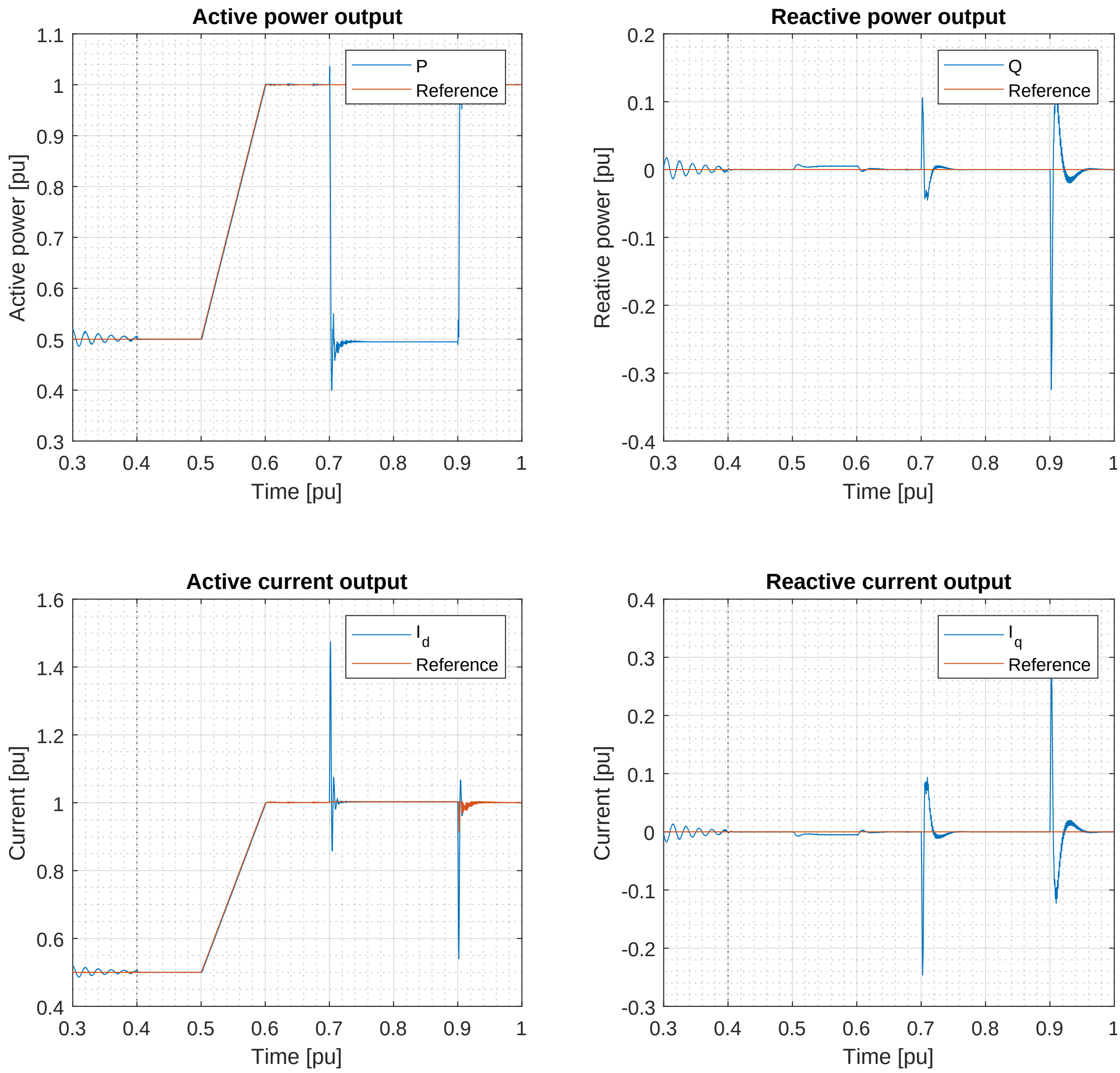

Figure 5.10:
Top left: P not directly constrained
Top right: Q not directly constrained
Bottom left: I_d constraint = [-0.15pu to 1.25pu]
Bottom right: I_q constraint = [-0.15pu to 1.25pu]

DC Link voltage

The reference for the DC link voltage is constant at 1 pu. Figure 5.11 shows the behaviour of the DC voltage during the test. Again the DC link voltage is lowered when the active power is ramping up.

The DC link is relatively well behaved during the fault. There is oscillatory behavior, which is linked to the chopper. The chopper is controlled by a driver, which translates the control signal [0-1] to a PWM signal [0%-100%]. This PWM signal opens and closes the chopper which couples to the DC link voltage. Figure 5.12 shows an enhanced view of the behavior.

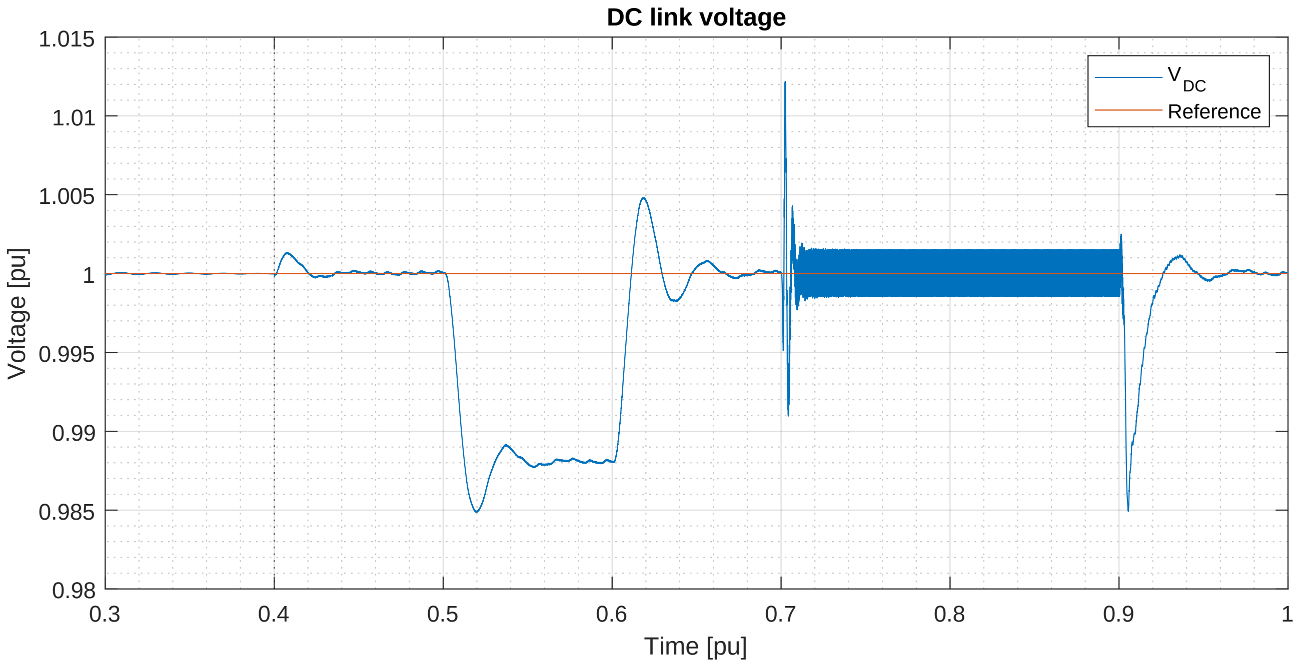

Figure 5.11: V_{DC} constraint = [0.95pu to 1.05pu]

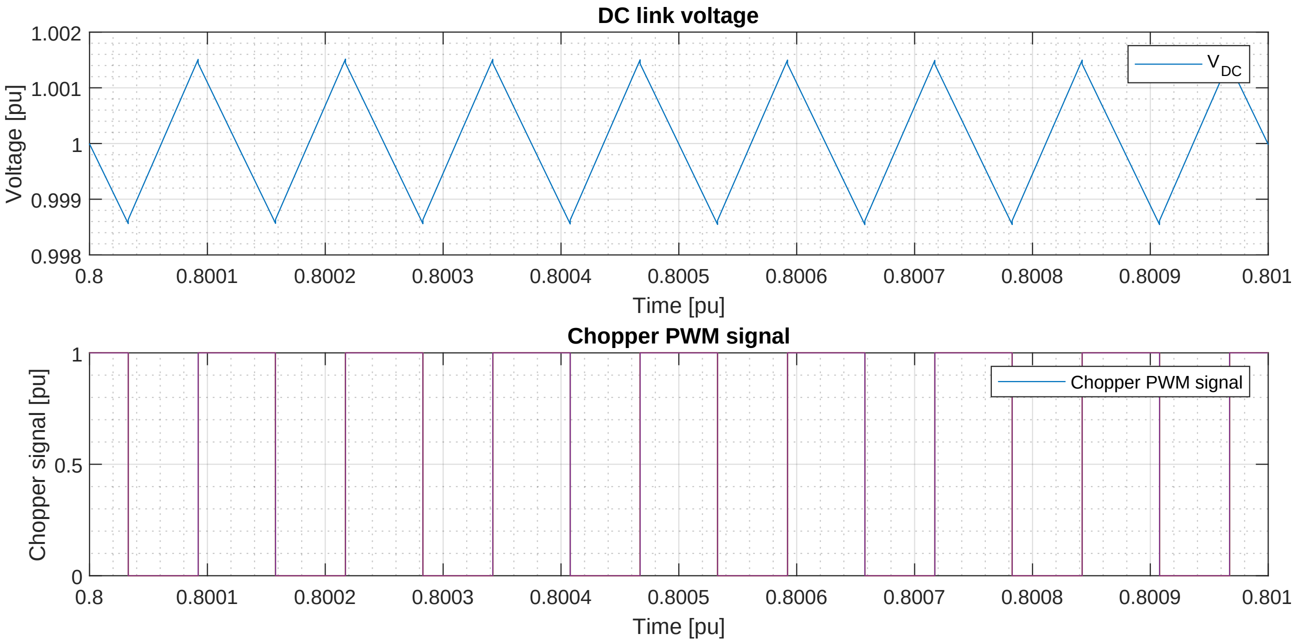

Figure 5.12:
Top: DC link voltage sawtooth behavior
Bottom left: Chopper PWM signal. Dutycycle is 50%

The single PWM signal which controls the chopper is a simplification of the simulations. In the practical application the chopper consists of several parallel resistor[1] and gates - typically 4 stacks. The PWM signals of these 4 stacks have the same dutycycle, but are offset in time from each other. Each stack is 0.25 of the PWM sample time delayed with respect to the next. This means for dutycycles above 25% there will always be at least one gate open, which helps to smooth out the behavior.

[1]Each parallel resistor is naturally larger that than the equivalent combined resistance.

Control signals

Figure 5.13 depicts the control signals of the test. During the FRT event the following behaviour is observed:

- There is a large spike in the q component of the voltage.
- The d component of the converter voltage is being lowered to match the grid voltage.
- The chopper gate is opened almost fully and the settles to approximately 0.5.
- The MSC current does not change during FRT.

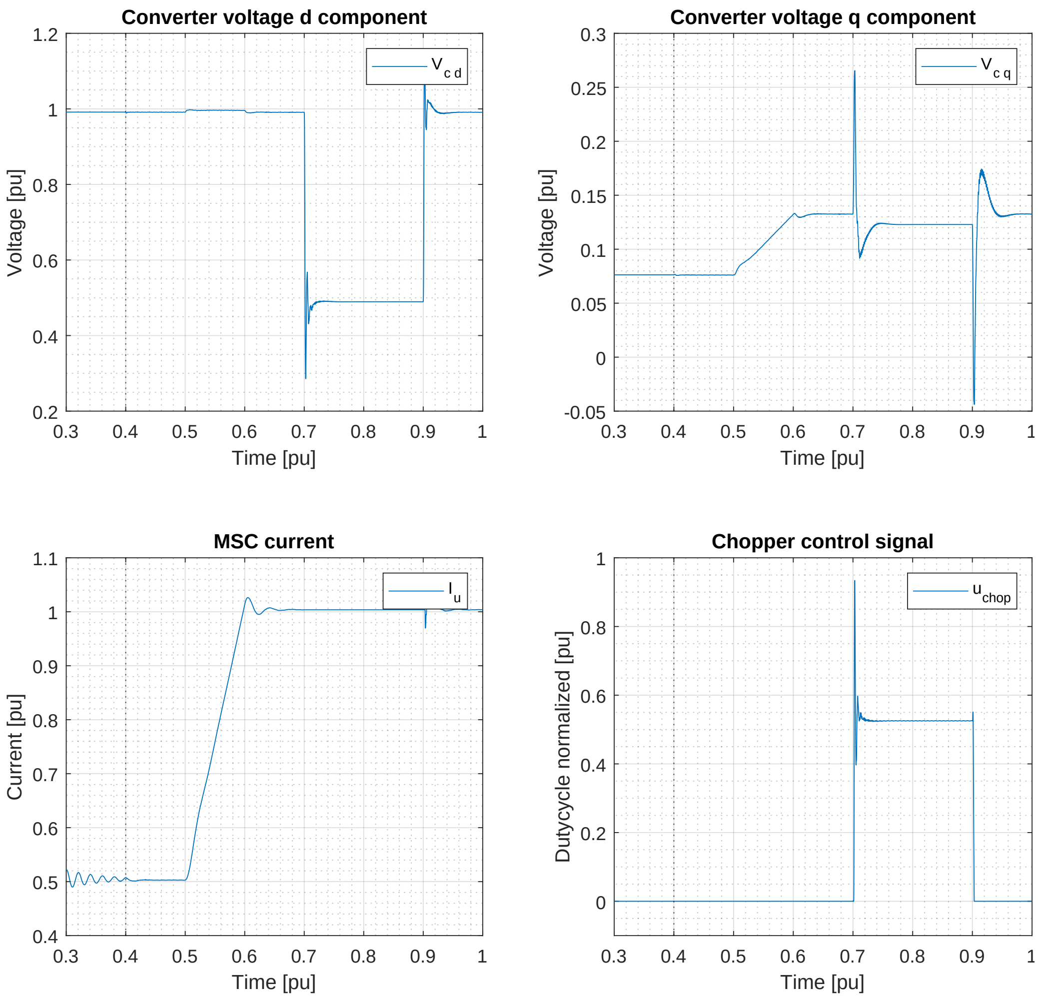

Figure 5.13:
Top left: V_{c_d} constraint = [-0.1pu to 1.1pu]
Bottom left: I_u constraint = [-0.15pu to 1.25pu]
Top right: V_{c_q} constraint = [-0.1pu to 1.1pu]
Bottom right: u_{chop} constraint = [0pu to 1pu]

Fault ride through test summary

The test has demonstrated that the controller is able to keep the system stable during a low voltage grid fault. By switching from power production to current control, the system avoids overcurrent situations - although the current does spike during transients.

The chopper resistor is being used properly to dissipate the MSC power. The chopper PWM driver creates a sawtooth wave in the otherwise stable DC link voltage. This is no concern as the movement is small.

The success-criteria were partially met:

- ✓ The system must be stable during and after the fault.
- ✓ There must be zero steady state error in P and Q before and after the fault.
- ✓ There must be zero steady state error in the active and reactive currents during the fault.
- ✘ The currents must not exceed their constraints
  The active current briefly exceeded its constraint when the fault began
- ✓ The controller must use the chopper to control the DC link voltage during the fault, and return the chopper signal to zero after the fault.
- ✓ The controller must not change the DC link current during the fault.

5.3.3 FRT with Q production

This test demonstrates the fault ride through performance when the current references are optimized for better performance. Better performance entails:

- The converter should produce reactive power during FRT, to help stabilize the grid and raise the voltage.
- The converter should limit the amount of active power during FRT.

During FRT-oriented control in this test the I_{dq} references are:

$$I_{d_{ref}} = 0.5\text{pu}$$
$$I_{q_{ref}} = -0.5\text{pu}$$

The fault begins at time = 0.7pu and ends at time = 0.9pu. The test is conduction with nominal grid: SCR = 20.

The success-criteria are:

- The system must be stable during and after the fault.
- There must be zero steady state error in P and Q before and after the fault.
- There must be zero steady state error in the active and reactive currents during the fault.
- The currents must not exceed their constraints
- The controller must use the chopper to control the DC link voltage during the fault, and return the chopper signal to zero after the fault.
- The controller must not change the DC link current during the fault.

Grid voltage

The upper plot of figure 5.9 depicts the grid voltage, which is lowered to 0.5pu when the fault occurs.

The lower plot depicts the resulting decrease of the converter output voltage V_f. The converter voltage stabilizes at 0.6pu, rather than 0.5pu, due to the reactive power production.

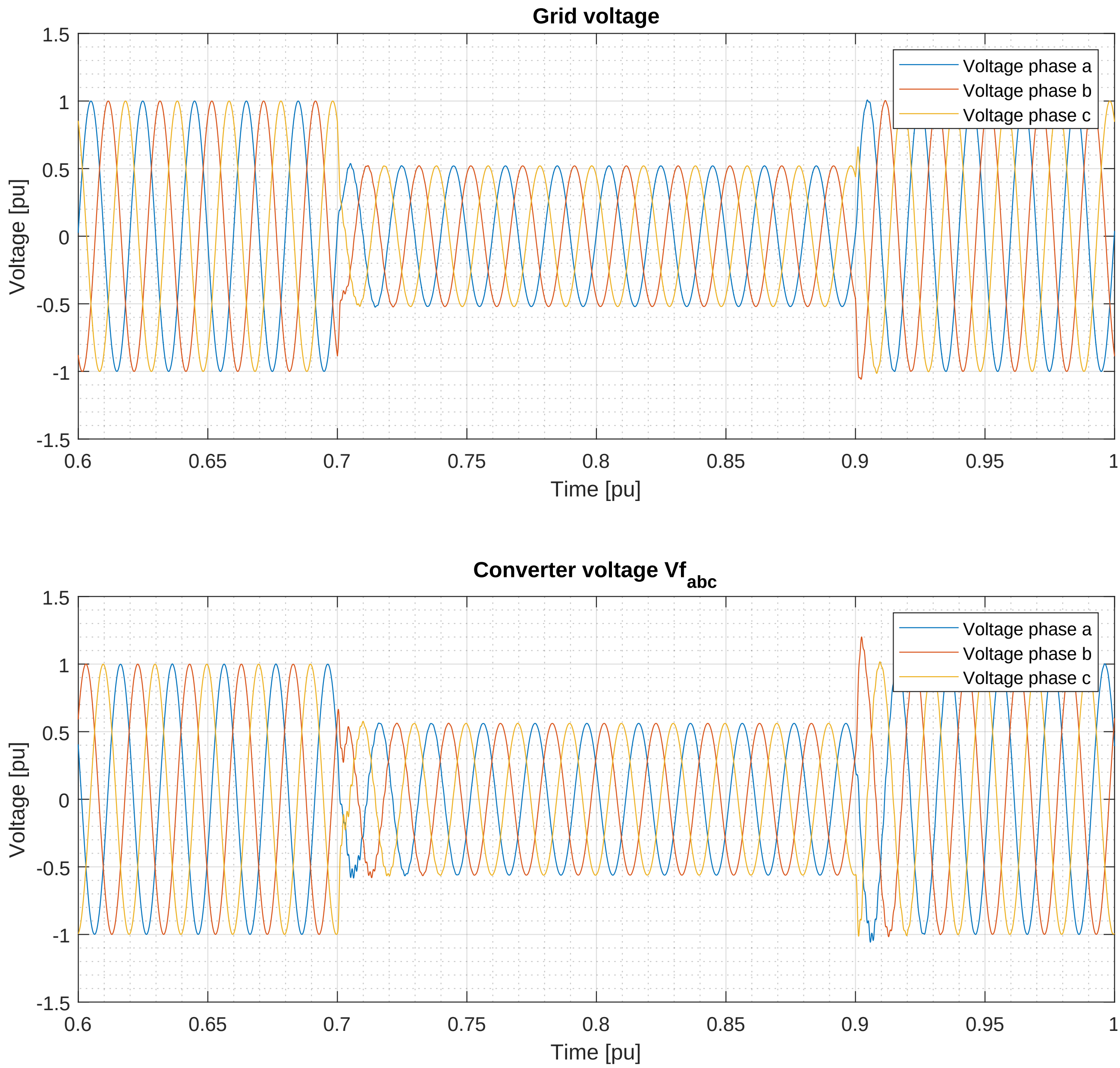

Figure 5.14:
Top: Grid voltage V_g **Bottom:** Converter voltage V_f

Power outputs and references

Figure 5.15 shows the active and reactive powers being delivered to the grid (upper plots). As before during the fault, the P and Q references are not being used.

During the fault the current references are being followed with zero steady state error. Reducing the I_d reference to 0.5pu, reduces the peak active current when the fault occurs. Previously the current would peak at 1.5pu, now it peaks at 1.2pu. This is a great improvement, as the current no longer violates its constraint.

The reactive power is being increased during the fault, to help stabilize the grid. -0.5pu reactive current is being produced, which results in 0.3pu reactive power. However when leaving the fault, a large spikes in reactive current happens. This hints that the simple on/off current references during the fault might not be the best reference implementation.

Consider what happens the moment the fault ends: the voltage is still low, but the current reference jumps from -0.5pu to 0pu. The controller is tuned to prioritize the reactive current less than the active current, so it doesnt change the current quickly. While the voltage increases the current is still large, which causes the spike in reactive power. No more studies has been conducted on the issue in this thesis.

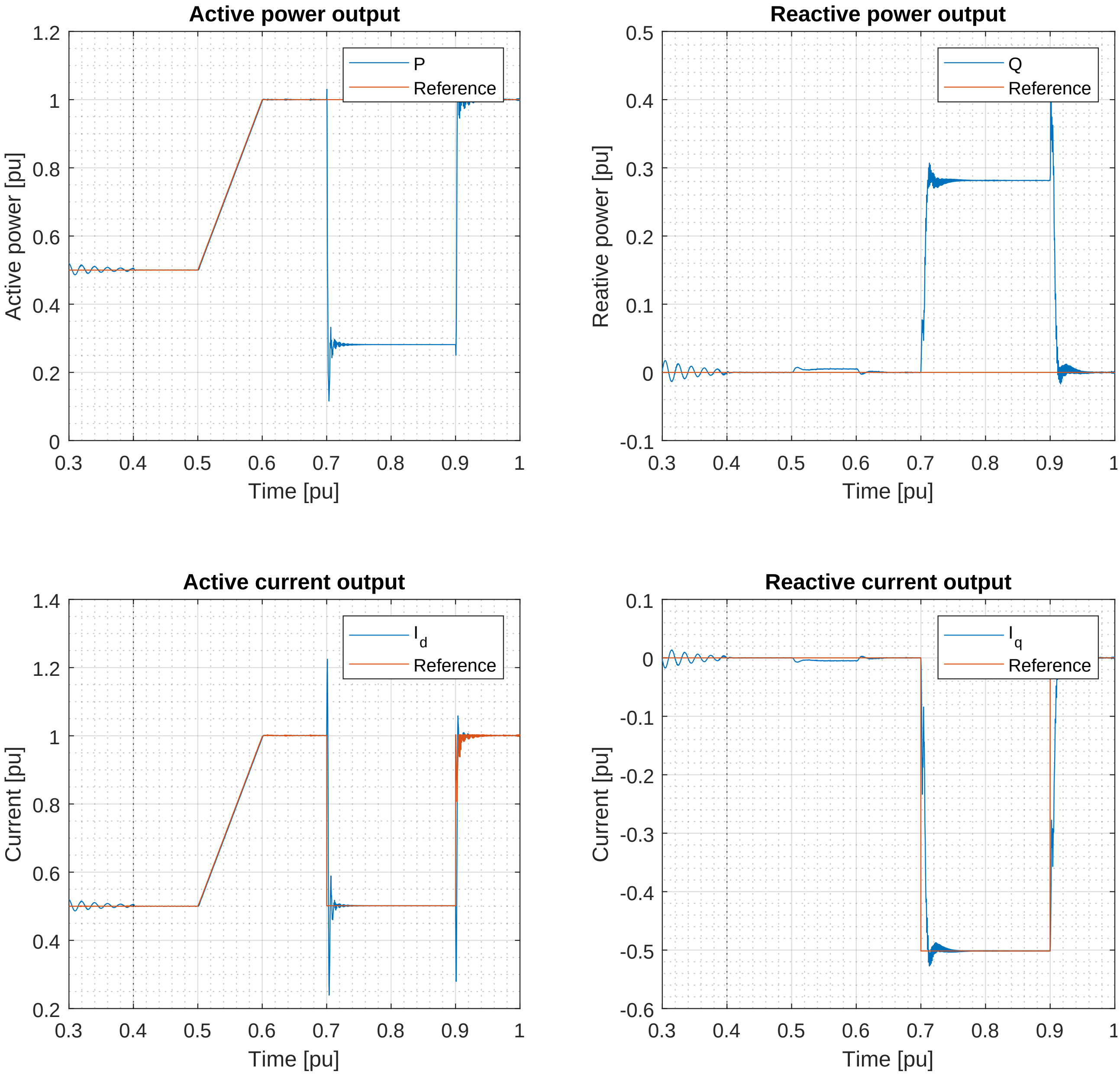

Figure 5.15:
Top left: P not directly constrained
Bottom left: I_d constraint = [-0.15pu to 1.25pu]

Top right: Q not directly constrained
Bottom right: I_q constraint = [-0.15pu to 1.25pu]

DC Link voltage

The reference for the DC link voltage is constant at 1 pu. Figure 5.16 shows the behaviour of the DC voltage during the test. Again the DC link voltage is lowered when the active power is ramping up.

The DC link voltage reacts a lot when leaving the fault. It falls to 0.96pu. This is because the LSC active power is very low during the fault, which results in power being drawn from the DC link capacitor when increasing the LSC power after the fault. This is unexpected behaviour, as the constant MSC current should ensure that the system does not need to draw energy from the DC link capacitor.

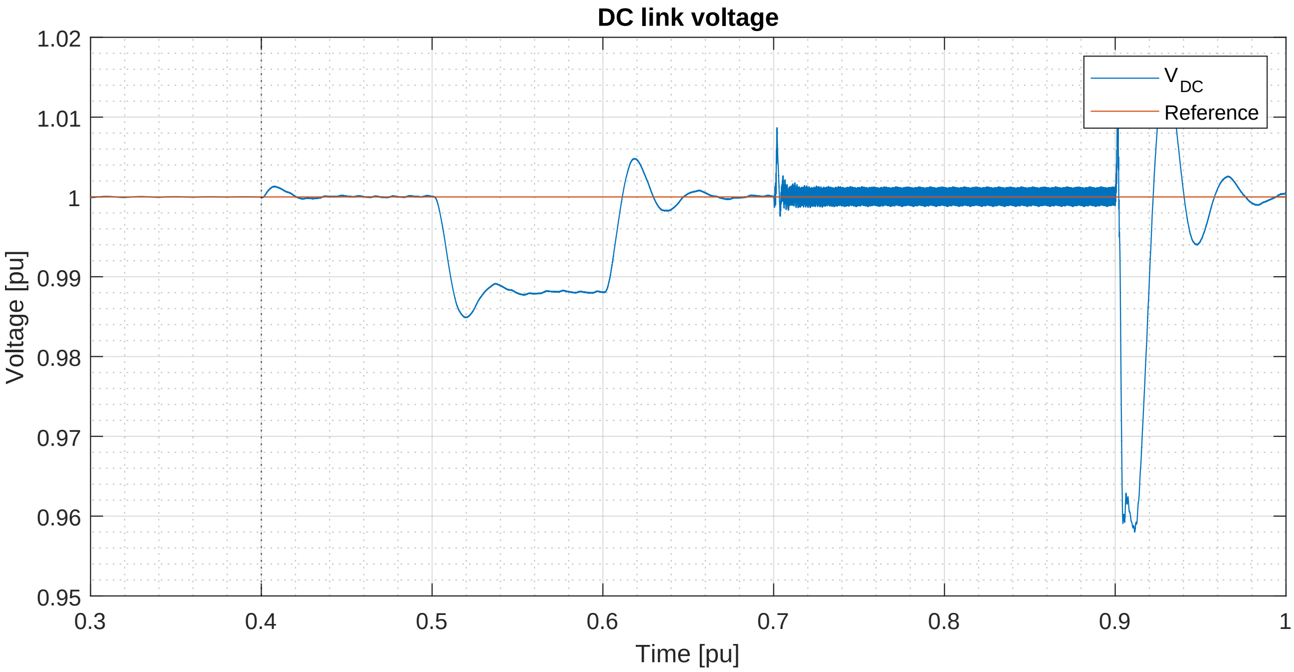

Figure 5.16: V_{DC} constraint = [0.95pu to 1.05pu]

Control signals

Figure 5.17 depicts the control signals of the test. The control signals are comparable to the previous FRT test.

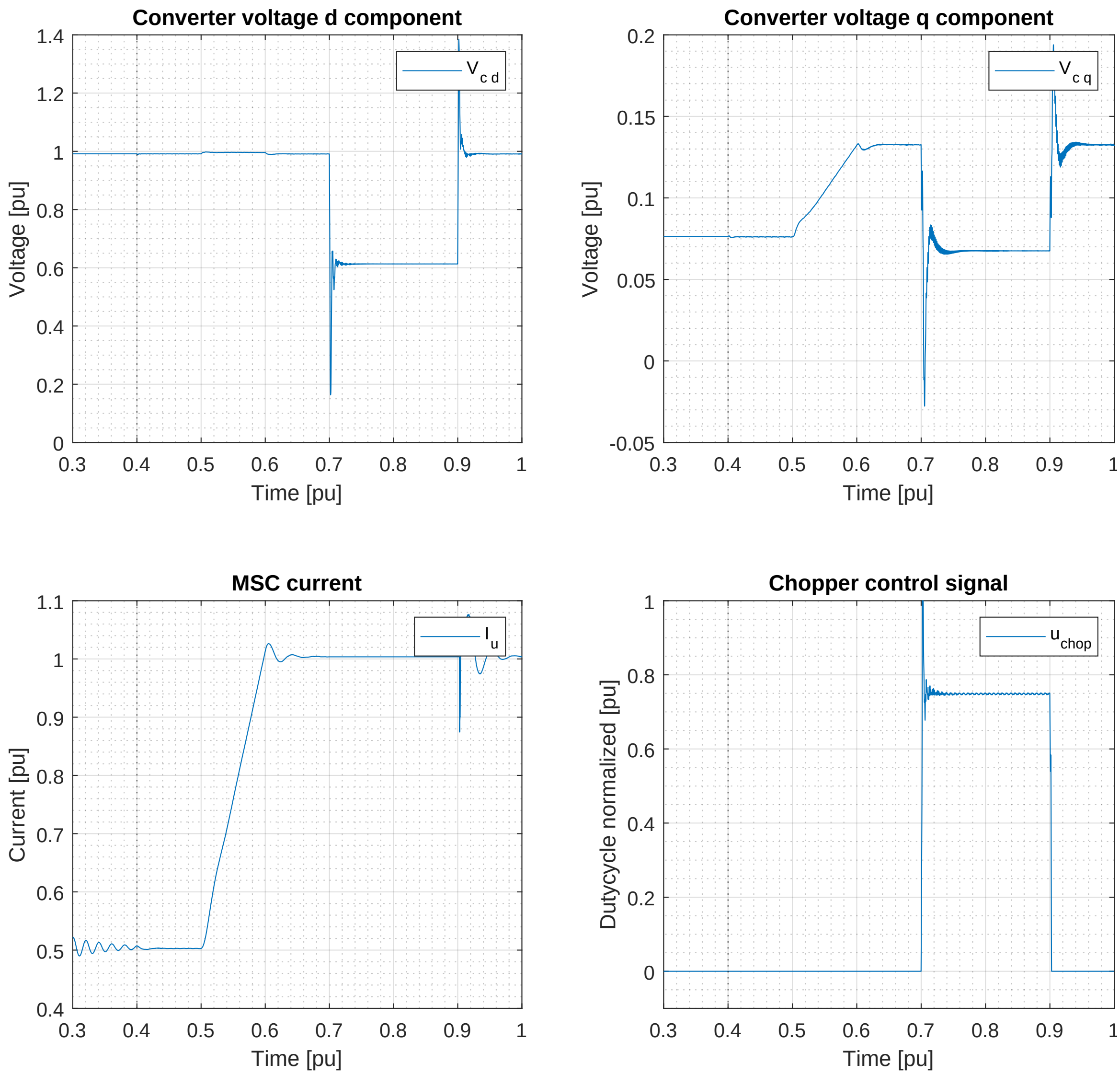

Figure 5.17:
Top left: V_{c_d} constraint = [-0.1pu to 1.1pu]
Top right: V_{c_q} constraint = [-0.1pu to 1.1pu]
Bottom left: I_u constraint = [-0.15pu to 1.25pu]
Bottom right: u_{chop} constraint = [0pu to 1pu]

FRT with Q production - test summary

The test demonstrated the FRT performance when producing reactive power during the fault. The performance increased on some parameters but decreased on others:

- The spikes in active current were reduced.
- The converter voltage was increased, which aids to stabilize the grid.
- The reactive power overshot greatly when leaving the fault.
- The DC link undershot when leaving the fault.

The success-criteria were met:

✓ The system must be stable during and after the fault.

✓ There must be zero steady state error in P and Q before and after the fault.

✓ There must be zero steady state error in the active and reactive currents during the fault.

✓ The currents must not exceed their constraints

✓ The controller must use the chopper to control the DC link voltage during the fault, and return the chopper signal to zero after the fault.

✓ The controller must not change the DC link current during the fault.

5.3.4 Low SCR test

This test demonstrates the MPC performance, when the grid has a low short circuit ratio. The previous tests were all conducted with SCR = 20. This test sees an increase in active power production from 0.5pu to 1pu, under varying grid conditions. The table below specifies the test cases.

Test case	**SCR**
TC.1	20
TC.2	10
TC.3	5
TC.4	3
TC.5	2

Test case 5 yields unstable behavior and will be plotted as a dotted line. The axis limits will often be chosen to best depict test case 1-4, which will sometimes mean that the full oscillations of test case 5 will be cut.

The success-criteria are:

- The system must be stable for all test cases.
- There must be zero steady state error in P and Q for all test cases.
- The currents must not exceed their constraints for any test cases.
- The controller must not use the chopper as no fault is applied.

Power outputs and references

Figure 5.18 depicts the active and reactive powers and their references. Under all grid variations the active and reactive power references are met. There is no apparent deviation in the active power output. The reactive power oscillates more, when the SCR is low, but the magnitudes are so small that it is negligible. The exception is SCR=2, where the system becomes incredibly oscillatory.

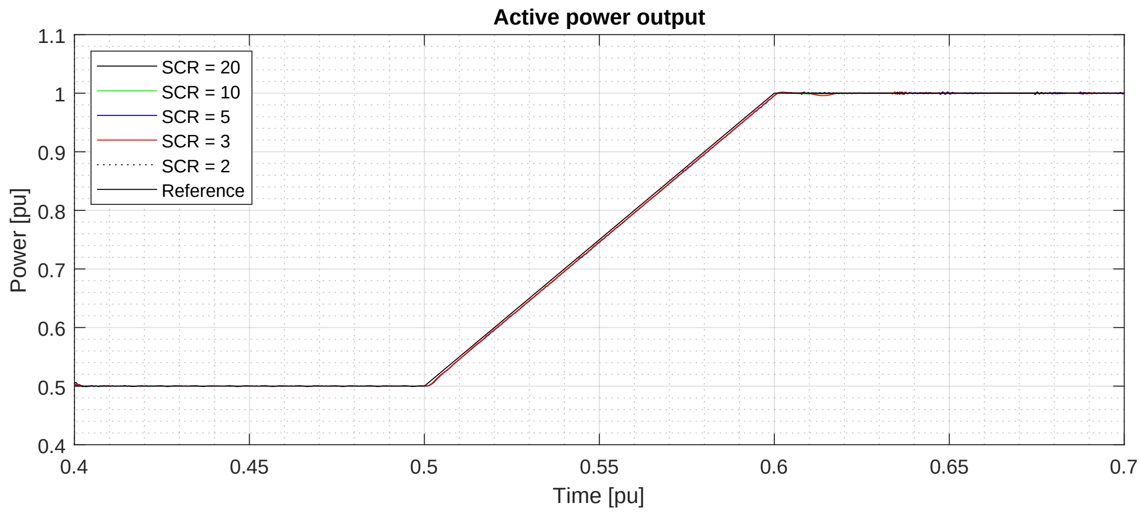

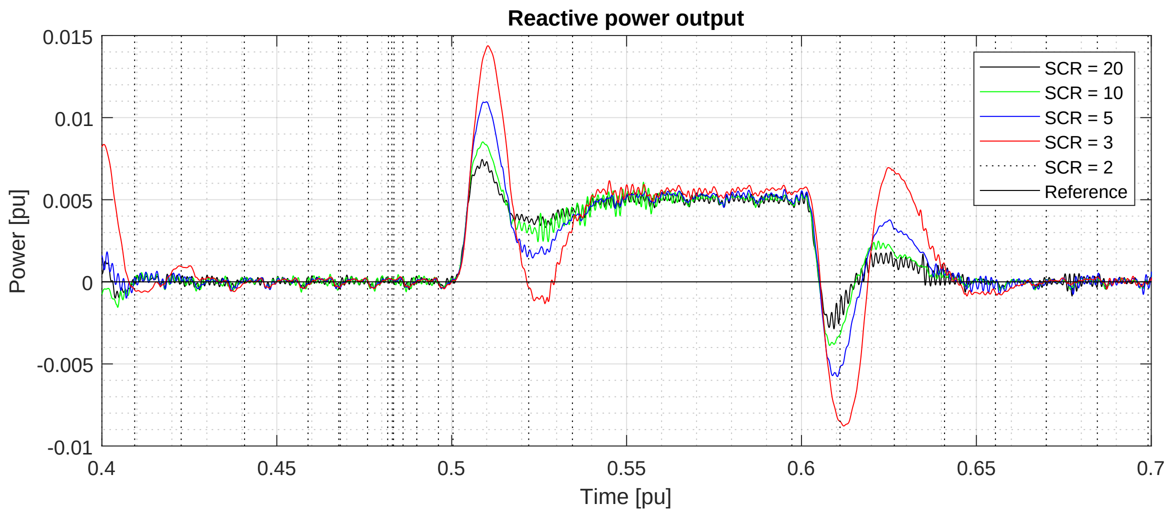

Figure 5.18:

Top: P not directly constrained **Bottom:** Q not directly constrained

Current outputs and references

The current references are being calculated based on the power references and the measured output voltage V_{f_d}. Figure 5.19 only depicts the reference associated with SCR=20. It is clear that lower short circuit ratios yields greater steady state active currents. This is because the converter output voltage is lower when the SCR is lower. This is demonstrated on figure 5.20.

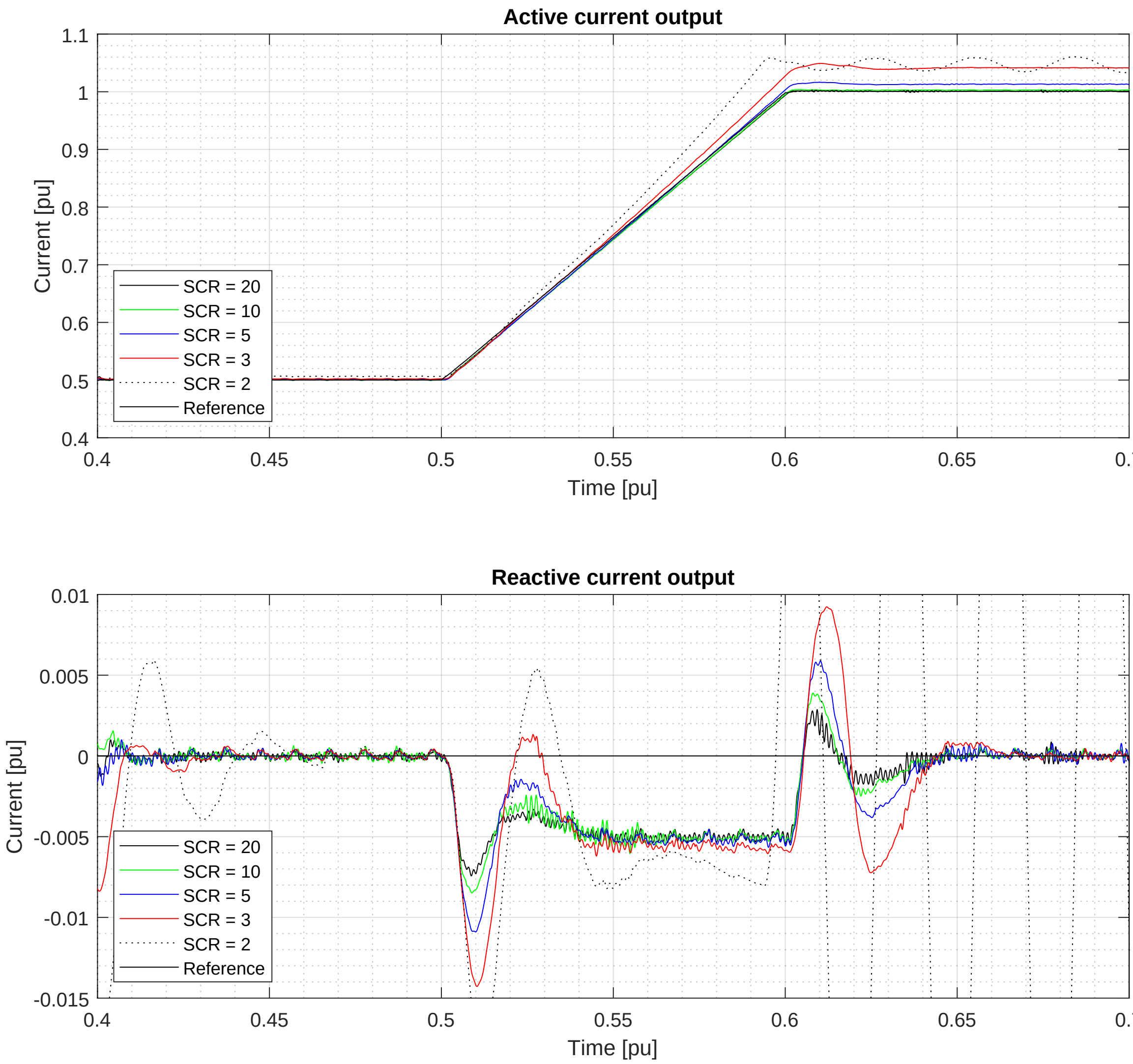

Figure 5.19:

Top: I_d constraint = [-0.15pu to 1.25pu] **Bottom:** I_q constraint = [-0.15pu to 1.25pu]

Converter voltage V_f

A trend that becomes apparent here is that the converter voltage V_f is lowered when the SCR is low. This causes the d current to be correspondingly larger to transfer the same power, as seen in the previous figures.

The lowered voltage is an interesting results of the increased grid impedance. Recall that the grid voltage has a fixed amplitude A in the time domain. Then consider that in the dq frame the voltage the d component corresponds to the amplitude and the q component to the phase[2]. Lastly recall that the d and q must sum quadratically to A, that is:

$$V_{g_d}^2 + V_{g_q}^2 = A^2$$

It is natural that a greater grid impedance causes a phase shift between V_g and V_f. This translates to an increase in V_{g_q} (V_{f_q} is always 0 due to the PLL). When V_{g_q} increases, then V_{g_d} decreases. This couples to V_{f_d}, which in turn decreases as well.

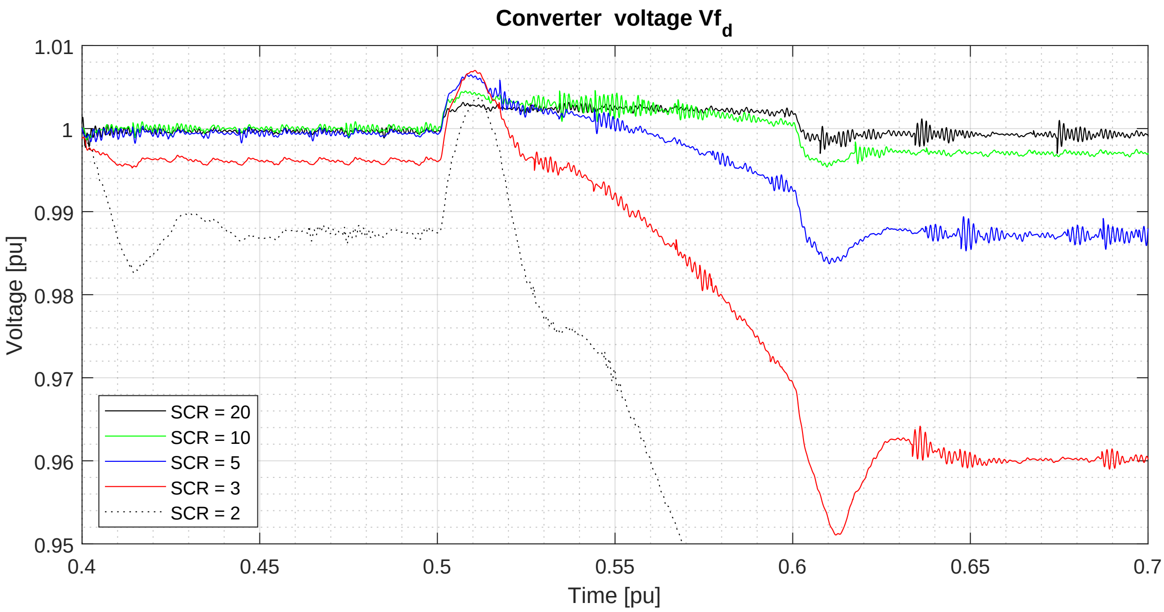

Figure 5.20: Converter voltage V_{f_d}

[2]When d » q

DC link voltage

The SCR has minimal impact on the DC link voltage regulation as long as SCR > 2. Once SCR = 2, the DC link becomes unstable.

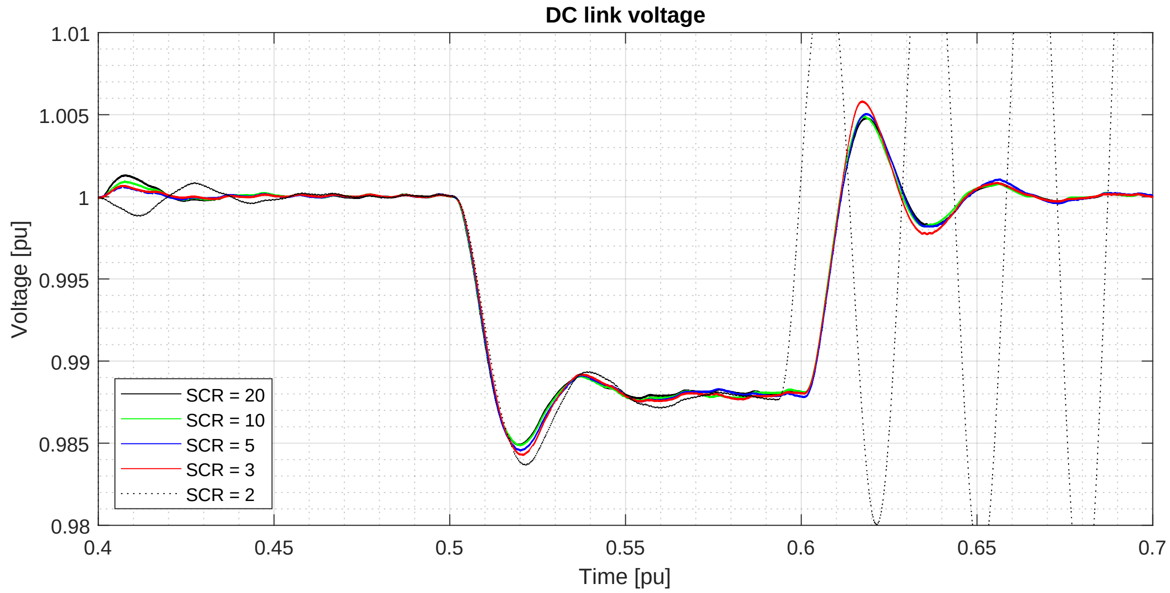

Figure 5.21: V_{DC} constraint = [0.95pu to 1.05pu]

Low SCR test summary

The test revealed that the MPC controller is robustly stable against short circuit ratios as low as 3. Lower SCR's cause unstable oscillations in the DC link voltage and the reactive current.

It was observed that lower short circuit ratios caused larger voltages, which in turn increased the current nessecary to meet the power references.

The success-criteria were partially met:

- ✓ [✘] The system must be stable for all test cases.
  Osciallations occured when SCR=2.
- ✓ [✘] There must be zero steady state error in P and Q for all test cases.
  Q was oscillating for SCR=2.
- ✓ The currents must not exceed their constraints for any test cases.
- ✓ The controller must not use the chopper as no fault is applied.

5.3.5 Low SCR FRT test

This test demonstrates the FRT performance, when the grid has a low short circuit ratio. The previous FRT tests were all conducted with SCR = 20. This test will reevaluate the FRT event with lower short circuit ratio. The test will be with Q production. During FRT-oriented control in this test the I_{dq} references are:

$$I_{d_{ref}} = 0.5\text{pu}$$
$$I_{q_{ref}} = -0.5\text{pu}$$

The fault begins at time = 0.7pu and ends at time = 0.9pu.

The success-criteria are:

- The system must be stable during and after the fault for all test cases.
- There must be zero steady state error in P and Q before and after the fault for all test cases.
- There must be zero steady state error in the active and reactive currents during the fault for all test cases.
- The currents must not exceed their constraints for any test cases.
- The controller must use the chopper to control the DC link voltage during the fault, and return the chopper signal to zero after the fault.
- The controller must not change the DC link current during the fault.

Power outputs and references

Figure 5.22 depicts the active and reactive powers and their references. As the fault occurs the power references are no longer used. The resulting power is a result of the current reference and the measured output voltage. The system is stable to all SCR's tested, but the general tendency is that lower short circuit ratio yields less stable behavior.

During the fault the lower SCR tests produce more active and reactive power. This is expected since they all deliver the same current, but the lower SCR tests deliver the currents to a larger impedance. This results in increased great power outputs.

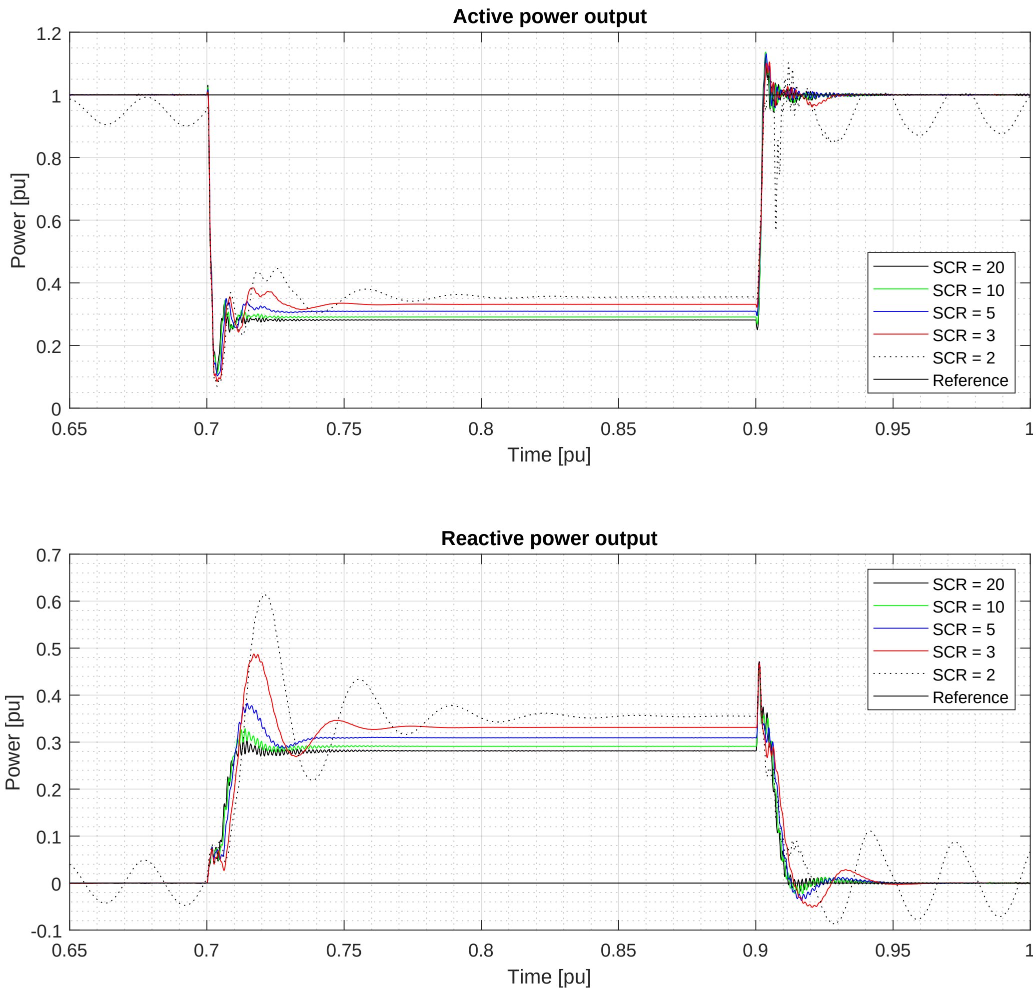

Figure 5.22:

Top: P not directly constrained **Bottom:** Q not directly constrained

Current outputs and references

During the fault the controller is able to stabilize the currents on the reference value. The weaker grid configuration requires more settling time and greater oscillations. Figure 5.23 only depicts the reference signals associated with SCR=20.

The low SCR tests produce smaller spikes in active current once the fault occurs.

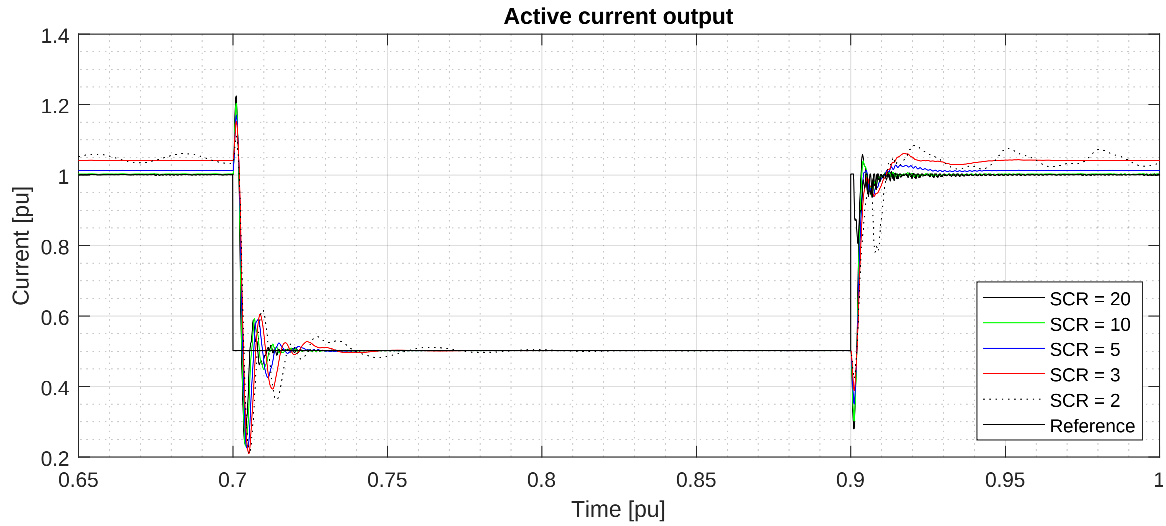

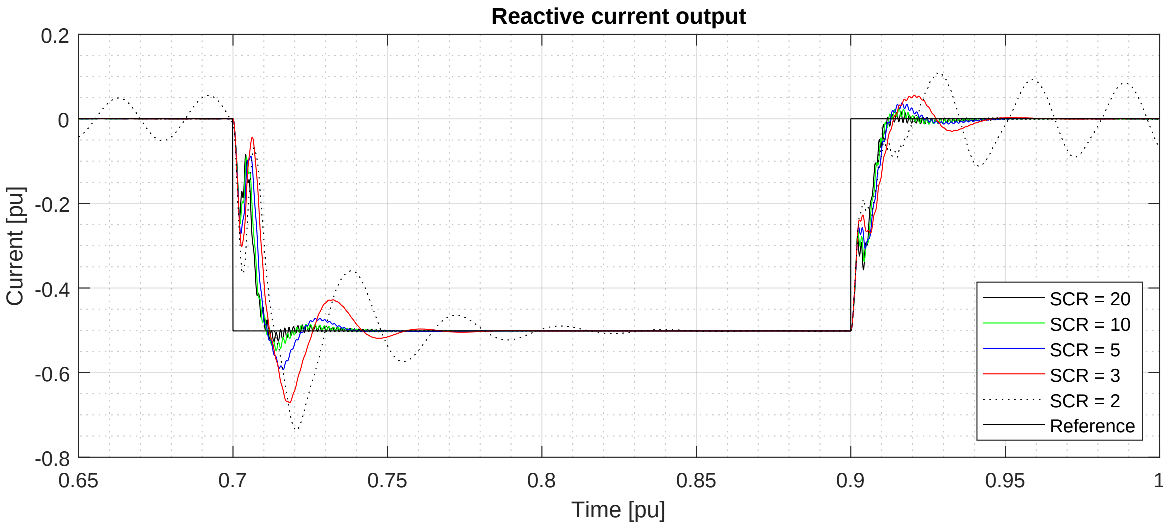

Figure 5.23:

Top: I_d constraint = [-0.15pu to 1.25pu] **Bottom:** I_q constraint = [-0.15pu to 1.25pu]

Converter voltage V_f

During the fault the converter voltage V_f settles to steady value for all test cases. The voltage is higher when the SCR is lower.

The test case with SCR=2 sees oscillations in the voltage, before and after the fault. These oscillations might be coupled to other oscillations in the currents and DC link. This is discussed later.

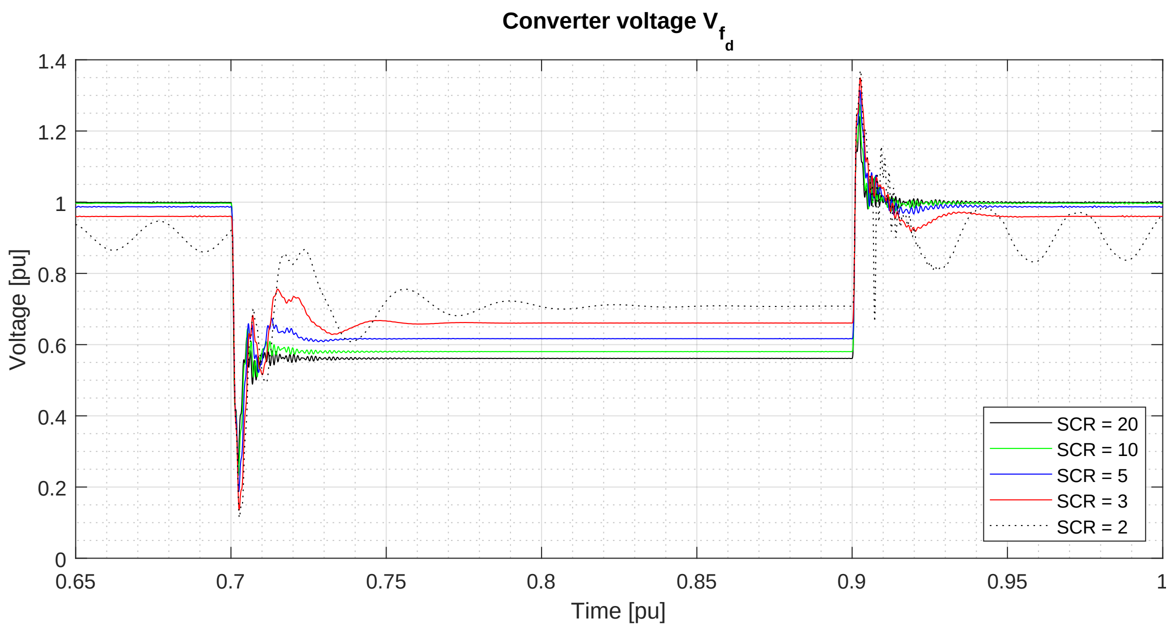

Figure 5.24: Converter voltage V_{f_d}

DC link voltage

The SCR has minimal impact on the DC link voltage regulation as long as SCR > 2. Once SCR = 2, the DC link becomes unstable.

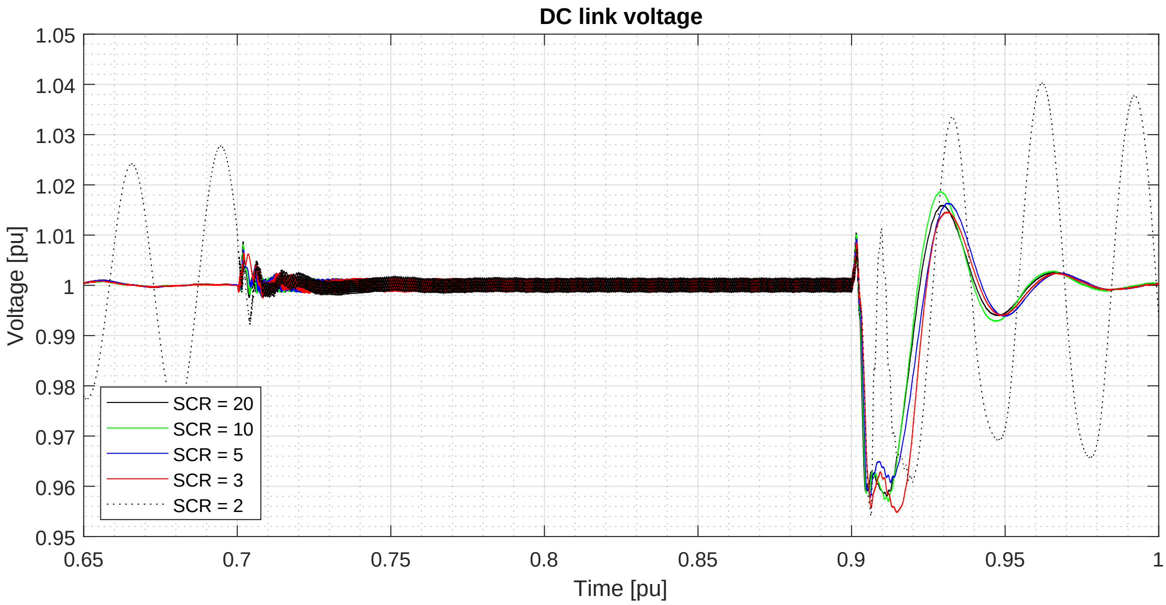

Figure 5.25: V_{DC} constraint = [0.95pu to 1.05pu]

Low SCR FRT test summary

The test revealed that the MPC controller is robustly stable against short circuit ratios as low as 3, even during fault ride through events.

An interesting phenomenom occurs for the extreme case where SCR=2. During the fault, the previously unstable signals (V_{DC} and I_q) would settle to a steady value with no oscillations. Once the fault ended they would resume oscillations.

A theory for why the low SCR ratio causes oscillations can be the current reference generation method. The references are created algebraically as

$$I_{dref} = \frac{P_{ref}}{1.5V_{f_d}}$$

$$I_{qref} = \frac{-Q_{ref}}{1.5V_{f_d}}$$

It is obvious that if V_{f_d} oscillates, so will the current references. This might cause a loop of oscillations, that can further couple to the DC voltage. The test results did indeed show that V_{f_d} was continuously oscillating when SCR=2. More research should be done on this topic, and another reference generating strategy should be proposed.

The success-criteria were partially met:

- ✓ [✘] The system must be stable during and after the fault for all test cases.
  Oscillations occur when SCR=2.
- ✓ [✘] There must be zero steady state error in P and Q before and after the fault for all test cases.
  Oscillations occur in Q when SCR=2.
- ✓ There must be zero steady state error in the active and reactive currents during the fault for all test cases.
- ✓ The currents must not exceed their constraints for any test cases.
- ✓ The controller must use the chopper to control the DC link voltage during the fault, and return the chopper signal to zero after the fault.
- ✓ The controller must not change the DC link current during the fault.

5.3.6 FRT with detection delay test

This test seeks to investigate the effects of a detection delay during FRT events. Previous tests assumed that the controller was informed of the fault the moment it happening. This test introduces a delay between the fault occuring and the controller switching to FRT-oriented control.

For this test the fault will begin at t=0.7pu, and the voltage will reach 0.5pu at t=0.701pu. The controller will switch to FRT-oriented control at t=0.701pu.

The test will be conducted with a SCR of 5. The controller will enter Q production, once FRT is "detected".

The success-criteria are:

- The system must be stable during and after the fault.
- There must be zero steady state error in P and Q before and after the fault.
- There must be zero steady state error in the active and reactive currents during the fault.
- The currents must not exceed their constraints.
- The controller must remain in "normal operation" until t=0.701pu, to simulate a delay in FRT detection.
- After t=0.701, the controller must use the chopper to control the DC link voltage during the fault, and return the chopper signal to zero after the fault.
- The controller can change the DC link current during the fault *before* FRT has been detected, but must not change the current *after* FRT is detected.

Control signals

Figure 5.26 depicts the control signals of the test.

- The d component of the converter voltage V_{c_d} goes to 0 during the beginning of the fault.
- The q component of the converter voltage V_{c_q} spikes rapidly when the fault begins. This, in combination with the d component distorts the abc voltage signal heavily.
- Before the controller switches to FRT-oritented control, it lowers the MSC current I_u drastically. This causes the chopper to not have to be open as much as previously. Previous tests of FRT with Q production saw steady state chopper values of 0.7pu.

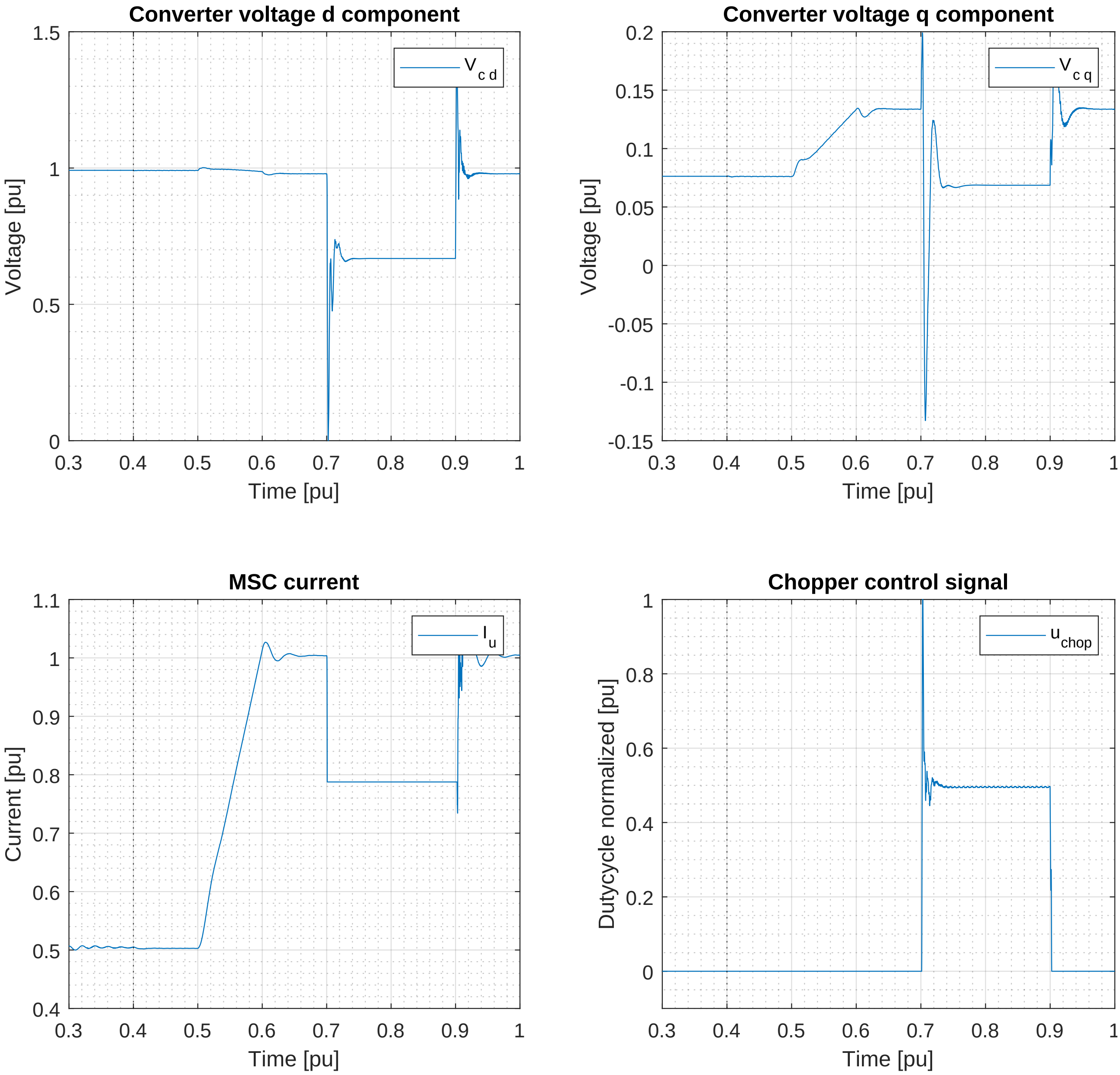

Figure 5.26:
Top left: V_{c_d} constraint = [-0.1pu to 1.1pu]
Bottom left: I_u constraint = [-0.15pu to 1.25pu]
Top right: V_{c_q} constraint = [-0.1pu to 1.1pu]
Bottom right: u_{chop} constraint = [0pu to 1pu]

Power outputs and references

The active and reactive powers behave as seen in previous tests. The active current overshoots by a large amount, but settles at the target value of 0.5pu - as does the reactive power. The active current violates its constraint of 1.25pu.

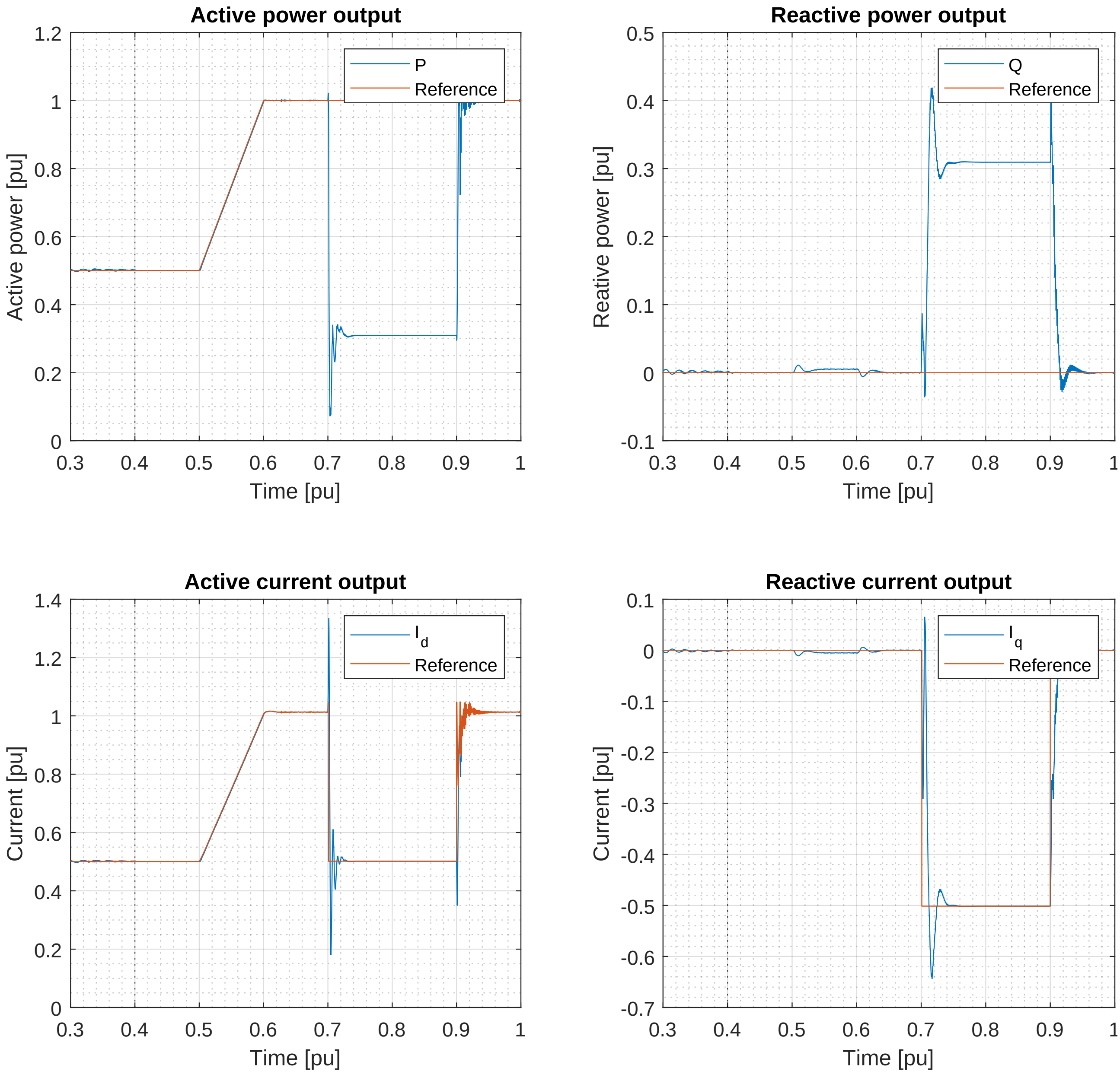

Figure 5.27:
Top left: P not directly constrained
Top right: Q not directly constrained
Bottom left: I_d constraint = [-0.15pu to 1.25pu]
Bottom right: I_q constraint = [-0.15pu to 1.25pu]

DC link voltage

The DC link voltage is affected more by the detection delay than the other signals. It spikes $\pm$ 0.01pu, which is noticably more than previous tests - however, not enough to be an actual issue.

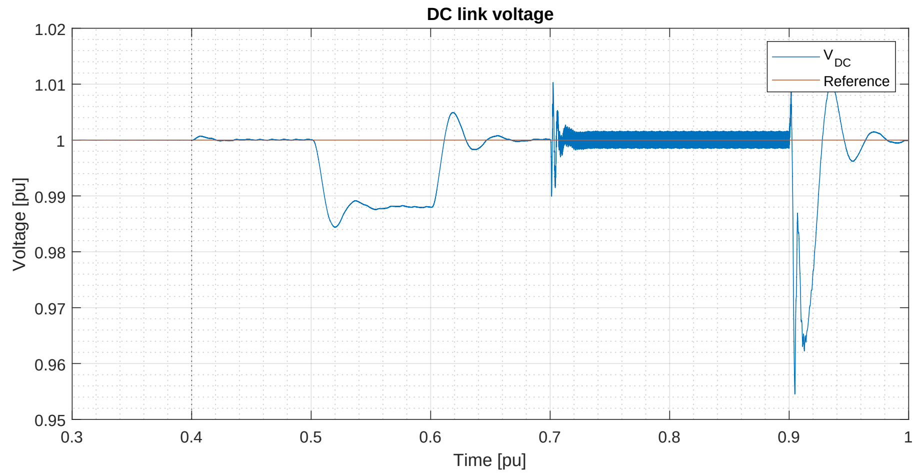

Figure 5.28: V_{DC} constraint = [0.95pu to 1.05pu]

FRT with detection delay - test summary

The test verified that a detection delay of 0.01pu (0.01pu is equal to the voltage fault fall and rise duration) did not affect system stability. The delay did however cause the active current to spike above its constraint. The control signal Vf_d went to 0 during the beginning of the fault. Further, the MSC current was lowered before the switch to FRT oriented control.

The success-criteria were partially met:

- ✓ The system must be stable during and after the fault.
- ✓ There must be zero steady state error in P and Q before and after the fault.
- ✓ There must be zero steady state error in the active and reactive currents during the fault.
- ✘ The currents must not exceed their constraints.
- ✓ The controller must remain in "normal operation" until t=0.701pu, to simulate a delay in FRT detection.
- ✓ After t=0.701, the controller must use the chopper to control the DC link voltage during the fault, and return the chopper signal to zero after the fault.
- ✓ The controller can change the DC link current during the fault *before* FRT has been detected, but must not change the current *after* FRT is detected.

5.3.7 Summary of Plecs test

The controller has been thoroughly tested on the high fidelity Plecs simulation. The highlights of the test results are as follows

- The MPC controller is able to stabilize the system during normal operation.
- The active power can be regulated without steady state error between 0pu and 1pu.
- The reactive power can be regulated without steady state error between -0.5pu and 0.5pu.
- The controller can stabilize the system during a fault ride through. Two reference strategies were tested:
  - Case 1: Keep the active current at 1pu and the reactive current at 0pu during the fault.
  - Case 2: Decrease the active current to 0.5pu during the fault, and decrease the reactive current to -0.5pu, which causes an increase in Q.
- Neither case was definitively better than the other on all parameters. Case 2 increased the voltage V_f, which helps stabilize the grid, and it decreased the current spikes. It did however cause a large spike in reactive power when the fault ended.

  - A potential issue can be the bang-bang change of current references, which is suboptimal.
- The MPC controller is robustly stable to grid variations as low as SCR=3. Lower than that system would start oscillating.
- The controller could stabilize the system during a fault ride through event with a SCR of 3.
- The controller could stabilize the system during a fault ride through event with a SCR of 5, even with a detection delay of t_{delay}=0.01pu.

5.4 MPC predictions investigation

The objective of this section is document a test of the internal function of MPC. As discussed in the controller design chapter, MPC will at every sample predict the trajectories of the system outputs over the prediction horizon. An example of these predictions are demonstrated an discussed here.

5.4.1 Prediction test

The test is similar to the base functionality test first conducted in Plecs. It is not necessary to recall the specific results or conclusions from the previous run, since this time the focus is on the MPC predictions. During the test, the active power is ramped slowly from 0.5pu to 1pu. Figure 5.29 depicts the resulting active current, and the MPC predicted trajectories.

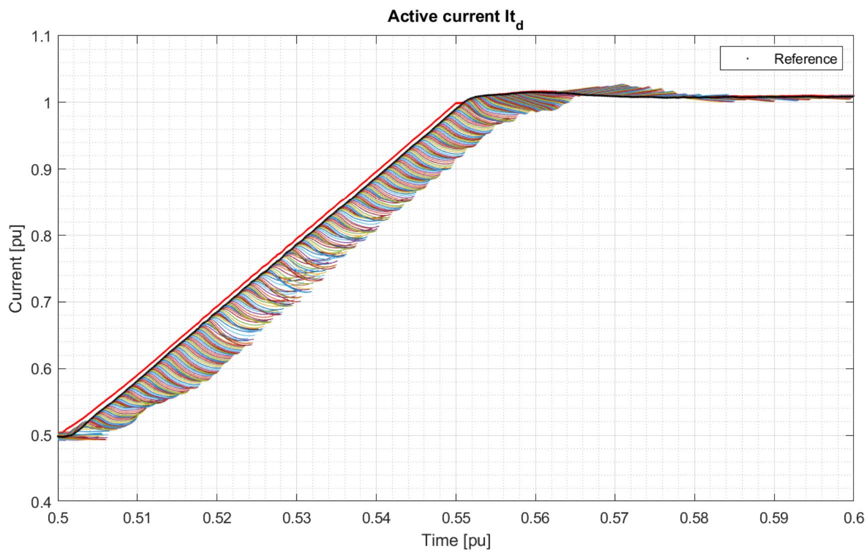

Figure 5.29: MPC predictions of the active current trajectories.

The red trace is the active current reference, and the black line is the actual measured active current. The trajectories are seen branching out from every sample.

Two things must be mentioned before analyzing the prediction behavior. The reference signals at each sample is assumed by the MPC algorithm to be constant over the entire prediction horizon.

Secondly the MPC controller has no terminal constraints: a common constraint which dictates that the last output value of the prediction **must** be equal to the reference.

An interesting phenomonen is seen. At each sample the controller predicts the the *optimal* action is a downwards movement followed by a rise up. This is because the controller understands that the current is increasing[3] but wants the output current to settle at the present value of the reference.

If the controller had terminal constraints, the trajectories would flatten and end at the reference values.

Consider now the DC link voltage trajectories in figure 5.30. The general tendency of these trajectories is that, when the DC link voltage is below the reference, the controller predicts that the optimal behavior is to cause a great rise DC link voltage. And vice versa, when the voltage is above the reference the voltage is predicted to shoot down.

One important thing here is the open loop instability of the system, as related to the horizons. The prediction horizon is 50 samples, while the control horizon is only 30 samples. This means that the final 20 samples demonstrate open loop behavior. This is likely why the DC link voltage appears to take off towards at the end of the prediction horizon.

One way to resolve this would be terminal constraints, which would ensure that every trajectory ends in 1pu. Another way could be to set the prediction and control horizon equal to eachother. Thus no open loop predictions are made.

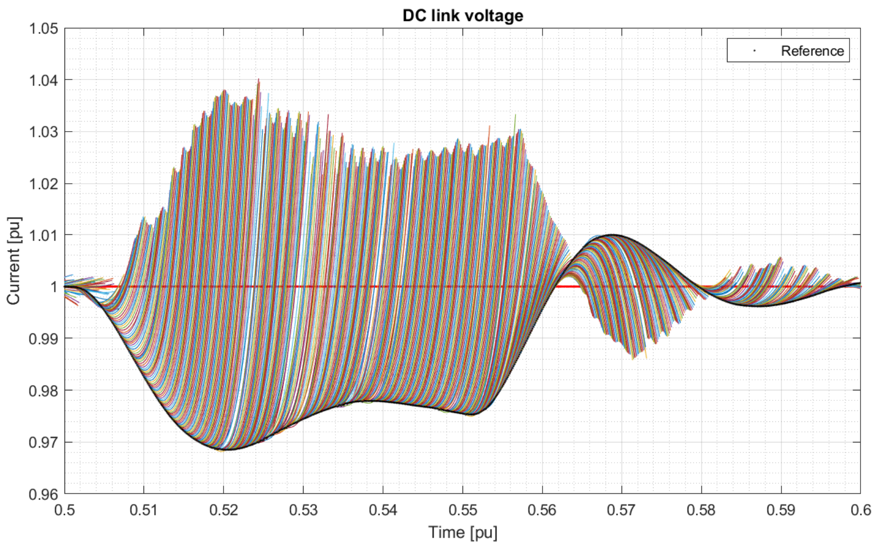

Figure 5.30: MPC predictions of the DC link voltage trajectories.

[3]MPC has information about the change in states from the previous sample, see model augmentation 3.3

Lastly figure 5.31 depicts the reactive power prediction trajectories. The tendencies are identical to that of the DC link voltage: when the measured value is below the reference, the trajectory takes off to plus infinity, and vice versa.

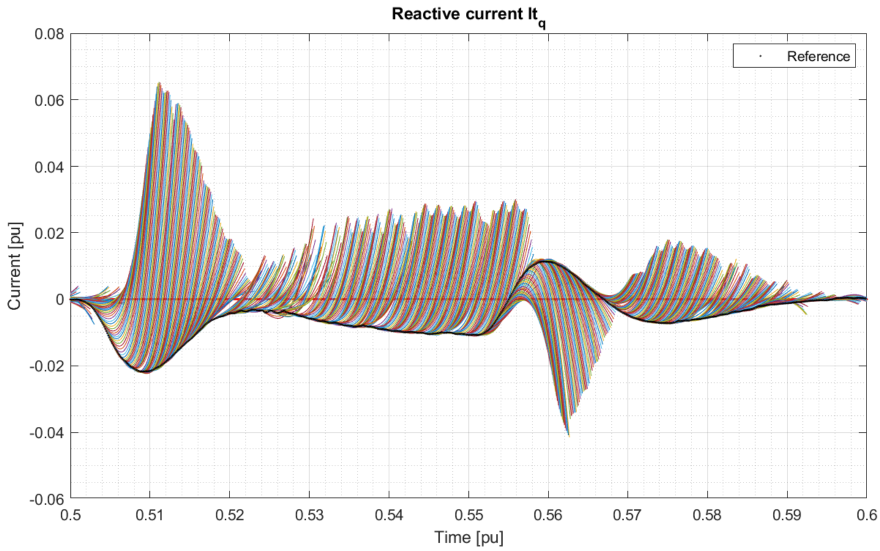

Figure 5.31: MPC predictions of the reactive current trajectories.

5.4.2 Summary

The tests has documented the prediction behavior of MPC. The main findings are that due to the absence of terminal constraints and due to the open loop control after H_u the trajectories tend to take off towards $\pm$ infinity.

This suggests that terminal constraints and equal horizons should be applied to future revisions of the control strategy. In spite of this, the test section has proven that the control strategy is stable. This is a very promising result for future work with MPC for power converters.

Chapter 6

Conclusion

This thesis has demonstrated the viability of model predictive control for wind turbine power converters. It has concluded that the proposed control strategy can stabilize the converter during normal operation, as well as during FRT events and under challenging operating conditions. The thesis has documented the development phase in four chronological parts.

The thesis statement was:

> How can a model predictive controller be implemented and used as a viable control strategy for a wind turbine full scale converter?

Parts 1 through 3 resolves the statement by documenting the full development of the model predictive control strategy for a full scale converter. Part 4 verifies the three hypotheses formulated in section 1.4.1.

Part 1: Modelling
The first part of the development, was the development of a LTI state space model, which accurately represents the system dynamics. The model was derived using first principles, and methods from previous work by the author. The model is used as a prediction model for the controller.

Part 2: Control design
The second part of the development, was the formulation of a model predictive control strategy. Initially the thesis presents the mathematical foundation for the controller, and demonstrates how MPC can be formulated as a quadratic optimization problem with LMI contraints. The MPC controller contains the previously developed prediction model, and information about the systems constraints. The control design section also provides information on how MPC tuning is handled, and how the controller in this thesis has been tuned.

Part 3: Implementation

The third part of the development is concerned with implementation of the MPC strategy on a platform. Two implementations are demonstrated. The first implementation is as a mex file, which can be executed in Simulink. This was done because previous work had developed a Simulink test framework, which in this thesis acts as the initial test platform. The second implementation is in C code. This success of this implementation was important, as functional c code is necessary for the potential future MPC hardware implementation.

Part 4: Test

The fourth part of the development is a test phase, which investigates the MPC controllers performance. Initial test in a controlled Simulink environment verified the baseline of the MPC functionality. Extensive tests were then conducted on a high fidelity converter simulation, provided by Vestas. Tests conducted on the HiFi simulation model include: Baseline functionality (normal performance), low voltage fault ride through events, robust stability to low grid SCR, and stability to FRT detection delays.

The proposed MPC controller proved to be able to stabilize and control the WTG full scale converter. The control strategy is able to control the active and reactive power delivered to the grid with zero steady state error, while keeping the DC link voltage steady. Under low voltage grid faults, the controller was able to switch to FRT-oriented control, which entailed switching from power control to current control. During these faults the active power output was lowered. To satisfy the power balance at the DC link, the chopper was used to dissipate excess power from the MSC; the DC link current was not lowered during FRT. The switching strategy between control of the MSC current and the chopper was successful.

The controller was robustly stable to grid short circuit ratios down to 3, and could even perform FRT with low SCR values. Although a SCR of 2 did not make the converter become strictly unstable, undamped oscillations in the DC link voltage and reactive current were observed. It is a great property of the MPC strategy, that stability can be obtained with a SCR of 3 without even changing the tuning. For comparison, classical control strategies utilize different tuning sets when connected to a grid with a SCR of below 5. The robust stability of MPC was obtained in the short span of 4 months, which reinformaces the belief that MPC will capable of producing superior robust performance when developed further.

The thesis has demonstrated that MPC is a stable control strategy for wind turbine power converters in simulation. There are however still many issues not investigated in this thesis. The most critical of these issues will be discussed in the following section.

6.1 Future work

Optimization of c code implementation

The implementation in c code in this thesis is being executed in a simulation, that has no limit on execution time. As such, there is no verification that the MPC algorithm calculates a valid control signal within one sample time. This consideration is deliberately omitted in the thesis, due to the extended scope optimization would require. Future research should investigate ways to ensure that the controller implementation is sufficiently efficient. Furthermore, strategies should be implemented to handle cases where for unknown reasons the MPC would fail to calculate a control signal within the sample time.

SCR capability improvement

The MPC controller was able to completely stabilize the system, when the SCR of the grid was above 2. Future research should investigate if and how the controller could be improved to facilitate robust control of even weaker grids. An interesting topic of research is to analyze if the SCR of the grid could be estimated online, and accounted for by the controller.

MPC improvements

The MPC controllers output predictions were investigated, which revealed that the last samples of the prediction tends to take off to $\pm$ infinity. To prevent this behavior, the controller could be improved by including terminal constraints, such that the predictions always end at the reference values. This would improve system stability. Furthermore due to the open loop instability of the system, the prediction horizon should not be longer than the control horizon, as that yields open loop behavior once the control horizon has ended.

Bibliography

[1] Mohammed Alhajeri and Masoud Soroush. "Tuning Guidelines for Model-Predictive Control". In: (2021).

[2] Joel A. E. Andersson et al. "CasADi - a software framework for nonlinear optimization and optimal control". In: *Mathematical Programming Computation* (2018).

[3] Oladimeji Ayamolowo, Patrick Manditereza, and Kanzumba Kusakana. "An overview of inertia requirement in modern renewable energy sourced grid: challenges and way forward". In: *Journal of Electrical Systems and Information Technology* 9 (2022). DOI: 10.1186/s43067-022-00053-2.

[4] Anca Hansen, ; Daniela, and Ioannis D Margaris. "General rights Type IV Wind Turbine Model". In: ().

[5] João P Hespanha. "Lecture notes on LQR/LQG controller design". In: (2005).

[6] Rasmus Kristiansen. *Model-based Control of Full-scale Converter Wind Turbines*. Tech. rep. Aalborg University, School of Information and Communication Technology, Department of Electronic Systems, 2022.

[7] Yoash Levron, Juri Belikov, and Dmitry Baimel. "A tutorial on dynamics and control of power systems with distributed and renewable energy sources based on the DQ0 transformation". In: *Applied Sciences (Switzerland)* 8.9 (Sept. 2018). ISSN: 20763417. DOI: 10.3390/APP8091661.

[8] Mathworks. *What is Model Predictive Control? - MATLAB & Simulink*. URL: https://www.mathworks.com/help/mpc/gs/what-is-mpc.html.

[9] Plexim GmBH. *PLECS Tutorial: Introduction to the C-Script Block*. URL: https://www.plexim.com/sites/default/files/tutorials/cscript_controller.pdf.

[10] *Renewable energy directive*. URL: https://energy.ec.europa.eu/topics/renewable-energy/renewable-energy-directive-targets-and-rules/renewable-energy-directive_en.

[11] S&P Global. *Current gas, electricity prices threaten European steelmaking viability: Eurofer | S&P Global Commodity Insights*. 2022. URL: https://www.spglobal.com/commodityinsights/en/market-insights/latest-news/metals/090922-current-gas-electricity-prices-threaten-european-steelmaking-viability-eurofer.

[12] Bartolomeo Stellato et al. “OSQP: an operator splitting solver for quadratic programs”. In: *Mathematical Programming Computation* 12 (2020), pp. 637–672. DOI: 10.1007/s12532-020-00179-2. URL: https://doi.org/10.1007/s12532-020-00179-2.

[13] Yueming Sun. “Impacts of the Ukraine Conflict on Energy and Food Shortages & Price Increase in UK and EU”. In: *BCP Business & Management* 40 (2023), pp. 253–259. DOI: 10.54691/bcpbm.v40i.4389.

[14] *Vestas Annual Report 2022 – A challenging year with negative profitability*. Feb. 2023. URL: https://www.vestas.com/en/media/company-news/2023/vestas-annual-report-2022---a-challenging-year-with-neg-c3710817.

Appendix A

System matrices from previous work

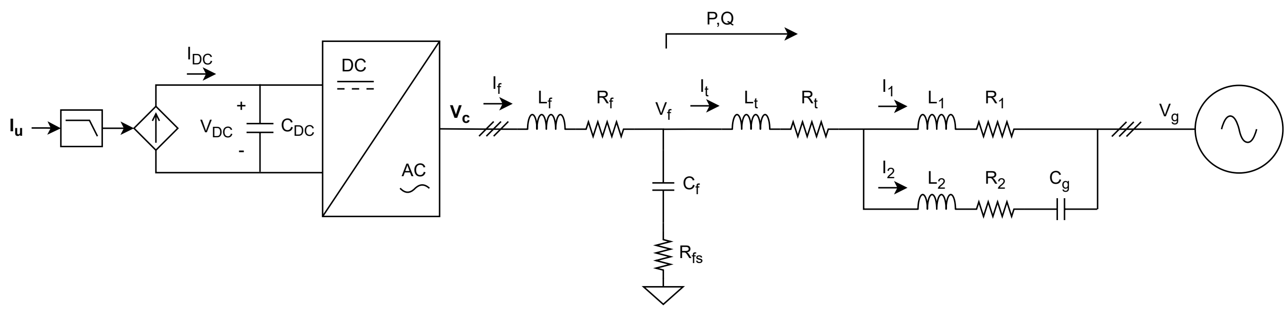

Figure A.1: Block diagram of the system modelled in previous work

The AC subsystem of the system presented in figure A.1 can be modelled as such:

$$\dot{x} = Ax + Bu \tag{A.1}$$
$$y = Cx \tag{A.2}$$

where

$$x = \begin{bmatrix} I_f \\ I_t \\ I_1 \\ I_2 \\ V_{C_f} \\ V_{C_g} \end{bmatrix}, \qquad u = \begin{bmatrix} V_c \\ V_g \end{bmatrix}, \qquad y = \begin{bmatrix} V_f \\ I_t \end{bmatrix} \tag{A.3}$$

and

$$A = \begin{bmatrix} \left(\frac{-R_{fs}}{L_f} - \frac{R_f}{L_f}\right) & \frac{R_{fs}}{L_f} & 0 & 0 & \frac{-1}{L_f} & 0 \\ \left(\frac{-R_{fs}}{L_t^2\sigma} + \frac{R_{fs}}{L_t}\right) & \left(\frac{R_{fs}}{L_t^2\sigma} + \frac{R_t}{L_t^2\sigma} + \frac{-R_{fs}}{L_t} - \frac{R_t}{L_t}\right) & \frac{-R_1}{L_1\sigma L_t} & \frac{-R_2}{L_2\sigma L_t} & \left(\frac{1}{L_t} - \frac{1}{L_t^2\sigma}\right) & \frac{-1}{L_2\sigma L_t} \\ \frac{R_{fs}}{L_t\sigma L_1} & \left(\frac{-R_{fs}}{L_t\sigma L_1} - \frac{R_t}{L_t\sigma L_1}\right) & \left(\frac{R_1}{L_1^2\sigma} - \frac{R_1}{L_1}\right) & \frac{R_2}{L_2\sigma L_1} & \frac{1}{L_t\sigma L_1} & \frac{1}{L_2\sigma L_1} \\ \frac{R_{fs}}{L_t\sigma L_2} & \left(\frac{-R_{fs}}{L_t\sigma L_2} - \frac{R_t}{L_t\sigma L_2}\right) & \frac{R_1}{L_1\sigma L_2} & \left(\frac{R_2}{L_2^2\sigma} - \frac{R_2}{L_2}\right) & \frac{1}{L_t\sigma L_2} & \left(\frac{1}{L_2^2\sigma} - \frac{1}{L_2}\right) \\ \frac{1}{Cf} & \frac{-1}{Cf} & 0 & 0 & 0 & 0 \\ 0 & 0 & 0 & \frac{1}{Cg} & 0 & 0 \end{bmatrix} \tag{A.4}$$

$$B = \begin{bmatrix} \frac{1}{L_f} & 0 \\ 0 & \left(\frac{-1}{L_1\sigma L_t} - \frac{1}{L_2\sigma L_t}\right) \\ 0 & \left(\frac{1}{L_1^2\sigma} + \frac{1}{L_2\sigma L_1} - \frac{1}{L_1}\right) \\ 0 & \left(\frac{1}{L_1\sigma L_2} + \frac{1}{L_2^2\sigma} - \frac{1}{L_2}\right) \\ 0 & 0 \\ 0 & 0 \end{bmatrix} \tag{A.5}$$

$$C = \begin{bmatrix} 0 & 1 & 0 & 0 & 0 & 0 \\ R_{fs} & -R_{fs} & 0 & 0 & 1 & 0 \end{bmatrix} \tag{A.6}$$

and the intermediate variable σ is defined as

$$\sigma = \frac{1}{L_t} + \frac{1}{L_1} + \frac{1}{L_2} \tag{A.7}$$

Appendix B

Derivation of AC subsystem differential equations

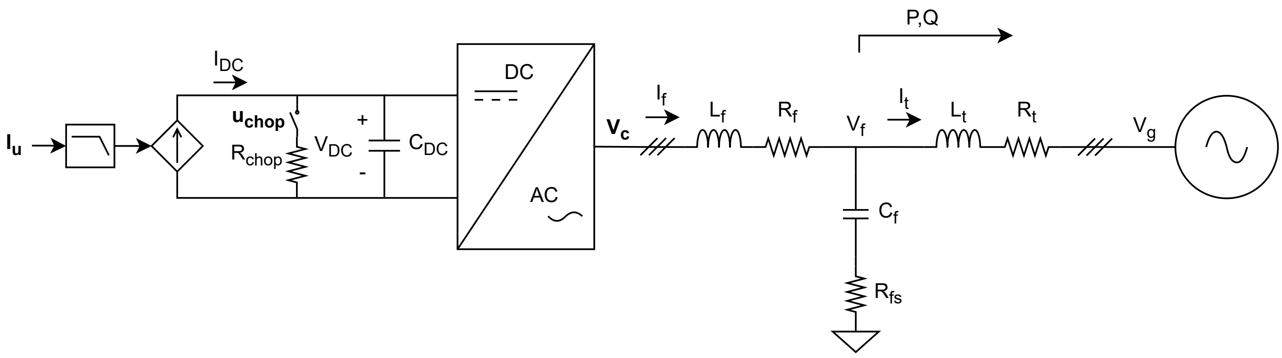

Figure B.1: Block diagram of the Type 4 wind turbine model considered in this thesis

$\mathbf{I_{Cf}}$

$$0 = I_f + (\text{-}I_t) + (\text{-}I_{C_f}) \tag{B.1}$$

$$I_{C_f} = I_f \text{ - } I_t \tag{B.2}$$

$\mathbf{V_f}$

$$V_f = V_{C_f} + I_{C_f} R_{fs} \tag{B.3}$$

Substituting equation B.2 yields

$$V_f = V_{C_f} + \left(I_f \text{ - } I_t\right) R_{fs} \tag{B.4}$$

Rearranging

$$V_f = V_{C_f} + I_f R_{fs} \text{ - } I_t R_{fs} \tag{B.5}$$

$\mathbf{I_f}$

$$\dot{I}_f = \frac{V_{L_f}}{L_f} \tag{B.6}$$

$$\dot{I}_f = \frac{V_c - I_f R_f - V_f}{L_f} \tag{B.7}$$

$$\dot{I}_f = \frac{V_c}{L_f} + \frac{-I_f R_f}{L_f} + \frac{-V_f}{L_f} \tag{B.8}$$

$$\dot{I}_f = V_c \frac{1}{L_f} + I_f \frac{-R_f}{L_f} + V_f \frac{-1}{L_f} \tag{B.9}$$

$$\dot{I}_f = V_c \frac{1}{L_f} + I_f \frac{-R_f}{L_f} + \left(V_{C_f} + I_f R_{fs} - I_t R_{fs} \right) \frac{-1}{L_f} \tag{B.10}$$

$$\dot{I}_f = V_c \frac{1}{L_f} + I_f \frac{-R_f}{L_f} + V_{C_f} \frac{-1}{L_f} + I_f \frac{-R_{fs}}{L_f} + I_t \frac{R_{fs}}{L_f} \tag{B.11}$$

$$\dot{I}_f = V_c \frac{1}{L_f} + I_f \frac{-R_f - R_{fs}}{L_f} + V_{C_f} \frac{-1}{L_f} + I_t \frac{R_{fs}}{L_f} \tag{B.12}$$

$\mathbf{I_t}$

$$\dot{I}_t = \frac{V_{L_t}}{L_t} \tag{B.13}$$

$$\dot{I}_t = \frac{V_f - I_t R_t - V_g}{L_t} \tag{B.14}$$

$$\dot{I}_t = \frac{V_f}{L_t} + \frac{-I_t R_t}{L_t} + \frac{-V_g}{L_t} \tag{B.15}$$

$$\dot{I}_t = V_f \frac{1}{L_t} + I_t \frac{-R_t}{L_t} + V_g \frac{-1}{L_t} \tag{B.16}$$

$$\dot{I}_t = \left(V_{C_f} + I_f R_{fs} - I_t R_{fs}\right) \frac{1}{L_t} + I_t \frac{-R_t}{L_t} + V_g \frac{-1}{L_t} \tag{B.17}$$

$$\dot{I}_t = V_{C_f} \frac{1}{L_t} + I_f \frac{R_{fs}}{L_t} + I_t \frac{-R_{fs}}{L_t} + I_t \frac{-R_t}{L_t} + V_g \frac{-1}{L_t} \tag{B.18}$$

$$\dot{I}_t = V_{C_f} \frac{1}{L_t} + I_f \frac{R_{fs}}{L_t} + I_t \frac{-R_t - R_{fs}}{L_t} + V_g \frac{-1}{L_t} \tag{B.19}$$

$\mathbf{V_{cf}}$

$$\dot{V}_{C_f} = \frac{I_{C_f}}{C_f} \tag{B.20}$$

$$\dot{V}_{C_f} = \frac{I_f - I_t}{C_f} \tag{B.21}$$

$$\dot{V}_{C_f} = I_f \frac{1}{C_f} + I_t \frac{-1}{C_f} \tag{B.22}$$

Appendix C

Lifting example

Let the system dynamics be given by 3.2, and define $H_p = 4$ and $H_u = 3$. The predictions of $\hat{x}(k+n|n \in \{1,2,3,4\})$ in terms of $\hat{x}(k)$ and $\hat{u}(k+n|n \in \{0,1,2,3\})$ can be written as

$$\hat{x}(k+1) = A\hat{x}(k) + B\hat{u}(k) \tag{C.1}$$

$$\begin{aligned} \hat{x}(k+2) &= A\hat{x}(k+1) + B\hat{u}(k+1) \\ &= A\left(A\hat{x}(k) + B\hat{u}(k)\right) + B\hat{u}(k+1) \\ &= A^2\hat{x}(k) + AB\hat{u}(k) + B\hat{u}(k+1) \end{aligned} \tag{C.2}$$

$$\hat{x}(k+3) = A^3\hat{x}(k) + A^2B\hat{u}(k) + AB\hat{u}(k+1) + B\hat{u}(k+2) \tag{C.3}$$

$$\hat{x}(k+4) = A^4\hat{x}(k) + A^3B\hat{u}(k) + A^2B\hat{u}(k+1) + AB\hat{u}(k+2) + B\hat{u}(k+3) \tag{C.4}$$

Now define the control signals $\hat{u}(k+n)$ in terms of $\Delta\hat{u}(k+n)$ and $\hat{u}(k-1)$

$$\hat{u}(k) = \hat{u}(k-1) + \Delta\hat{u}(k) \tag{C.5}$$

$$\hat{u}(k+1) = \hat{u}(k-1) + \Delta\hat{u}(k) + \Delta\hat{u}(k+1) \tag{C.6}$$

$$\hat{u}(k+2) = \hat{u}(k-1) + \Delta\hat{u}(k) + \Delta\hat{u}(k+1) + \Delta\hat{u}(k+2) \tag{C.7}$$

$$\hat{u}(k+3) = \hat{u}(k-1) + \Delta\hat{u}(k) + \Delta\hat{u}(k+1) + \Delta\hat{u}(k+2) \tag{C.8}$$

Notice, there is no $\Delta\hat{u}(k+3)$, since that would be the 4^{th} predicted input action. $H_u = 3$ dictates that only 3 input actions are only being predicted, which implies that $\Delta\hat{u}(k+3) = 0$.

Substituting the reformulated control signal equations C.5-C.8 into the state prediction equations C.1-C.4 yields the following

$$\hat{x}(k+1) = A\hat{x}(k) + B\Delta\hat{u}(k) + B\hat{u}(k-1)$$

$$\hat{x}(k+2) = A^2\hat{x}(k) + (AB+B)\Delta\hat{u}(k) + B\Delta\hat{u}(k+1) + (AB+B)\hat{u}(k-1)$$

$$\hat{x}(k+3) = A^3\hat{x}(k) + (A^2B+AB+B)\Delta\hat{u}(k) + (AB+B)\Delta\hat{u}(k+1) + B\Delta\hat{u}(k+2) + (A^2B+AB+B)\hat{u}(k-1)$$

$$\begin{aligned}\hat{x}(k+4) = {} & A^4\hat{x}(k) + (A^3B+A^2B+AB+B)\Delta\hat{u}(k) + (A^2B+AB+B)\Delta\hat{u}(k+1) + (AB+B)\Delta\hat{u}(k+2) \\ & + (A^3B+A^2B+AB+B)\hat{u}(k-1)\end{aligned}$$

The colors aid to reveal the pattern of the lifted system matrices. The state trajectory sequence can be written in matrix form as such

$$\mathcal{X}(k) = \mathcal{A}\hat{x}(k) + \mathcal{B}_u u(k-1) + \mathcal{B}_{\Delta u}\Delta\mathcal{U}(k)$$

where

$$\mathcal{X}(k) = \begin{bmatrix} \hat{x}(k+1) \\ \hat{x}(k+2) \\ \hat{x}(k+3) \\ \hat{x}(k+4) \end{bmatrix}$$

$$\Delta\mathcal{U}(k) = \begin{bmatrix} \Delta\hat{u}(k) \\ \Delta\hat{u}(k+1) \\ \Delta\hat{u}(k+2) \end{bmatrix}$$

$$\mathcal{A} = \begin{bmatrix} A \\ A^2 \\ A^3 \\ A^4 \end{bmatrix}$$

$$\mathcal{B}_u = \begin{bmatrix} B \\ AB+B \\ A^2B+AB+B \\ A^3B+A^2B+AB+B \end{bmatrix}$$

$$\mathcal{B}_{\Delta u} = \begin{bmatrix} B & 0 & 0 \\ B+AB & B & 0 \\ B+AB+A^2B & B+AB & B \\ B+AB+A^2B+A^3B & B+AB+A^2B & B+AB \end{bmatrix}$$

Appendix D

Constraint matrices

For a constrained model, the following LMIs can be used to define the constraints:

Actuation slew rate constraint:

$$\mathcal{E}\begin{bmatrix}\Delta\mathcal{U}(k)\\ 1\end{bmatrix} \leq 0, \qquad \Delta\mathcal{U}(k) = \begin{bmatrix}\Delta\hat{u}(k)\\ \vdots\\ \Delta\hat{u}(k+H_u-1)\end{bmatrix} \tag{D.1}$$

Actuation range constraint:

$$\mathcal{F}\begin{bmatrix}\mathcal{U}(k)\\ 1\end{bmatrix} \leq 0, \qquad \mathcal{U}(k) = \begin{bmatrix}\hat{u}(k)\\ \vdots\\ \hat{u}(k+H_u-1)\end{bmatrix} \tag{D.2}$$

Output range constraint:

$$\mathcal{G}\begin{bmatrix}\mathcal{Y}(k)\\ 1\end{bmatrix} \leq 0, \qquad \mathcal{Y}(k) = \begin{bmatrix}\hat{y}(k)\\ \vdots\\ \hat{y}(k+H_p)\end{bmatrix} \tag{D.3}$$

The matrices $\mathcal{E}$, $\mathcal{F}$ and $\mathcal{G}$ contain the information about the constraints. This appendix will show how they are constructed.

Consider a state space model with 2 inputs and 1 output, controlled by a MPC controller. Let the controller have the following horizons: $H_p = 3$ and $H_u = 2$.

D.1 Actuator slew rate constraint

Let the actuator slew rate be limited by

$$-2 \leq \Delta\hat{u}_1 \leq 3 \tag{D.4}$$

$$-10 \leq \Delta\hat{u}_2 \leq 15 \tag{D.5}$$

The constraint can be rewritten over the entire control horizon as as

$$\begin{array}{rrl} -\Delta\hat{u}_1(k) & -2 & \leq 0 \\ \Delta\hat{u}_1(k) & -3 & \leq 0 \\ -\Delta\hat{u}_2(k) & -10 & \leq 0 \\ \Delta\hat{u}_2(k) & -15 & \leq 0 \\ -\Delta\hat{u}_1(k+1) & -2 & \leq 0 \\ \Delta\hat{u}_1(k+1) & -3 & \leq 0 \\ -\Delta\hat{u}_2(k+1) & -10 & \leq 0 \\ \Delta\hat{u}_2(k+1) & -15 & \leq 0 \end{array} \tag{D.6}$$

Which can be written as a matrix inequality as

$$\begin{bmatrix} -1 & 0 & 0 & 0 & -2 \\ 1 & 0 & 0 & 0 & -3 \\ 0 & -1 & 0 & 0 & -10 \\ 0 & 1 & 0 & 0 & -15 \\ 0 & 0 & -1 & 0 & -2 \\ 0 & 0 & 1 & 0 & -3 \\ 0 & 0 & 0 & -1 & -10 \\ 0 & 0 & 0 & 1 & -15 \end{bmatrix} \begin{bmatrix} \Delta\hat{u}_1(k) \\ \Delta\hat{u}_2(k) \\ \Delta\hat{u}_1(k+1) \\ \Delta\hat{u}_2(k+1) \\ 1 \end{bmatrix} \leq 0 \tag{D.7}$$

This LMI can be expressed compactly as

$$\mathcal{E} \begin{bmatrix} \Delta\mathcal{U}(k) \\ 1 \end{bmatrix} \leq 0 \tag{D.8}$$

D.2 Actuator range constraint

Let the actuator range be limited by

$$0 \leq \hat{u}_1 \leq 100 \tag{D.9}$$

$$-10 \leq \hat{u}_2 \leq 10 \tag{D.10}$$

Using the same procedure as for the actuator slew rate constraint, the constraint can be defined as an LMI:

$$\begin{bmatrix} -1 & 0 & 0 & 0 & 0 \\ 1 & 0 & 0 & 0 & -100 \\ 0 & -1 & 0 & 0 & -10 \\ 0 & 1 & 0 & 0 & -10 \\ 0 & 0 & -1 & 0 & 0 \\ 0 & 0 & 1 & 0 & -100 \\ 0 & 0 & 0 & -1 & -10 \\ 0 & 0 & 0 & 1 & -10 \end{bmatrix} \begin{bmatrix} \hat{u}_1(k) \\ \hat{u}_2(k) \\ \hat{u}_1(k+1) \\ \hat{u}_2(k+1) \\ 1 \end{bmatrix} \leq 0 \tag{D.11}$$

As before, this LMI can be expressed compactly as

$$\mathcal{F}\begin{bmatrix}\mathcal{U}(k)\\ 1\end{bmatrix} \leq 0 \tag{D.12}$$

D.3 Output range constraint

Lastly, let the output range be limited by

$$-20 \leq \hat{y} \leq 100 \tag{D.13}$$

$$\begin{bmatrix} \text{-}\hat{y}(k) & -20 & \leq 0 \\ \hat{y}(k) & -100 & \leq 0 \\ \text{-}\hat{y}(k+1) & -20 & \leq 0 \\ \hat{y}(k+1) & -100 & \leq 0 \\ \text{-}\hat{y}(k+2) & -20 & \leq 0 \\ \hat{y}(k+2) & -100 & \leq 0 \end{bmatrix} \tag{D.14}$$

which can be written as matrices

$$\begin{bmatrix} -1 & 0 & 0 & -20 \\ 1 & 0 & 0 & -100 \\ 0 & -1 & 0 & -20 \\ 0 & 1 & 0 & -100 \\ 0 & 0 & -1 & -20 \\ 0 & 0 & 1 & -100 \end{bmatrix} \begin{bmatrix} \hat{y}(k) \\ \hat{y}(k+1) \\ \hat{y}(k+2) \\ 1 \end{bmatrix} \leq 0 \tag{D.15}$$

$$\mathcal{G}\begin{bmatrix}\mathcal{Y}(k)\\ 1\end{bmatrix} \leq 0 \tag{D.16}$$